Spring 4-17-2017

DEVELOPING FLUOROGEN ACTIVATING PROTEIN-FLUORESCENT PROTEIN FRET PAIRS FOR LIVE CELL IMAGING

Genevieve Kate Phillips
University of New Mexico

Genevieve Phillips
_____

Candidate

Biomedical Sciences
_____

Department

This thesis is approved, and it is acceptable in quality and form for publication:

Approved by the Thesis Committee:

Dr. Diane Lidke, Chairperson
_____

Dr. Angela Wandinger-Ness
_____

Dr. Heather Ward
_____

Dr. Bill Shuttleworth
_____

_____

_____

_____

_____

**DEVELOPING FLUOROGEN ACTIVATING PROTEIN-FLUORESCENT PROTEIN FRET PAIRS
FOR LIVE CELL IMAGING**

BY

GENEVIEVE KATE PHILLIPS

BACHELOR OF SCIENCE, BIOLOGY

BACHELOR OF ARTS, PSYCHOLOGY

THESIS

Submitted in Partial Fulfillment of the

Requirements for the Degree of

Master of Science

Biomedical Sciences

The University of New Mexico

Albuquerque, New Mexico

May, 2017

ACKNOWLEDGEMENTS

DEVELOPING FLUOROGEN ACTIVATING PROTEIN-FLUORESCENT PROTEIN FRET PAIRS

FOR

LIVE CELL IMAGING

by

Genevieve Phillips

B.S., Biology, Central Washington University, 2003

B.A., Psychology, Central Washington University, 2003

M.S., Biomedical Sciences, University of New Mexico, 2017

ABSTRACT

Fluorogen activating proteins (FAPs) are genetically encoded tags made from single chain antibody fragments (scFv) designed to bind fluorogens with high specificity. Both the fluorogen and FAP can be modified to provide flexibility in properties such as affinity, membrane permeability, spectra, and quantum yield. The fluorogen Malachite Green (MG) has two excitation peaks, the maximum at 630 nm and a secondary peak at 450 nm. The emission spectra of blue-emitting fluorescence proteins, such as mCerulean (mCer), overlap with the MG secondary peak, generating a FRET pair with large Stokes shift emission. Using 405 nm excitation of mCer, we observe acceptor

sensitized emission at wavelengths greater than 650 nm with no spectral crosstalk between the donor and acceptor channels. Additionally, donor only controls can be acquired for all cells as the acceptor is not present until after the addition of the fluorogen, providing intra-cellular control.

The FAP-FRET system has been characterized using proof of principle constructs: FAP-mCer-transmembrane (TM) as a positive FRET control and FAP-TM-mCer as a negative FRET control and expressed in HeLa cells. Multiple MG derivatives were compared and imaging parameters were optimized to determine the optimal FRET pair. Analysis was performed using code written in Matlab to mask the cell membrane and quantify FRET efficiencies, based on donor intensity before and after addition of fluorogen. Data from several fluorogen showed high energy transfer efficiency (~30%) with the FAP-mCer-TM construct compared to negligible FRET (~4%) for FAP-TM-mCer. Additional techniques were performed to support the FRET efficiency data, including spectral imaging and FLIM, which also reported FRET efficiency around 30% with the positive constructs and negligible FRET with the negative constructs. The FAP-FRET system is currently being used to study the kinetics of signaling proteins within the FcεRI pathway.

TABLE OF CONTENTS

LIST OF FIGURES

LIST OF TABLES

Chapter 1

Introduction

1.1 Fluorescence

Fluorescence microscopy has been a powerful tool used for decades to investigate

biological questions because of the ability to specifically label and visualize only the

cellular components of interest in either live or fixed specimens. Fluorescence was first

described by G. G. Stokes in 1852 after observing that a mineral emitted red light when

illuminated with ultraviolet light, and determined that the emission of fluorescence is

always a longer wavelength than that used for excitation. The Stokes shift is the

difference in wavelength between maximum excitation and emission of a fluorescent

molecule (Lavis & Raines, 2007) (Figure 1.1 A).

Identification and evaluation of a number of naturally occurring fluorescent substances,

including aromatic amino acids such as tryptophan, showed that these molecules

typically contain polyaromatic hydrocarbons or heterocyclic structures where electrons

within pi bonds can become excited through interactions with photons (Teale & Weber,

1957) (Zgierski, Fujiwara, & Lim, 2010) (Figure 1.1 B). Depending on the chemical

structure of the fluorescent molecule, a photon of specific energy can excite an electron

to a higher energy state and emit a photon of less energy during relaxation. A Jablonski

diagram is frequently used to describe this event, where the ground state of an electron

is labeled S_0 and the excited singlet states are denoted S_1 and S_2 (Figure 1.1 C).
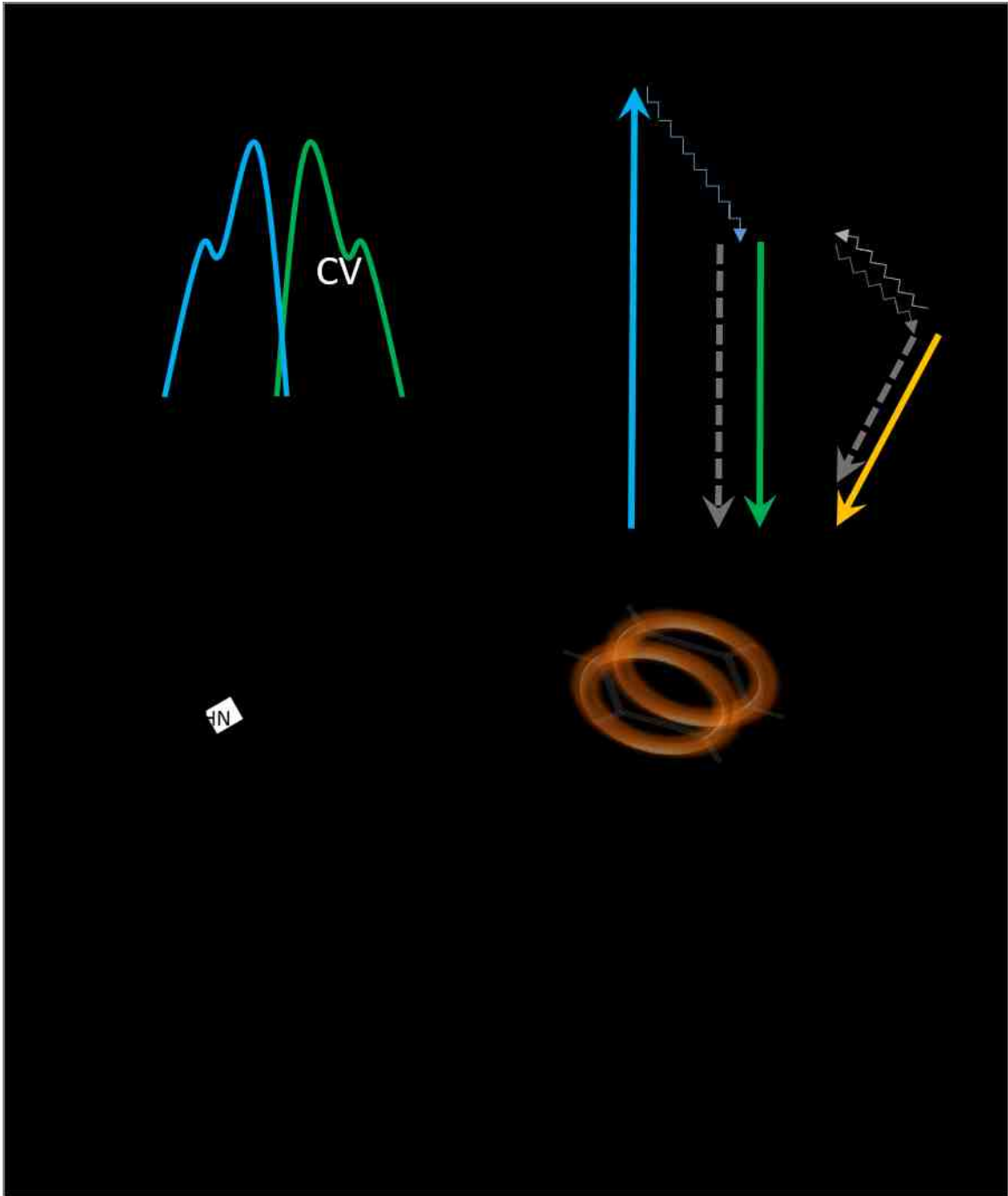
Each energy state is subdivided into additional vibrational energy states, indicated with thin horizontal lines. Excitation of an electron occurs within femtoseconds and is represented by a blue upward arrow. Vibrational relaxation within the higher energy states occurs within picoseconds and is represented by stepped lines. The energy lost

through this relaxation is what causes fluorescence emission of a longer wavelength

(Lavis & Raines, 2007). The relaxation of an electron from the lowest level of S_1 to the

ground state, when released as a photon, occurs within nanoseconds and is termed

fluorescence, represented by a green downward arrow. The molecule can also be

quenched, where electrons return to the ground state without emitting a photon,

shown as a dashed downward arrow in the Jablonski diagram (Berezin & Achilefu, 2010).

Additionally, energy can be non-radiatively transferred to another molecule through a

process termed Förster Resonance Energy Transfer (FRET).

Excited electrons can also cross to the excited triplet state, sometimes referred to as the

dark state, shown as T_1 in Figure 1.1 C. Molecules can remain in the dark state for a long

period of time, up to milliseconds, but eventually either return to an excited singlet

state or the ground state. If it relaxes down to the ground state, this process occurs at a

much longer time scale than fluorescence, up to hundreds of seconds, and is termed

phosphorescence. The presence of molecular oxygen can push electrons out of the dark

state to the singlet state, allowing them to become excitable again, but oxygen can also

cause irreversible photobleaching (Vogelsang et al., 2008). Molecules can cycle through

the excitation and relaxation process up to millions of times but the formation of singlet

oxygen from triplet state quenching can oxidize the structure leaving them permanently

dark (Aitken, Marshall, & Puglisi, 2008).

Each fluorophore has a specific absorption and emission spectrum that may change

depending on the environment, but remains a characteristic of the fluorophore as the

spectra are based on the chemical structure and the extent of electron delocalization

3

across the molecule. (Voicescu, Ionescu, & Gatea, 2014) (Liu, Zhang, & Jin, 2013) The excitation and emission spectra and chemical structures of Alexa Fluor® 488 and Alexa Fluor® 647 (Thermo Fisher Scientific) are shown as examples (Figure 1.2 A). The excitation spectrum is a representation of how well the molecule absorbs photons of different energy levels or wavelengths. The maximum absorbance peak (λ_{max}) is the wavelength at which the fluorophore best absorbs photons. The emission spectrum of a fluorophore is a plot of the various wavelengths at which the molecule will emit light during relaxation, where the maximum peak (λ_{em}) represents the wavelength most likely to be emitted. The emission spectrum is independent of the wavelength used for excitation and simply shifts proportionally in intensity as the excitation wavelength deviates from maximum (Figure 1.2 B).
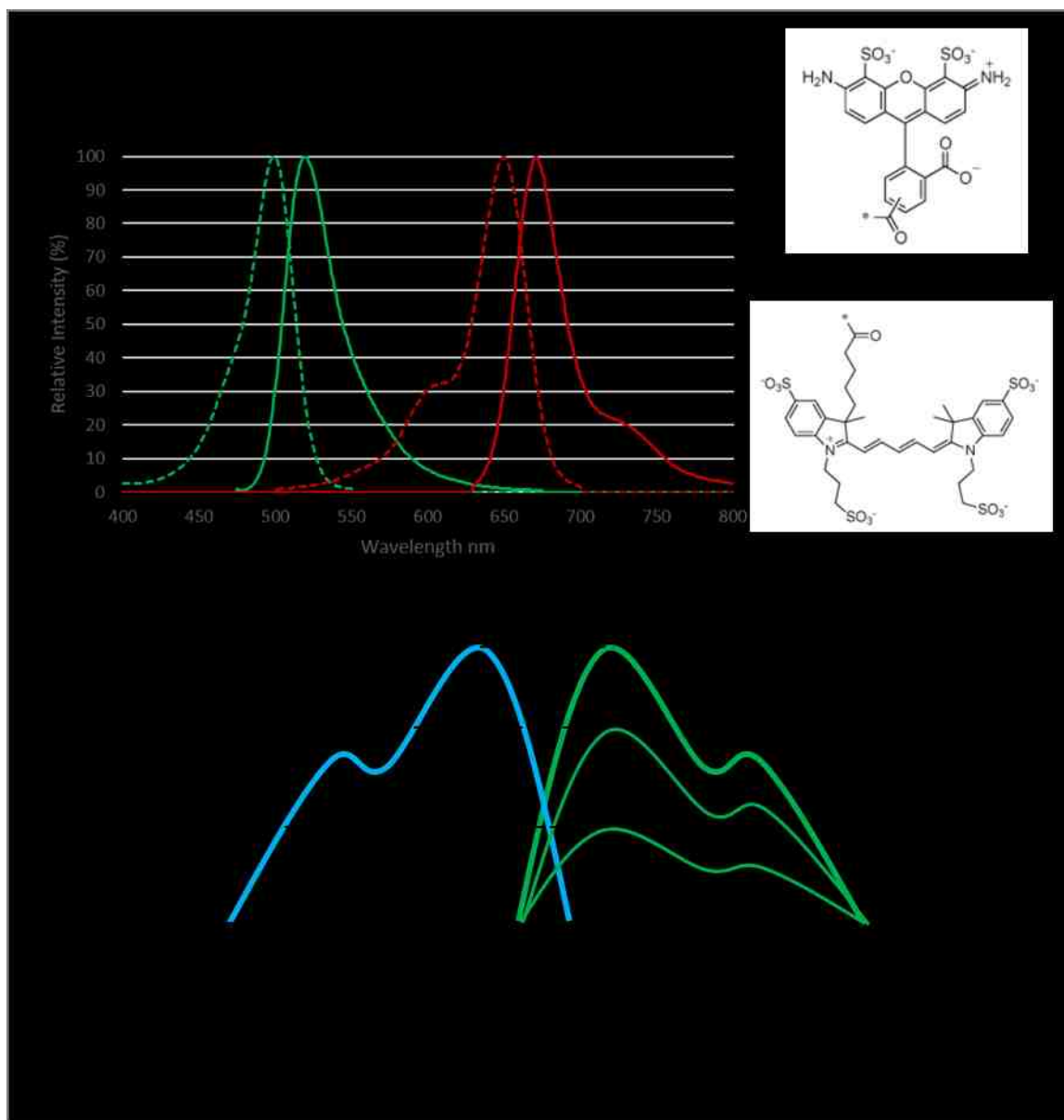
In addition to spectral characterization of a fluorophore, there are several other

descriptive photophysical properties frequently used. The efficiency of a molecule to

absorb a photon, the extinction coefficient (ε), can be determined using the Bouguer-

Lambert-Beer law, which defines the absorbance (A) of light by a sample with the

following equation: $A = \varepsilon \cdot c \cdot d$, where ε = molar absorption coefficient, c =

concentration, and d = path length (Mäntele & Deniz, 2016). The higher the extinction

coefficient, the better the molecule can absorb energy to produce fluorescence. The efficiency of a molecule to emit a photon after excitation, as opposed to non-radiative relaxation, is termed the quantum yield or quantum efficiency (ϕ). This is a ratio of the number of photons in to the number of photons out, with a maximum efficiency of 1.0. Molecules with a quantum yield as low as 0.05 can still be visualized but higher quantum yields are preferred. The brightness of a fluorophore can be defined by the product of the extinction coefficient and the quantum yield ($\varepsilon \times \phi$) (Lavis & Raines, 2007). The lifetime (τ) of the fluorophore is the average length of time a molecule spends in an excited state before returning to the ground state. As an excited molecule can relax through both radiative and non-radiative decay, the lifetime can be described as the inverse of the sum of both rate constants, k_r the radiative rate constant and k_{nr} the non-radiative rate constant, with the following equation: $\tau = \frac{1}{k_r + k_{nr}}$ (Berezin & Achilefu, 2010). Lifetime is independent of concentration, photobleaching, or other intensity based fluorescence parameters but is very sensitive to environment and is therefore a useful measurement for scientists. Using Alexa Fluor® 488 (Thermo Fisher Scientific) again as an example, the extinction coefficient is 73,000 M^{-1} cm^{-1}, the quantum yield is 0.92, and the lifetime is 4.1 ns (www.thermofisher.com).

1.2 Fluorophores

While the understanding of fluorescence has grown, its application in biology was limited until Albert Coons was able to chemically conjugate a fluorophore to an antibody in 1942 and directly target pneumococci in fixed tissue (Coons, 1961). This was the

beginning of immunofluorescence and incredible scientific progress in the field of cell biology. Direct and indirect labeling methods were developed to identify proteins of interest in cells or tissue using the specificity of the antigen-antibody reaction (Mellors, 1968). Direct labeling uses a small organic fluorophore directly conjugated to an antibody against an antigen, while the indirect method utilizes a dark primary antibody to the antigen and a fluorophore-conjugated secondary antibody against the primary antibody (Figure 1.3). While the direct method is simpler, the indirect method allows for more flexibility and brighter fluorescence as multiple secondary antibodies can bind the primary. Hundreds of organic fluorophores have been developed and applied to immunofluorescence and used within an expansive body of biological research.
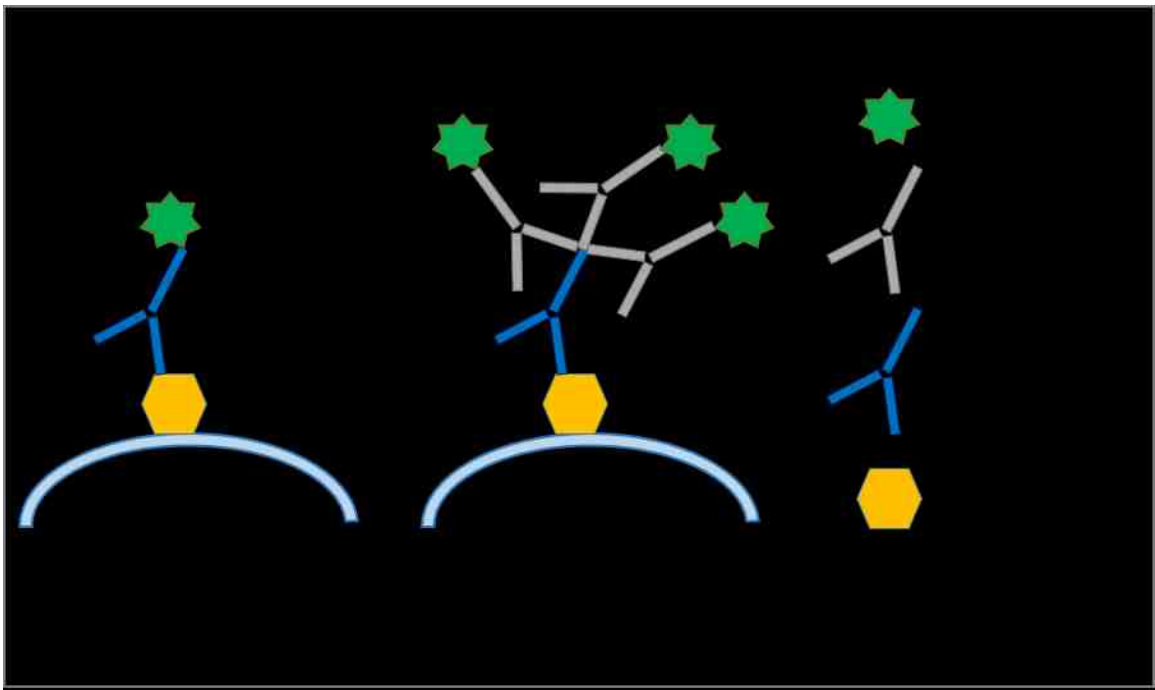
Improvements are continuously being made to enhance features such as the brightness and photostability of fluorophores. Quantum dots (QD) were developed in 1998 as a

biologically applicable fluorophore with several unique properties, including negligible

photobleaching (Wegner & Hildebrandt, 2015). QDs are nanoparticles that range from

2.7 nm to 4.8 nm, while the fluorescence emission increases with size, consisting of a

CdSe fluorescent core with a protective shell of either ZnS or CdS, surrounded by

functional groups that interact with other molecules, including antibodies, to target

cellular components of interest (Figure 1.4).
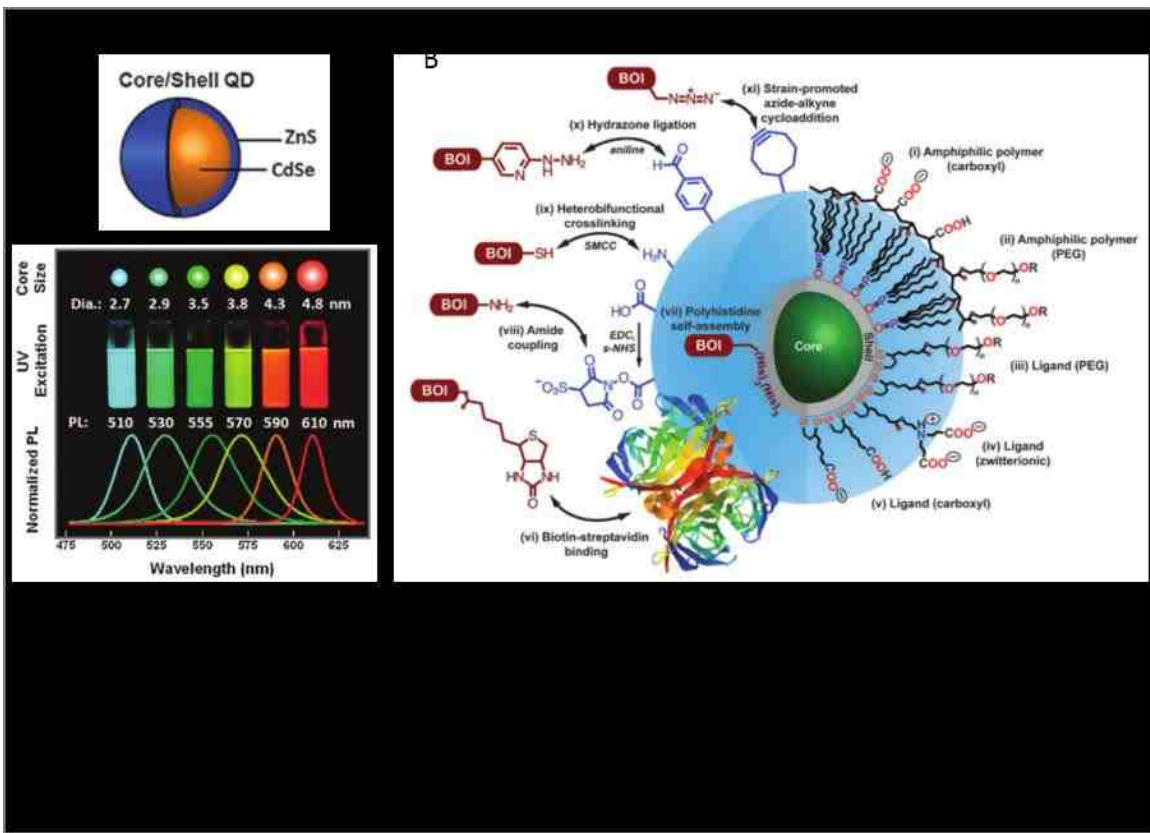
Although a powerful technique, immunofluorescence is limited to evaluation of fixed

samples as labeling intracellular structures with an antibody requires permeablization of

the cell membrane. In the early 1990's, decades of work by many people including

Roger Tsien and Martin Chalfie culminated in the cloning of the Green Fluorescent

Protein (GFP) as an expressible fluorescent marker after GFP was identified in the 1960's

by Osamu Shimomura from jellyfish, *Aequorea victoria* (Zimmer, 2009). GFP is a 27 kDa

protein that is approximately 24 Å wide and 42 Å long with a barrel of beta sheets

surrounding a fluorophore, which helps to reduce photobleaching (Figure 1.4 A) (Walker

et al., 2015) (Yang, Moss, Phillips, Phillips Jr., & Phillips, 1996). In the early 1990's,

Chalfie expressed and visualized GFP in *Escherichia coli* and then neurons of

Caenorhabditis elegans, introducing GFP as an expressible fluorescent protein (FP) for

live cells, while Tsien was responsible for developing the first GFP variant, a blue FP

(Sanders & Jackson, 2009). Continued modifications to the GFP molecule has led to

brighter fluorescence, enhanced GFP (EGFP), and many other color variants, such as

Cyan FP (CFP) and Yellow FP (YFP) (Zimmer, 2009) (Figure 1.5). In 1999, Lukyanov

discovered naturally red-shifted fluorescent proteins in reef coral, *Discosoma*, which

allowed for expansion of FPs throughout the visible spectrum (Campbell et al., 2002;

Matz et al., 1999).
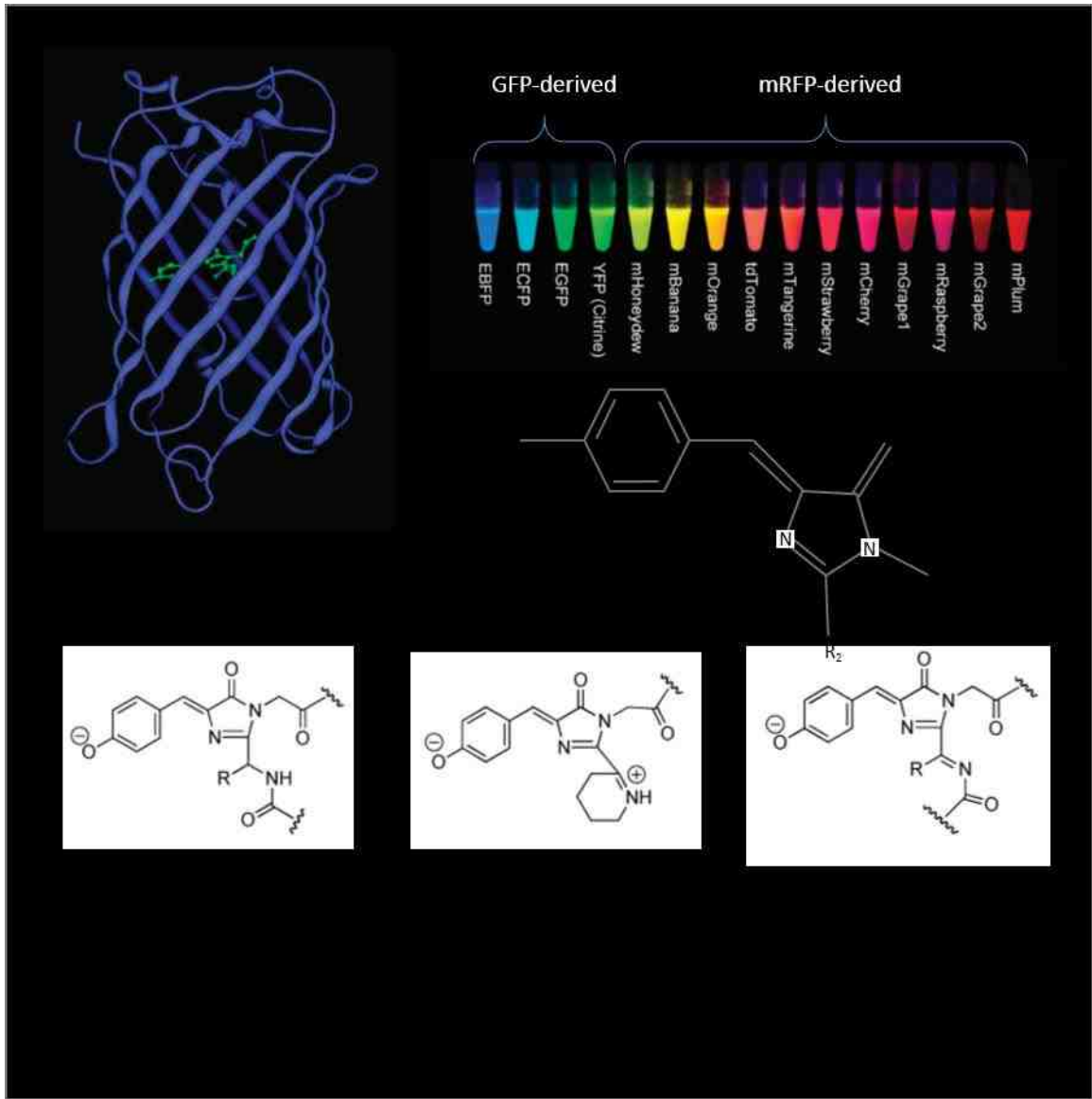
The fusion of FPs to proteins of interest has been a powerful tool for cell biologist to visualize proteins of interest in living cells, but even the enhanced FPs still suffered from photobleaching and low quantum yields making quantification difficult. After continued work to improve fluorescent proteins, mCerulean3 was developed in 2011, an ECFP variant with 10 mutations and an increase in quantum yield from 0.37 to 0.87 (Mérola et al., 2014). mCerulean is a monomeric form that prevents dimerization due to a common

FP point mutation, A206K, that changes a hydrophobic residue to a positively charged residue (Zacharias, Violin, Newton, & Tsien, 2002). Dimerization has been shown to increase FRET efficiencies but can be an undesirable occurrence when studying protein function.

1.3 Microscopy Basics

As the advancement of fluorophores has grown, so has the technology to image them. The fluorescence microscope was first developed by two German physicists, Otto Heimstaedt and Heinrich Lehmann, between 1911 and 1913 to visualize autofluorescence in biological materials. A filter cube is necessary to separate the bright light used for excitation from the relatively dim fluorescence emission. The filter cube typically contains a bandpass excitation filter, a dichroic mirror, and an emission filter, either bandpass or long pass (Figure 1.6 A). Filter cubes are often designed to excite and detect a specific fluorophore or groups of spectrally similar fluorophores. Using the Alexa Fluor® 488 filter set from Chroma as an example, the excitation filter is a 10 nm bandpass filter centered at 488 nm, the dichroic reflects light below and transmits light longer than 498 nm, and the emission filter is a 50 nm bandpass centered at 525 nm (Figure 1.6 B). Bandpass emission filters are important when looking at multiple fluorophores to reduce crosstalk between fluorophores. Longpass emission filters are beneficial because they transmit more light. A fluorescence microscope will often have multiple filter cubes to look at a variety of fluorophores.
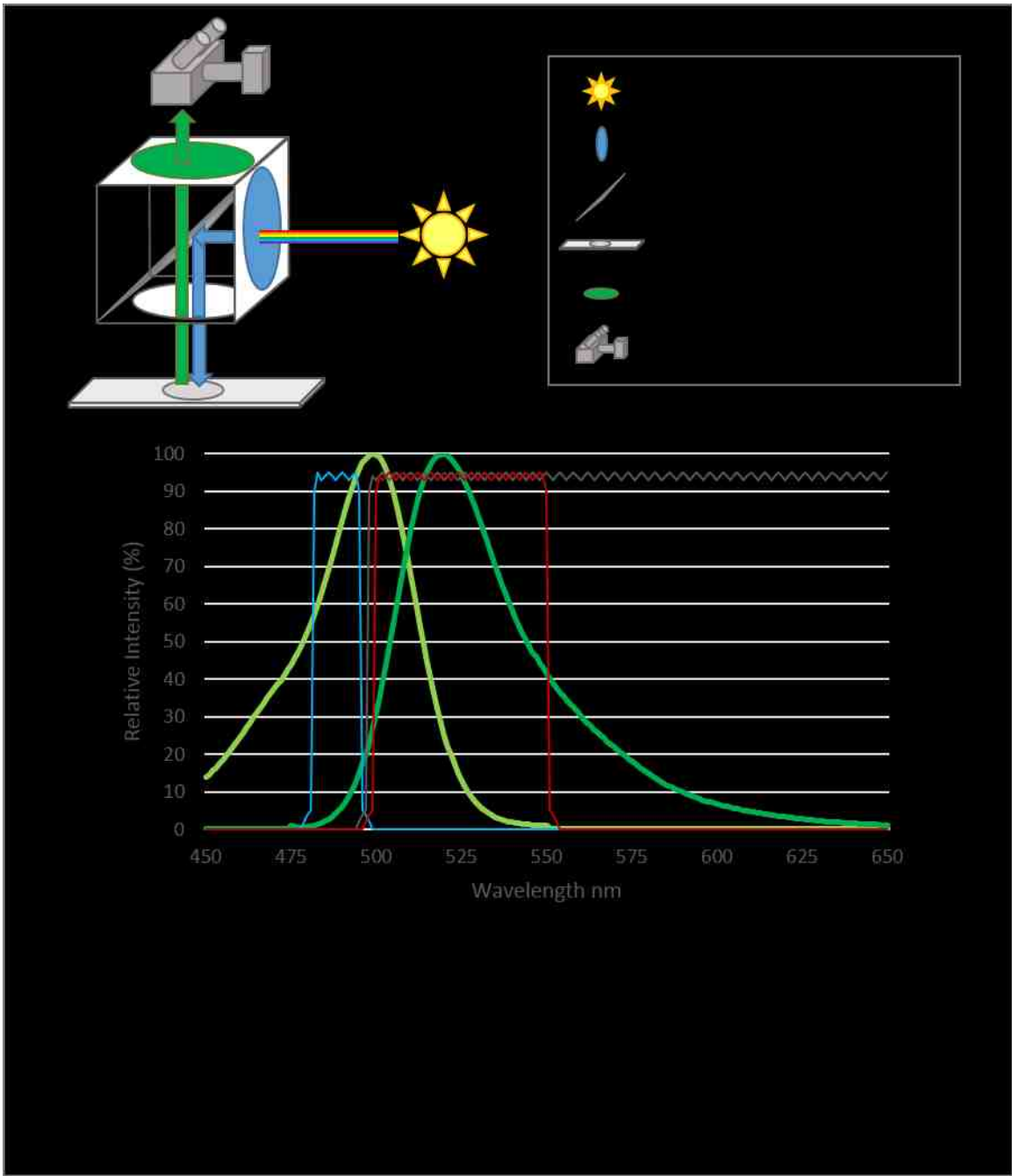
There are a several light sources as options for fluorescence excitation. Mercury lamps have been the standard for many years on fluorescence microscopes, as they are very bright and have a broad spectrum across the visible range with large peaks near excitation maximums for common fluorophores. While mercury lamps are a powerful

and flexible excitation source, they must be replaced frequently and disposed of as hazardous waste. Additionally, they can explode if not cool during ignition. Xenon lamps are similar to mercury lamps except they have a longer life and although less powerful, they provide a relatively even spectral profile across the visible range – a preferred feature for quantitative microscopy. Alternative options have been developed recently, including metal halide and L.E.D., and are quickly replacing mercury and xenon lamps. These new light sources last much longer and do not risk explosion while still providing high intensity across the visible spectrum.

Fluorescence is often detected with a camera and there are a number of different options available depending on the application and budget. Images were traditionally acquired with film cameras but were quickly replaced with charge coupled device (CCD) cameras when the technology became available, with the significant advantage of the digital format allowing for instant image display. Electron multiplying-CCD (EM-CCD) cameras were developed in the early 2000s to be more sensitive than standard CCD through the addition of an electron multiplying register positioned before the standard amplification, enhancing the signal without introducing read noise. Recently, scientific complementary metal-oxide-semiconductor (sCMOS) cameras have gained popularity as they have a larger field of view and higher resolution than EM-CCD cameras, as well as better signal to noise when more than 5 photons are detected. The high sensitivity of both EM-CCD and sCMOS have allowed for increased acquisition speed, advancing live cell imaging.

1.4 Microscopy Techniques

Microscopy has been such a powerful technique because of the ability to image live cells

with fairly high resolution, approximately 200 nm laterally and 600 nm axially

(Fernández-Suárez & Ting, 2008). Ernst Abbe first described the limit to the resolution of

light in 1873 with the equations $\Delta x, \Delta y = \frac{\lambda}{2n \sin \alpha}$ and $\Delta z = \frac{2\lambda}{n \, sin^2 \, \alpha}$ (Figure 1.7 A),

where λ is the emission wavelength of the fluorophore and $n \sin \alpha$ is the numerical

aperture (NA) of the objective, with n as the refractive index of the imaging medium and

α as half the angle of light that the objective can collect (Hell, Dyba, & Jakobs, 2004)

(Figure 1.7 B). A point of light in a sample will be refracted as it passes through the

optics of the microscope. The refraction pattern is called an airy disc and the size of the

disc depends on the NA of the objective – the larger the NA, the smaller the airy disc

pattern and the better the resolution (Figure 1.7 C). The wavelength of the fluorophore

also effects the size of the airy disc, with a longer wavelength resulting in a larger airy

disc (Figure 1.7 D).
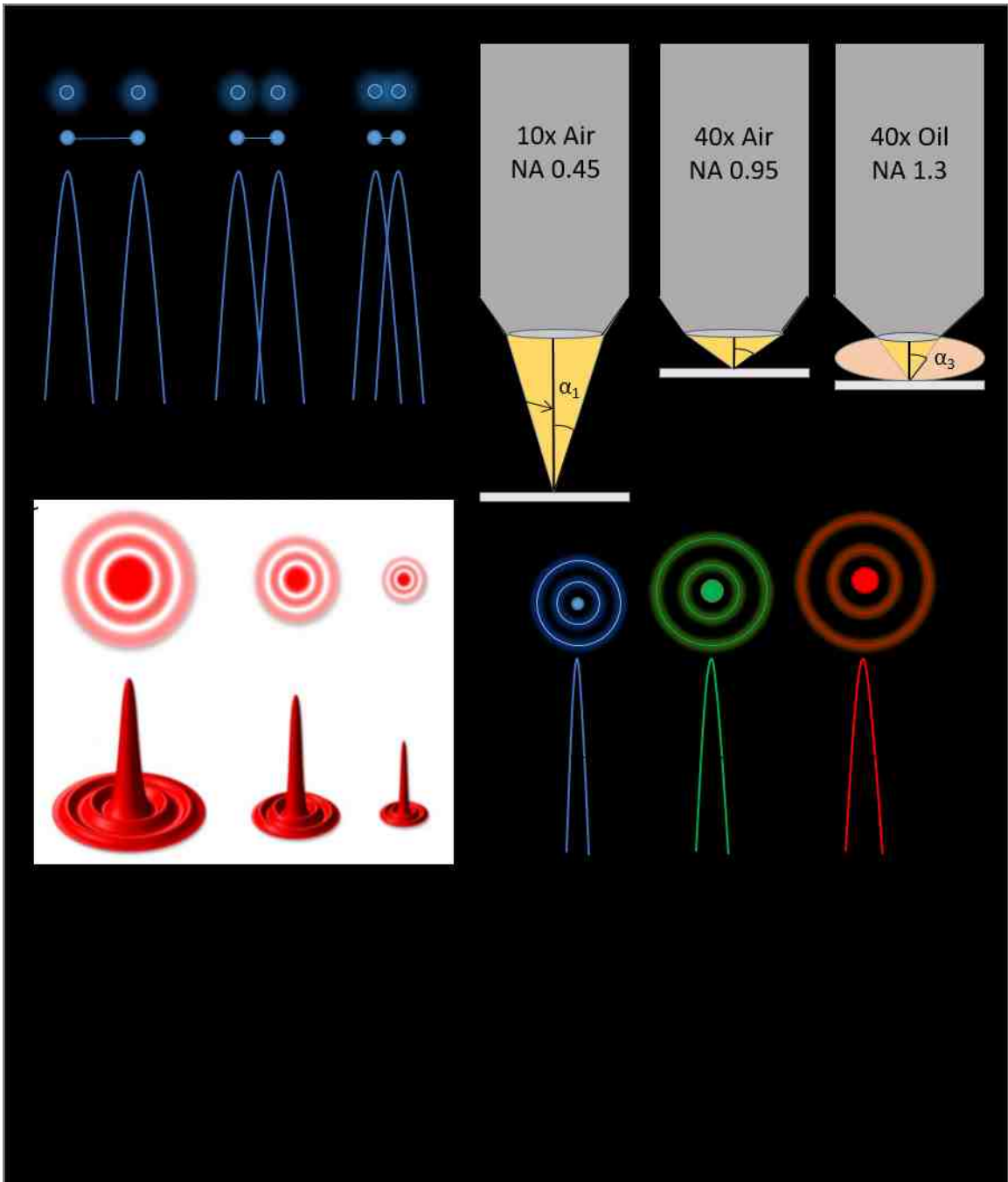
Confocal microscopy was introduced in the 1980's to improve axial resolution and image clarity by removing out of focus light using a pinhole in the emission path. Although the entire z-plane is illuminated as in widefield, only fluorescence originating from the focal plane is detected, while out of focus light falls outside of the pinhole and is rejected

(Figure 1.8). Typically, the diameter of the pinhole can be adjusted to optimize the
optical section thickness and collect one airy unit, based on the objective and the
wavelength of light. Collecting more than one airy unit decreases the axial resolution
and collecting less than one airy unit will quickly reduce the amount of light that can be
detected.
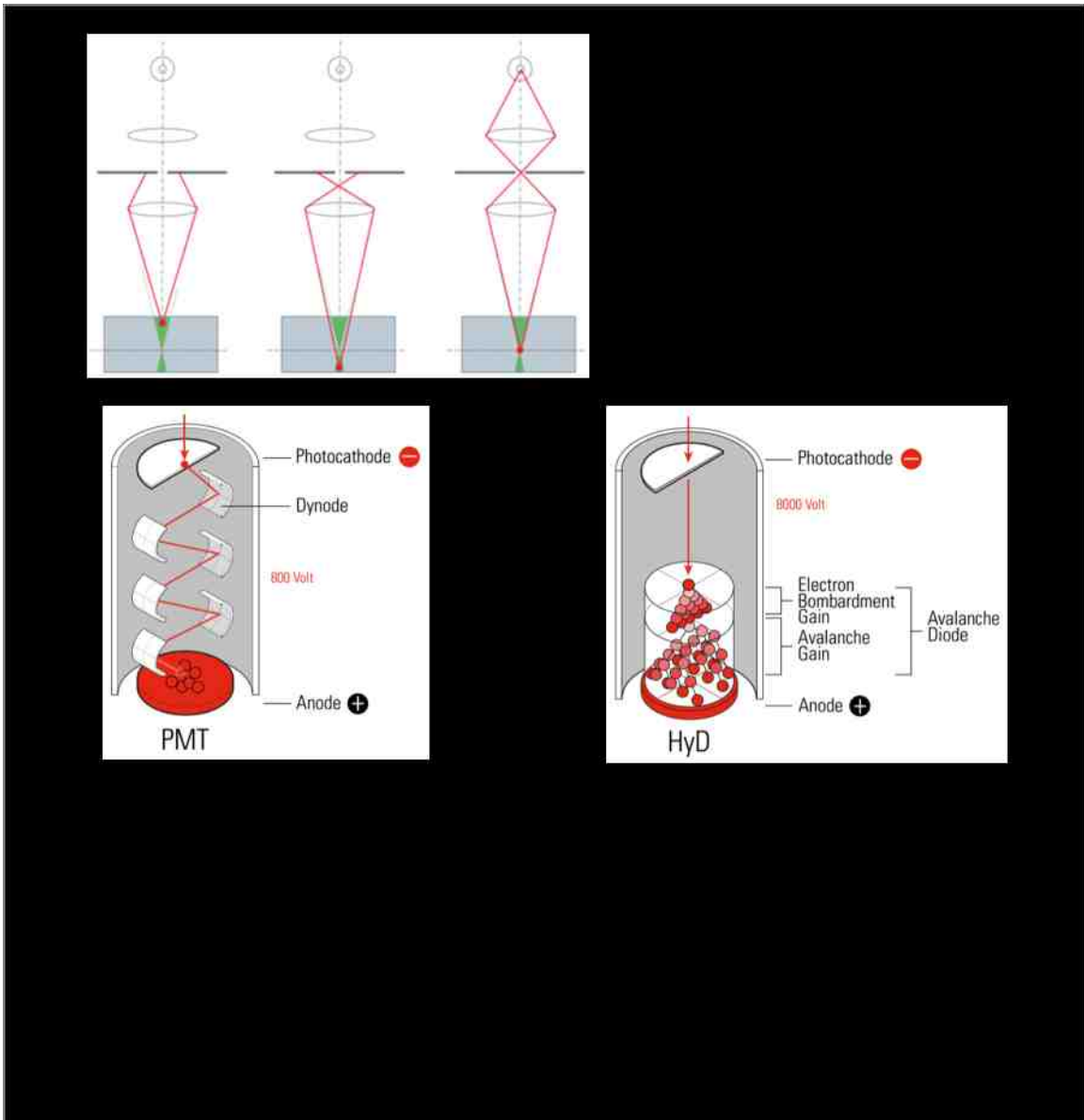
Gas lasers, such as Argon and Helium-Neon, have been commonly used light sources for confocal microscopy because of their narrow spectral lines at wavelengths useful for exciting many fluorophores, but due to their inefficiency and large size have recently been replaced with diode lasers. Most confocal microscopes acquire an image by scanning the laser across a field of view and collecting the emitted photons with a photomultiplier tube (PMT) or more recently, GaAsP or Hybrid (HyD) detectors. A PMT is a vacuum tube that detects photons that pass through a window and hit a photocathode within the tube. The photon is converted to an electron which is then amplified through a series of dynodes before reaching the anode and recorded as current (Figure 1.8 B). A GaAsP detector is a PMT with a gallium-arsenide-phosphide coating on the photocathode, increasing the quantum efficiency of the detector from approximately 25% to 40%. HyD detectors are a hybrid of an avalanche photodiode detector and a GaAsP PMT, which offers the high dynamic range of a PMT with the low noise and sharp pulse of an avalanche photodiode detector, allowing for photon counting (Figure 1.8 C).

Although many advancements in biology have been made and questions addressed within the resolution of light, there are a number of cellular events and structures that require higher resolution. A number of super resolution techniques have been recently developed to overcome this limit, such as Stochastic Optical Reconstruction Microscopy (STORM) or Photoactivated Localization Microscopy (PALM) which localize photons through photobleaching or photoswitching, Stimulated Emission Depletion (STED) which increases precision by reducing the area of a point of light, and Structured Illumination

Microscopy (SIM) which uses shifting interference patterns to collect high-frequency information. These techniques significantly increase resolution compared to standard fluorescence microscopy, bringing the resolution limit down to approximately 50 nm, 70 nm, and 100 nm respectively (Schermelleh, Heintzmann, & Leonhardt, 2010).

<u>1.5 Introduction to FRET</u>

Although these super-resolution techniques have pushed imaging beyond the resolution of light there are still dynamic molecular interactions that occur at distances that remain unresolved, such as protein-protein interactions or conformational changes of proteins. In 1946, Theodor Förster proposed the theory that energy can transfer non-radiatively from one fluorescent molecule, a donor, to another molecule, an acceptor, within a distance of 10 nm, and the efficiency of transfer is distance dependent to the inverse sixth power (Bajar, Wang, Zhang, Lin, & Chu, 2016). This theory has been termed Förster Resonance Energy Transfer (FRET) and can be described using a Jablonski diagram (Figure 1.9). It is a powerful technique that can be used to visualize interactions that occur within 10 nm, below the resolution of super-resolution techniques. FRET has an advantage over biochemical techniques to optically localize and quantify transient interactions within intact cells. The development of GFP and the many derivatives have proven to be effective FRET pairs and allowed for these interactions to be studied in live cells (Bajar et al., 2016).
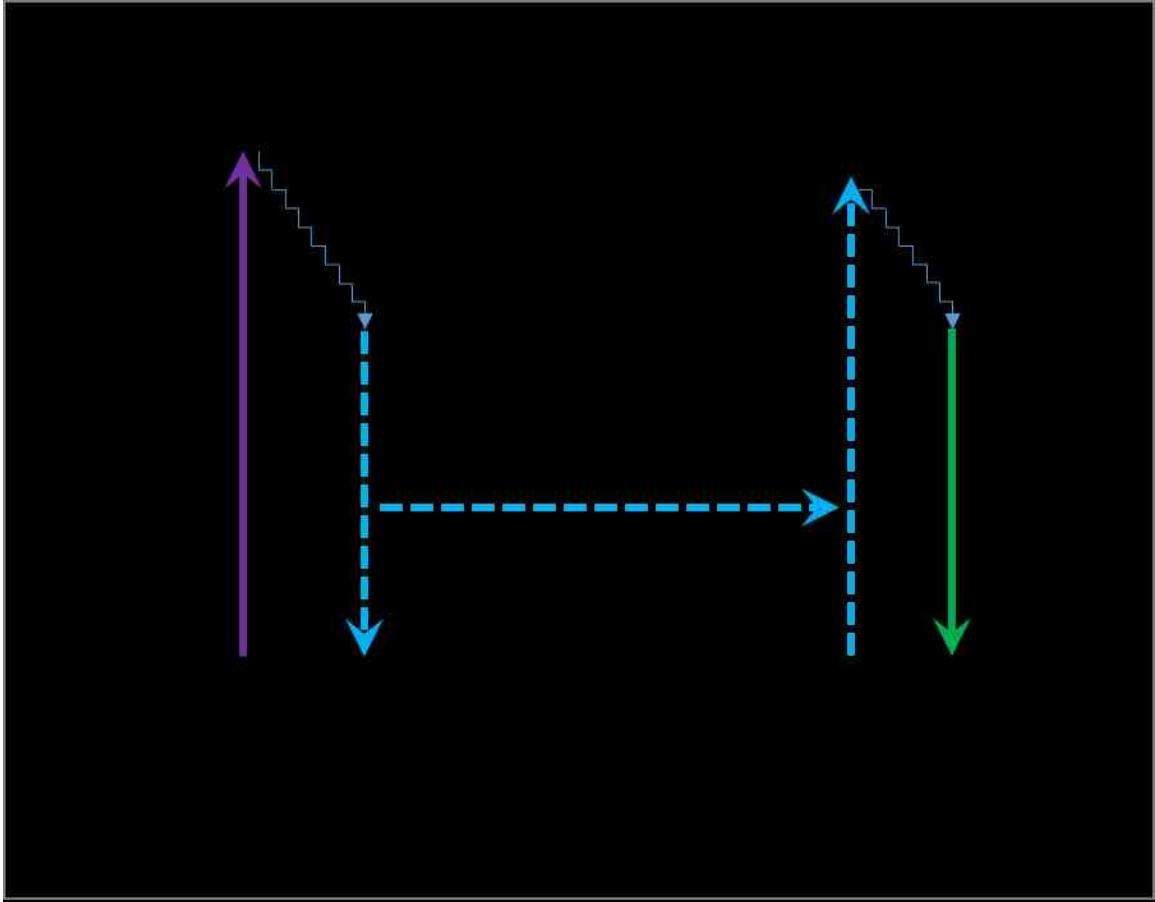
The first experiments using FRET were performed in cuvettes, before fluorescence
microscopy was routine. In 1978, Lubert Stryer demonstrated that FRET could be used
as a "spectroscopic ruler" to measure distances within proteins using intrinsic
fluorescence or through chemical insertion of fluorophores, determining the distance
between several positions of tRNA, for example, that agree with distances measured
using crystallography (Stryer, 1978). With the development of fluorescence microscopy,
FRET became a tool to visualize protein-protein interactions, as demonstrated by Anne
Kenworthy using Cy3 and Cy5 as FRET pairs (Kenworthy, 2001). Fluorescent proteins
have allowed for the development of FRET biosensors, in which biological changes such
as the conformational change of a protein or the cleavage of a molecule leads to a

change in FRET signal (Li, Pham, & Truong, 2006). Seong et al. used a FRET biosensor to elucidate the activation of focal adhesion kinase within membrane microdomains (Seong et al., 2011).

The occurrence of FRET can be described through several equations, most basically as a ratio of the FRET signal before and after a biological change. FRET efficiency is a more rigorous measurement of FRET and can be used to quantify the extent of FRET occurring. The equation for FRET efficiency (E) can be written as $E = 1 - \frac{I_{DA}}{I_D}$, where I_{DA} is the donor fluorescence intensity when the acceptor is present and I_D is the donor intensity when the donor is alone. Intensity can be substituted with donor lifetime values to calculate FRET efficiency (Kremers, Goedhart, Van Munster, & Gadella, 2006).

The Förster radius (R_0) is described as the distance between the donor and acceptor at which the FRET efficiency is 0.50 and written with the following equation: $R_0 = (JK^2 Q_0 n^{-4})^{\frac{1}{6}} \times 9.7 \times 10^3 \text{Å}$, where J is the integral of the spectral overlap of donor emission and acceptor absorption, K^2 is the orientation factor for a dipole-dipole interaction, Q_0 is the quantum yield of the donor, and n is the refractive index of the medium (Stryer, 1978). This value is useful to determine if a fluorophore pair is likely to FRET within the distance of the interactions in question.

1.6 Requirements for FRET

There are three physical requirements for FRET to occur: spectral overlap, distance, and orientation. The probability of FRET increases as these parameters are optimized and are discussed in the paragraphs below (Hochreiter, Garcia, & Schmid, 2015). The

emission spectrum of the donor must overlap with the acceptor absorption spectrum, ideally greater than 30% (Figure 1.10 A). FRET is very sensitive to distance, where the efficiency decreases with distance between fluorophores with a maximum distance around 10 nm (Figure 1.10 B). Third, the relative orientation of the donor and acceptor molecules is important for proper dipole-dipole coupling to occur (Figure 1.10 C).
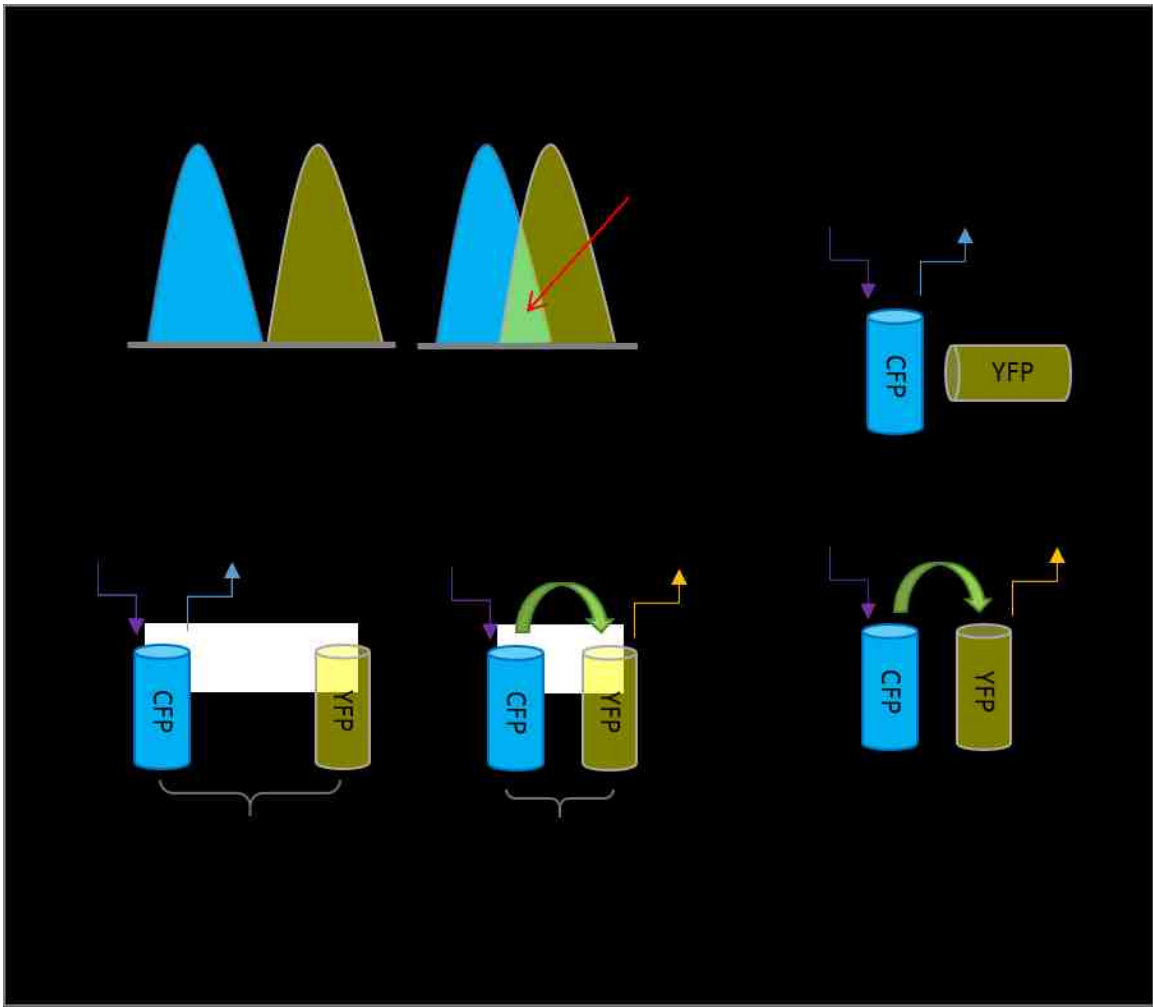
The degree of overlap between the donor emission and acceptor absorption spectra is an important consideration when selecting fluorophores to be used as FRET pairs – the higher the overlap, the better the FRET pair. The integral of spectral overlap (J or J_{DA})

can be determined with the following equation, $J = \int_0^\infty F_D(\lambda)\varepsilon_A(\lambda)\lambda^4 d\lambda$, where $F_D(\lambda)$

is the normalized, wavelength dependent fluorescence intensity of the donor, and $\varepsilon_A(\lambda)$

is the wavelength dependent extinction coefficient of the acceptor (Bajar et al., 2016).

The J_{DA} of CFP and YFP is 2.0320e-13, for example.

The sensitivity of FRET efficiency to distance can be expressed with the equation: $E = $

$\frac{1}{1+\left(r/R_0\right)^6}$ with efficiency decreasing to the 6th power with distance. It can be useful to

plot E vs r for a given donor and acceptor to determine the range at which FRET is likely

to occur. Calculating R_0 and plotting E vs r for the common FRET pair, CFP and YFP,

shows that FRET can be detected at distances up to 7.3 nm, as reported by Müller et al.

(Müller, Galliardt, Schneider, Barisas, & Seidel, 2013).

The third requirement for FRET is the orientation of the fluorophores, with efficiency

decreasing as the angle between the dipole-dipole transition moments increases. The

orientation factor can be calculated with the following formula: $K^2 = [d \times a - $

$3(d \times r_{da})(a \times r_{da})]^2$, where d and a are the dipole moments of the donor and acceptor,

respectively, and r_{da} is the vector between the two. Often K^2 is simply estimated to be

2/3, assuming free rotation of the dye molecules and complete sampling of all possible

orientations (Khrenova, Topol, Collins, & Nemukhin, 2015).

1.7 Standard Techniques for Measuring FRET

Although incredibly informative, quantifying FRET can be quite complicated, which has

limited the application of this technique. There are several methods for acquiring and

analyzing FRET, including intensity-based methods, such as acceptor photobleaching and sensitized emission, and measuring fluorophore lifetime with FRET-FLIM (Hochreiter et al., 2015). There are advantages and limitations to each method, which will be discussed with a description of each technique.

Acceptor photobleaching reports FRET by measuring an increase in donor intensity after bleaching the acceptor, although this technique should only be used with fixed samples as there could be diffusion after bleaching live cells. Using cells expressing both the donor and the acceptor, the donor is excited and emission is measured. Next, the acceptor is photobleached and the donor emission is again measured with direct excitation. If FRET was occurring and the acceptor was sufficiently bleached, the donor signal will increase when the acceptor no longer available. A ratio of this change can be used to determine relative changes in FRET and imaging the same cell before and after bleaching controls for variability in protein expression.

FRET efficiency could be calculated with the following equation: $E = 1 - \frac{I_{DA}}{I_D}$, where I_{DA} is the donor fluorescence intensity before bleaching the acceptor and I_D is the donor intensity after bleaching, although a correction for cross-talk of YFP into the CFP channel must be applied. Including the corrections, the equations is the following: $1 - \frac{I_{DA} - \alpha A}{I_D - \alpha A}$, where αA is the normalized cross-excitation cross-talk, determined using cells only expressing the acceptor. Acceptor only control samples are also important to determine proper bleaching of the acceptor, as donor bleed-through can make this difficult to determine in cells expressing both fluorescent proteins. Donor only control samples are

necessary to determine the settings required to prevent unintentional bleaching of the donor.

Sensitized emission is the measurement of the acceptor emission from donor excitation. Unfortunately, the spectral overlap that is required for FRET to occur also makes identifying this signal difficult using typical fluorophores, such as CFP and YFP; excitation of CFP and detection of YFP in the FRET channel will include CFP emission. There are several controls required to determine the FRET signal: CFP only expressing cells, YFP only expressing cells, and untransfected cells to identify the contribution of autofluorescence. Images of these control samples as well as the CFP and YFP expressing cells are acquired under three imaging conditions to calculate for cross-talk (Table 1.1 A): donor channel (A) with donor excitation, FRET channel (B) with donor excitation, and acceptor channel (C) with acceptor excitation. An additional complication when using fluorescent proteins is variability in protein expression, which must be normalized using correction factors (Table 1.1 B). Mean intensity data from these images are then used to determine the contribution of cross-talk and calculate sensitized emission with the following equation: $E = \frac{B - A \times \beta - C \times (\gamma - \alpha \times \beta)}{C \times (1 - \beta \times \delta)}$ (Qian, Yao, Wu, & Wu, 2014). Although sensitized emission directly calculates the FRET signal and can be used with live cells, the numerous control images and calculations required are prohibitive.

Specimen	(A) CFP Channel 470/40 nm	(B) FRET Channel 550/50 nm	(C) YFP Channel 550/50 nm
CFP Only (D)	CFP signal (A_D)	CFP cross-talk (B_D)	
A	A_A	B_A	C_A

β (B_D/A_D)	Corrects for donor cross-talk
A_A/C_A	
γ (B_A/C_A)	Corrects for acceptor cross-excitation
A_A/B_A	

The change in lifetime of a fluorophore can also be used to measure FRET as lifetime is very sensitive to environmental changes, such as pH or the availability of an acceptor for FRET. Lifetime can be measured several ways, including Fluorescence Lifetime Imaging Microscopy (FLIM). Time correlated single photon counting FLIM records the lifetime of a fluorophore using a picosecond pulsed laser and precisely clocked detectors that can measure the time between the laser pulse and the detection of a photon per pixel of an image (Figure 1.11 A). As the relaxation of a fluorophore is a stochastic process, the lifetime of a fluorophore must be measured many times, generating a histogram of the decay rate (Figure 1.11 B).
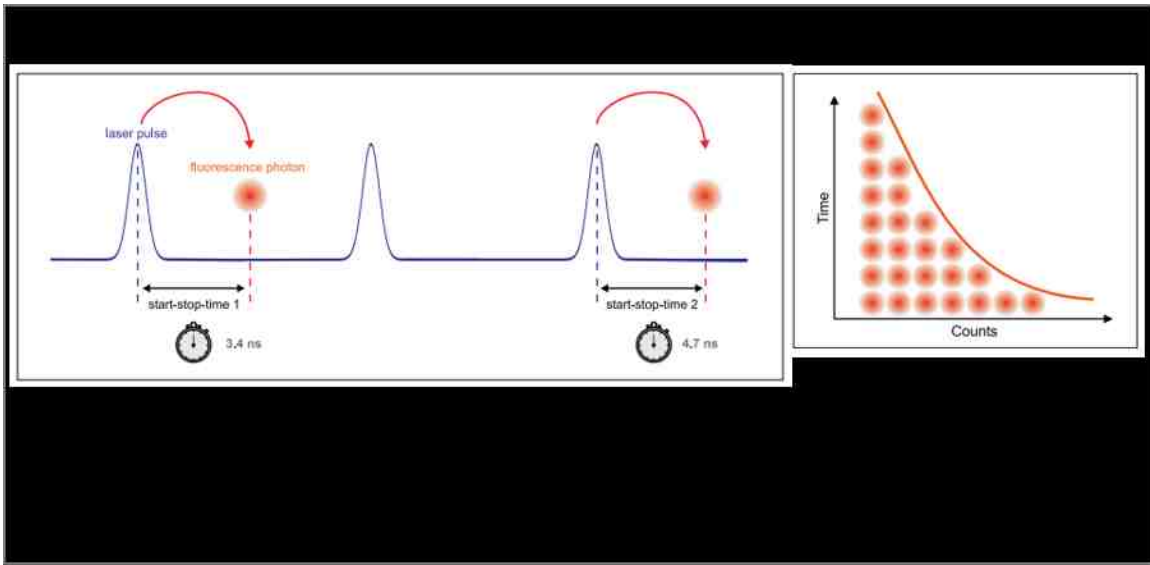
The lifetime of a fluorophore can be described as the inverse of the sum of both rate

constants, k_r the radiative rate constant and k_{nr} the non-radiative rate constant, with

the following equation: $\tau = \frac{1}{k_r + k_{nr}}$ (Berezin & Achilefu, 2010). The rate constant for

FRET can be described with the equation $k_T = r^{-6}K^2Jn^{-4}k_F \times 8.71 \times 10^{23} sec^{-1}$, where

r is the distance between the center of the chromophores, K^2 is the orientation factor,

J is the integral of the spectral overlap, n is the refractive index, and k_F is the donor rate

constant for fluorescence emission (Stryer, 1978). The rate of energy transfer can be

added as an additional rate constant when calculating the lifetime of a fluorophore

participating in FRET, $\tau = \frac{1}{k_r + k_{nr} + k_T}$, showing the lifetime of the fluorophore decreases

with FRET. FRET efficiency based on lifetime can be calculated as $E = 1 - \frac{\tau_{DA}}{\tau_D}$, where

τ_{DA} is the donor lifetime when the acceptor is present and τ_D is the donor lifetime when

the donor is alone. The lifetime of the donor alone can be obtaining by imaging cells

expressing only the donor and as lifetime is not influenced by concentration, the

variability of protein expression is not an issue. Although the acquisition of lifetime data

is simpler compared to intensity based measurements, it demands an understanding

beyond basic fluorescence and requires expensive, specialized hardware that is not

routinely available. Additionally, the time required to excite enough photons to

generate a decay curve eliminates the potential to measure events occurring within

several seconds.

1.8 Fluorogen Activating Protein

Unfortunately, the many complications involved with measuring FRET has limited the

application of the technique; intensity-based measurements require many control

samples and images to correct for cross-talk, while FLIM-FRET is an advanced technique

requiring specific hardware. Our group is developing a technique to overcome these

inherent complications and simplify FRET measurements using a unique expressible

protein, a Fluorogen Activating Protein (FAP), with a fluorogen as a FRET acceptor.

A FAP is a non-fluorescent, modified antibody that can be expressed by cells, developed

by our collaborators at Carnegie Mellon University. It is composed of only the single-

chain variable fragment (scFv) region of an antibody, either the light chain and heavy

chain together or two light chains, which were randomly mutated and screened for

binding specific fluorogens (Christopher Szent-Gyorgyi et al., 2008). The two

components are joined by a linker and are arranged in parallel (Figure 1.12). The FAP

can be genetically tagged to a protein of interest and expressed in tandem.
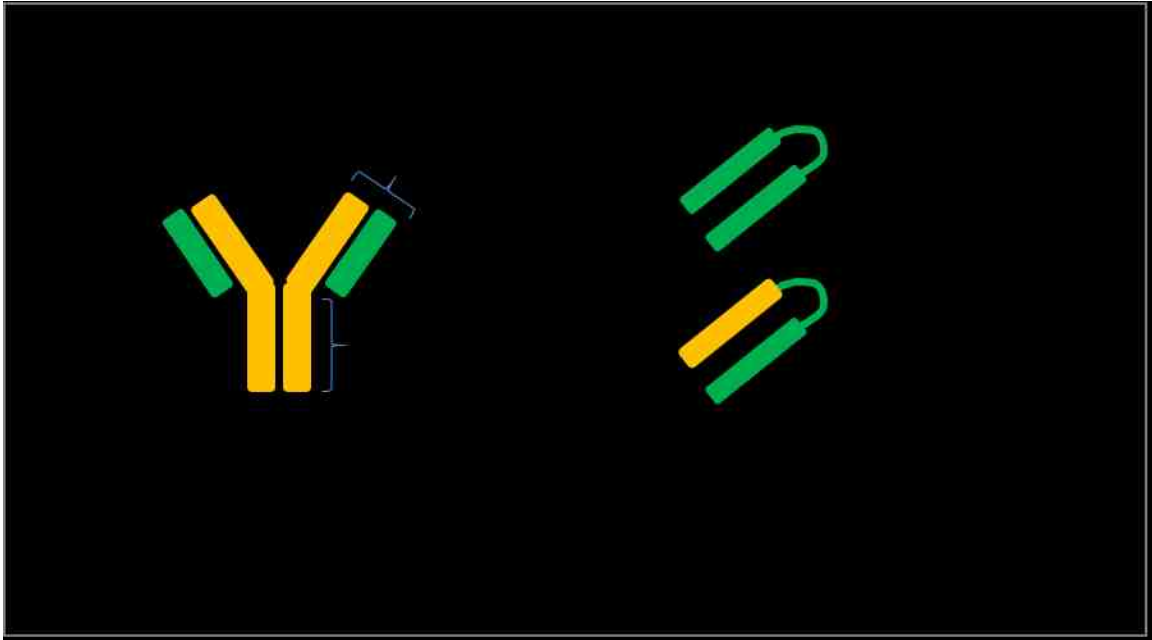
The fluorogen is a small organic molecule that is only fluorescent when bound to a FAP.

It can be added to cells at any time during an experiment, binding rapidly and with high

specificity; the fluorogen does not bind to cells that are not expressing the FAP.

Additionally, two different FAPs can be expressed within a population of cells and their

respective fluorogens can be added without crosstalk (Christopher Szent-Gyorgyi et al.,

2008). Depending on the demands of the experimental design, the fluorogen can be

modified in several ways, including the affinity to the FAP, the permeability through the

plasma membrane, the spectral properties, and the quantum yield. The permeability of

the fluorophore is an extremely useful modification that can be exploited to limit

labeling to the extracellular portion of the plasma membrane or to allow for binding to

FAPs tagged to intracellular proteins.

FAP-tagged proteins have been used successfully in conjunction with several imaging

techniques including confocal imaging, single particle tracking, and super-resolution.

Pratt et al. has shown that a single expressing FAP that binds both a green membrane permeable fluorogen and a red membrane impermeable fluorogen can be used to visualize endocytosis of membrane proteins using live cell confocal microscopy (Pratt, He, Wang, Barth, & Bruchez, 2015). FAP expressed on the extracellular region of FcεR1 has allowed for single particle tracking of the receptor without labeling with IgE (Schwartz et al., 2015). It has been demonstrated that super-resolution images of FAP-tagged actin could be acquired with STED in fixed cells and in live cells using the technique, FAP-Binding Activated Localization Microscopy (Fitzpatrick et al., 2009; Yan et al., 2014).

Malachite green (MG) is a fluorogen commonly used with the FAP and has a unique excitation spectrum; the excitation maximum is around 630 nm but has a secondary excitation peak near 450 nm (Figure 1.13 A). When MG is free in solution, the molecule can absorb energy but is not fluorescent; non-radiative relaxation releases energy as vibration due to rotational freedom of the dye (Figure 1.13 B). When bound to a FAP, the mobility is restricted and can release energy as far red photons. The fluorescence is approximately 10,000 times brighter when the fluorogen is bound to a FAP compared to when unbound, with a maximum emission peak around 650 nm.
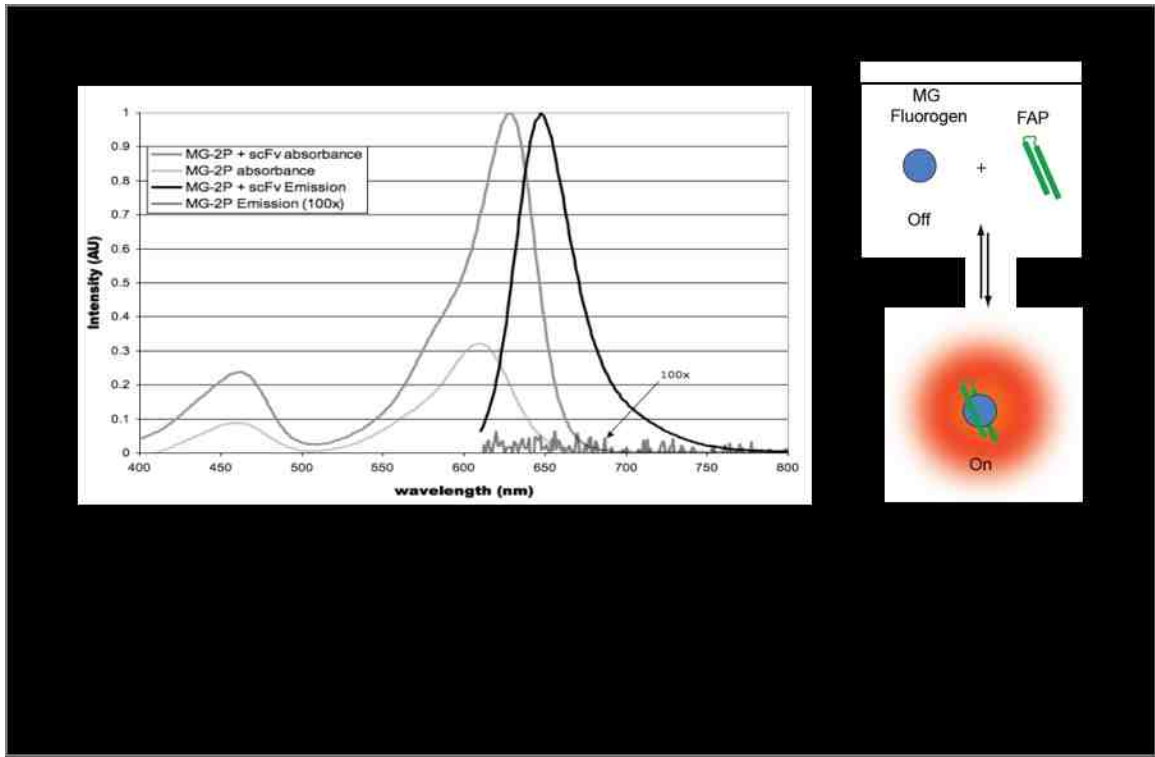
1.9 Using FAP/MG for FRET

There are two properties of the FAP/MG pair that make this system ideal for FRET: the unique excitation spectrum of MG and the ability to add the fluorogen at any time. Using a blue-shifted fluorescent protein as a donor, such as mCerulean, the emission spectrum overlaps with the secondary excitation peak of MG (Figure 1.14). As the emission of MG is far red, there is no crosstalk of donor signal into the FRET channel, allowing for direct detection of sensitized emission without the need for corrections. The flexibility to add MG as a FRET acceptor at any time allows for donor intensity to be measured before and after adding the fluorogen for the same cell, providing intracellular control for variability in protein expression.

Spectral Overlay of mCerulean with MG
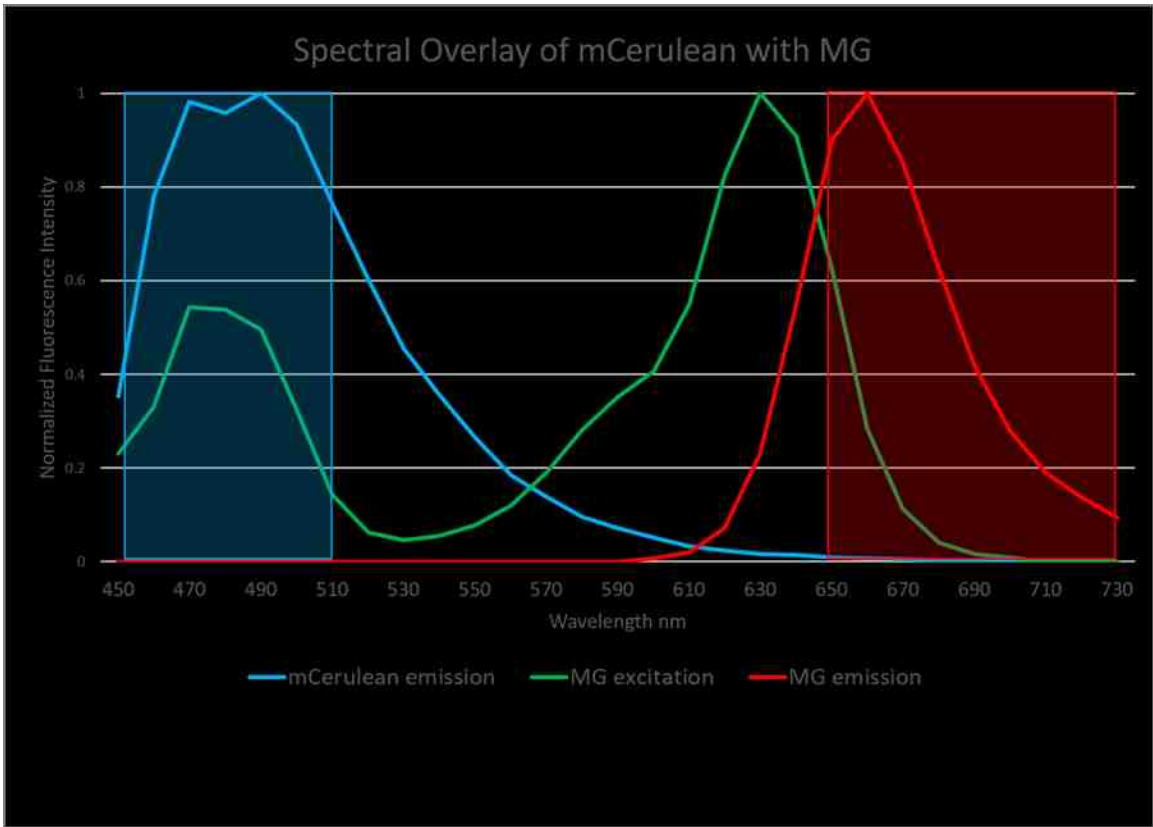
These two major benefits provide significant advantages over using traditional FRET pairs, such as CFP and YFP. When measuring FRET through intensity-based measurements, single expression control images for crosstalk correction are not necessary to detect sensitized emission. The FRET signal can be measured directly as the crosstalk is negligible. Additionally, acceptor photobleaching is not necessary to acquire intensity data for donor with acceptor and donor alone for calculating FRET efficiency with the equation, $E = 1 - \frac{I_{DA}}{I_D}$; I_D can be measured before adding MG and I_{DA} can be measured after adding MG. Lifetime measurements are also simplified as independent donor only control samples are not necessary to determine the lifetime of the donor alone; the lifetime can be measured before and after adding MG.

1.10 Additional Microscopy Techniques to Measure FRET

 Intensity based FRET and FLIM-FRET as described above will primarily be used in this work to measure FRET. However, a number of other imaging methods can be used to monitor FRET and are briefly described below.

Spectral imaging is a technique frequently used to separate fluorophores with overlapping spectra or to remove autofluorescence from an image. These images are typically acquired by applying a narrow emission window, such as 10 or 20 nm, and stepping through wavelength across the desired range, while the excitation wavelength, power, and exposure time remain constant. This produces a series of images where the intensity changes based on the emission of the fluorophores and can be used to create an emission spectrum. Control images of individual fluorophores and autofluorescence can then be used to generate spectra to linearly unmix multicomponent images. The image series can also be evaluated by selecting a region of interest (ROI) to determine the spectral properties within different regions of the image. Spectral imaging can be used to measure FRET by evaluating the change in the emission profile between positive and negative FRET samples when exciting the donor and collecting the acceptor emission.

TIRF is a technique that is used to visualize membrane events occurring at the coverslip. This is accomplished by using a high NA objective, ideally 1.45 or greater, and setting the angle of the excitation light such that it reaches the critical angle for TIRF (Figure 1.15). Beyond the critical angle, excitation light is reflected at the coverslip back into the

objective but creates an evanescent wave that can excite fluorescent molecules within approximately 100 nm of the coverslip. The result is a very thin optical section at the membrane, where fluorescence originating from within the cell are not illuminated. TIRF can be used to measure FRET in live cells using standard methods with the advantage of only exciting fluorophores at the basal membrane.
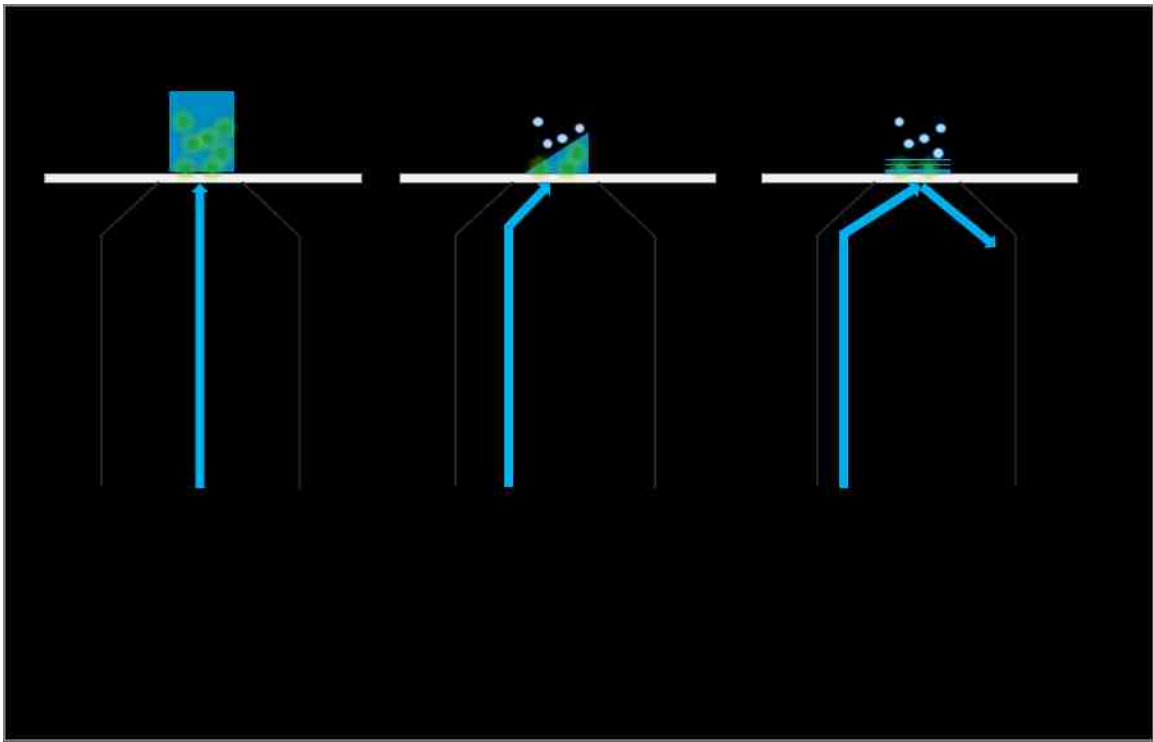
Single molecule imaging is useful to look at molecular interactions, such as receptor dimerization. This is frequently done using TIRF with a subpopulation of labeled molecules to allow for localization of individual fluorophores. Multiple fluorophores, such as two different quantum dots, can be used to spectrally distinguish spatially overlapping and potentially interacting molecules. These interactions can be further evaluated using single molecule FRET to confirm the distance between two molecules is less than 10 nm.

1.11 Hypothesis and Specific Aims

Based on preliminary work with MG-FAP and understanding the properties of fluorescent proteins and FRET, we hypothesize that MG-FAP will make a robust FRET acceptor with blue-shifted fluorescent proteins donors for live cell imaging. The following aims were developed to test our hypothesis.

- Aim 1: Demonstrate the feasibility of FAP-FP FRET.
- Aim 2: Quantify FRET efficiency of mCerulean-FAP FRET pair.
- Aim 3: Determine if YFP-FAP make a good FRET pair using FLIM.

Chapter 2

Methods

2.1 Proof of Concept Constructs

The Bruchez lab has provided us with two proof of principle constructs, FAP-mCer-TM and FAP-TM-mCer, to determine if FAP-MG can be used as an acceptor for FRET. FAP-mCer-TM is a positive FRET control; the FAP and mCerulean are expressed in tandem so that when MG is added, FRET is likely to occur (Figure 2.1 A). FAP-TM-mCer is a negative FRET control; there is a transmembrane domain that separates mCerulean from the FAP. The plasma membrane is approximately 6 to 8 nm in thickness, which positions the fluorophores far enough apart that FRET is unlikely to occur (Figure 2.1 B).

Each construct contains an Ig κ-chain leader sequence and Platelet-Derived Growth Factor Receptor Transmembrane domain (PDGFR-TM) that target the proteins to the membrane. In the positive FRET construct, both mCerulean and the FAP are located extracellularly. In the negative FRET construct, the FAP is positioned on the extracellular side of the membrane and mCerulean is intracellular. The FAP is the dL5** variant and is approximately 26 kD (Saunders et al., 2013). It is composed of two light chain portions of an antibody coupled with a glycine-serine linker $(G_4S)_4$, that form an antiparallel dimer (Chris Szent-Gyorgyi et al., 2013) (Figure 2.1 C). mCerulean3 is the fluorescent protein, which is a brighter derivative of Cerulean with a quantum yield of 0.87 compared to 0.49 for Cerulean and 0.60 for mCerulean2 (Goedhart et al., 2012). It

contains the common point mutation A206K that prevents dimerization. The constructs

are expressed in pcDNA vectors and include a myc tag.
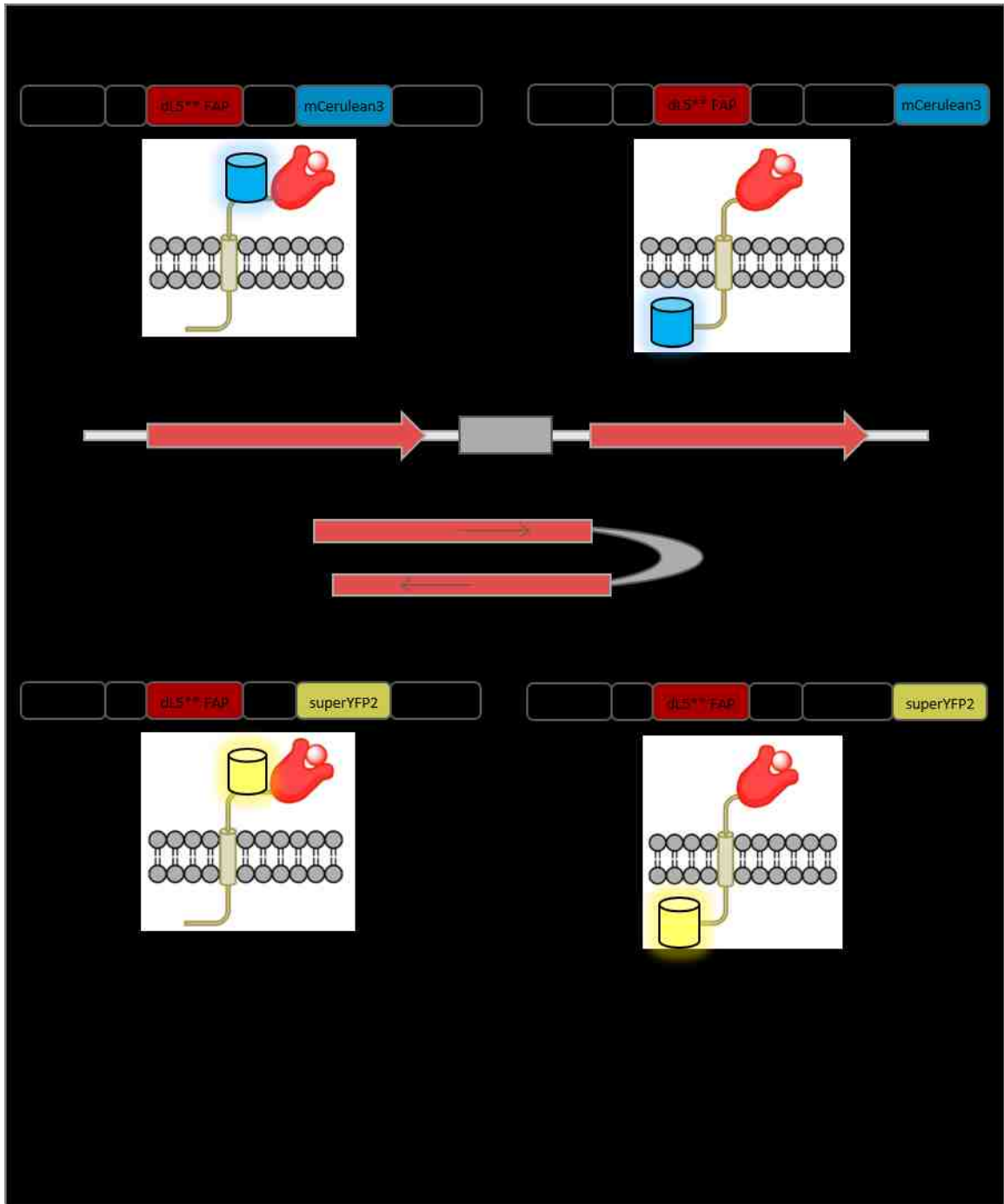
Similar constructs were developed that replace mCerulean3 with SuperYFP2 as a second option for a fluorescent protein donor for FRET with FAP-MG (Figure 2.1 D). SuperYFP2 is a brighter variant of EYFP with a higher extinction coefficient, 101,000 $M^{-1}cm^{-1}$ compared to 72,000 $M^{-1}cm^{-1}$ for EYFP. Other than replacing the fluorescent protein, the YFP constructs are identical to the mCerulean proof of concept constructs.

2.2 Fluorogens

We received a number of fluorogens from the Bruchez lab at Carnegie Mellon University that display various properties, including membrane permeability, quantum yield, and spectral properties (Table 2.1). The MG fluorogen has a primary excitation maximum, the x band, as well as a secondary excitation peak, the y band, whereas the other fluorogen, MHN, does not have a secondary peak. The peaks have been shifted in some of the variants to be used for different purposes, such as optimizing compatibility with other fluorophores. Modifications that increase the quantum yield of the fluorogen is always desirable in microscopy and improves efficiency of FRET.

Modifying the fluorogen to regulate permeablization through the plasma membrane is an important property to control. Preventing the fluorogen from passing through the membrane provides confidence that measurements are from the extracellular surface of the membrane and not FAP that may be intracellular. Alternatively, if the FAP is expressed with an intracellular protein, it is important for the fluorogen to be able to pass through the membrane of living cells. The membrane impermeable fluorogens contain a hydrophilic linker preventing passage through the plasma membrane, whereas

the permeable fluorogens are small enough and the right charge that they can passively

diffuse through the cell membrane (Yan et al., 2015).

Dye	Excitation max y band (nm)	Excitation max x band (nm)	Emission max (nm)	Membrane Permeable	Quantum Yield
MG-EDA-DMA	476	633	668	yes	0.14
MG-CN	442	680	726	yes	0.013
MG-Ester	460	633	668	yes	0.12
MG-nBu	460	633	668	yes	0.19
MHN-CN2	-	490	588	yes	-
MG-4F	464	710	750	yes	0.003
MG-EDA-Dcarb	476	633	668	no	0.14
MG-2P	460	633	668	no	0.2
MG-βTau	460	633	668	no	0.19
MHN-Tau	-	476	533	no	0.27

2.3 Cell Culture, Transfections, and Plating

Three cell lines were used for the initial experiments: HeLa, Chinese Hamster Ovary

(CHO), and Rat Basophilic Leukemia (RBL) cells. Before transfection, cells were grown to

approximately 80% confluency and transfected through electroporation with the Amaxa

Nucleofector. For transfection of HeLa cells, 3 µg of DNA were used per 1.5 million cells,

using program I-013 and solution R, as recommended by the manufacturer for high

transfection efficiency. When transfecting RBL cells, program T-020 was used with

solution L. CHO cells required a higher concentration of DNA per transfection, 4 µg per 1 million cells, and program U-023 was used with solution V. After transfection, cells were plated at low density on #1 or #1.5 piranha etched 15 mm round coverslips in 6-well plates and left to grow for at least one day before imaging.

2.4 Confocal Imaging

Live cells grown on 15 mm coverslips were placed into quick release (QR) magnetic imaging chambers from Warner Instruments (Order No. 64-1945; Model No. QR-42LP) with 150 µl of Tyrode's medium. Cells are imaged one, two, and three days after transfection on a Leica SP8 confocal microscope with a 63x 1.2NA water objective with the correction collar set to 0.17 for #1.5 coverslips or 0.15 when using #1 coverslips. For the mCerulean constructs, a 405 nm laser diode is used at 1% laser power for excitation. The 633 nm line from the White Light Laser (WLL) is used at 5% for direct excitation of the MG dye. Emission is collected from 450-550 nm for mCerulean and 640-740 nm for direct MG excitation (ex 633 nm) or FRET (ex 405 nm) with HyD detectors in photon counting mode. The 514 nm laser line from the WLL is used at 3.5% to excite YFP. Emission is collected from 520 – 575 nm for the donor signal and 660 – 750 nm was used for the FRET (ex 514 nm) channel and direct excitation of MG (ex 633 nm). The FRET channel is red-shifted from the mCerulean settings to reduce cross-talk of YFP into the FRET channel. See supplement for detailed acquisition settings exported from LAS X (S2.1).

For FRET efficiency data, the 'Mark and Find' feature is used to acquire images at multiple positions before adding dye and then returning to image the same positions after adding dye. The Adaptive Focus Control within the Leica software is used to maintain focus over time. Images are acquired with the 405 nm or 514 nm laser only to measure intensity in the donor channel before and after addition of dye for use in the FRET efficiency calculation, to confirm there is no bleed-through of mCerulean or autofluorescence into the FRET channel before adding dye, and to measure intensity in the FRET channel after adding dye. Images with the 633 nm laser only are acquired to measure any background or autofluorescence of cells from 633 nm excitation before adding dye and to confirm direct excitation after adding dye. When adding dye, 50 µl of 2 µM MG is added to the 150 µl of Tyrode's buffer to make a final concentration of 500 nM. For the membrane impermeable dyes, the after dye images are acquired shortly after addition of dye. For the membrane permeable dyes, a 15 min wait time is added to ensure dye has time to pass through the membrane and bind to internal FAP.

2.5 Confocal Image Analysis

To calculate intensity based FRET efficiency, we used the average intensity value from the donor mCerulean images acquired on the Leica SP8 confocal microscope, before and after addition of dye. To ensure that we only included properly localized construct, we created an automated script using Matlab to extract only donor signal from the cell membrane. The script opens the images from the original Leica file (.lif), masks the membrane of the cells using a defined thickness, and uses the average intensity values

within the mask to calculate the FRET efficiency per image (Figure 2.2). The script can be found in the supplement (S2.2).
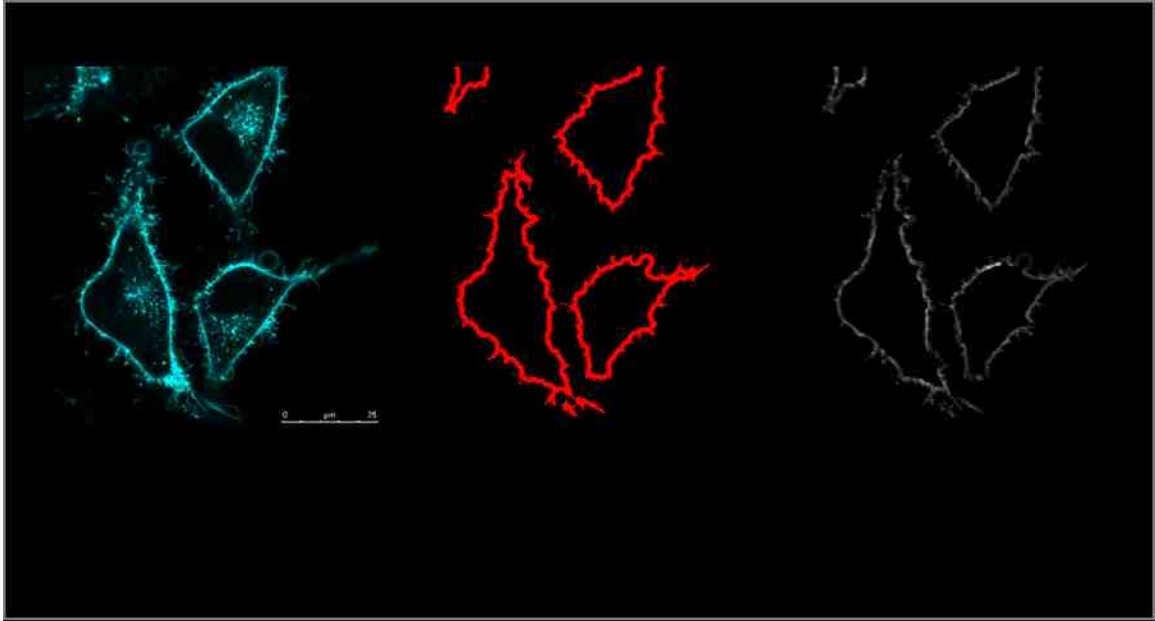
The equation used to calculate FRET efficiency is $E = 1 - \frac{I_{DA}}{I_D}$, where I_{DA} is the mean intensity from the donor with acceptor image (after dye addition) and I_D is the mean intensity from the donor only image (before dye addition), calculated for individual cells. A student's two-tailed t-test was used to compare groups. The R_0 value was calculated for several FRET pairs using a script written by Joshua Vaughan (http://web.mit.edu/5.33/www/5.33%20R%20Exp%203%20Laser_Appendix2-05.pdf). The equation used to determine the Förster radius is $R_0 = 8.8 \times 10^{-25}(Q_D K^2 n^{-4} J_{DA})^{1/6}$ cm, which is described in detail in the introduction.

2.6 Spectral Imaging

Spectral images were acquired on the Leica SP8 confocal microscope and the 63x 1.2 NA water objective, using LAS X software in xyλ mode. The 405 nm laser was used to excite mCerulean and images were acquired from 450 nm – 750 nm, acquiring images with a 20 nm band and a 10 nm step between images. See supplement for detailed spectral imaging parameters (S2.3).

2.7 FLIM Imaging

The YFP proof of concept constructs were used for acquiring FLIM data for YFP-MG FRET. The pulsed WLL is required for FLIM and the shortest wavelength from that laser is 470 nm, which does not excite mCerulean well. The 514 nm line is used at 3.5% laser power to excite YFP and lifetime values were recorded from the donor channel, 520 – 575 nm. The FLIM wizard from the LAS X software is integrated with PicoQuant's PicoHarp 300 TCSPC and SymPhoTime 64 software to acquire lifetime measurements. FLIM data was acquired until 1000 photons were accumulated in a pixel within the image. Mark and Find is disabled while using the FLIM wizard so images acquired before and after dye are not necessarily the same cell. See supplement for detail of FLIM imaging parameters (S2.4).

2.8 FLIM Analysis

SymPhoTime 64 software was used to quantify lifetime values. Masked pixels for analysis were selected using the magic wand tool and actively selecting membrane regions of the cells (Figure 2.3 A). A two-component fit was used and a χ^2 value near 1

was considered a good fit (Figure 2.3 B). Lifetime from amplitude weighted tau (τ_{AvAmp})

from five images in each condition were averaged to calculate lifetime and FRET

efficiency values using the equation: $\tau_{AvAmp} = \dfrac{A_1\tau_1}{A_1+A_2} + \dfrac{A_2\tau_2}{A_1+A_2}$.
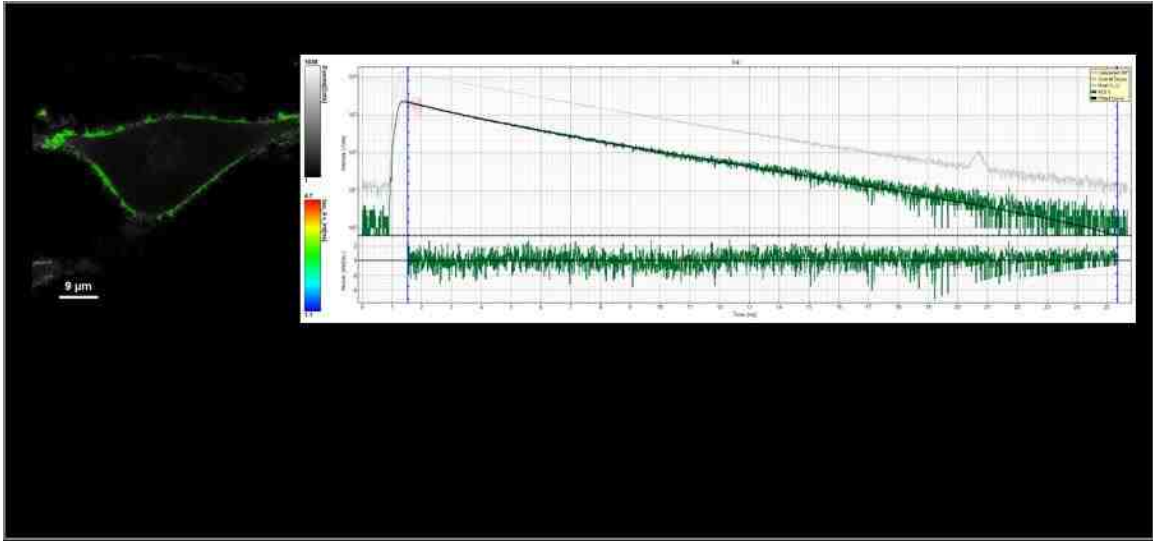
Chapter 3

Results

Aim 1: Demonstrate the feasibility of FAP-FP FRET

3.1 FAP-mCer-TM and FAP-TM-mCer constructs express at the membrane and bind MG

Two proof of concept constructs, FAP-mCer-TM and FAP-TM-mCer shown in Figure 2.1, were used to characterize FRET between mCerulean and FAP-MG and determine if they make a good FRET pair. As described in the methods, FAP-mCer-TM is a positive FRET construct and FAP-TM-mCer is a negative FRET construct, but both have a transmembrane domain that target the proteins to the plasma membrane. In the positive FRET construct, the FAP and mCerulean are expressed in tandem on the extracellular side of the membrane; when the fluorogen binds the FAP, the donor and acceptor are close enough that FRET should occur. In the negative construct, the transmembrane domain separates the FAP from mCerulean so that even when the fluorogen is bound, the distance between the donor and acceptor is large enough that FRET is unlikely to occur.

As the proof of concept constructs are large compared to most expressed proteins, initial experiments were performed to optimize expression and confirm that the constructs express properly, localizing to the plasma membrane with the ability to bind the fluorogen, MG. The constructs were expressed in three cell lines and imaged using confocal microscopy to evaluate expression of the constructs. In two cell lines, RBL and CHO, MG bound to the FAP but localization to the membrane was rare and large

44

aggregates formed within the cytosol. Expression in HeLa cells showed expression at the membrane and fewer cytosolic aggregates (Figure 3.1 A). As the constructs expressed best in HeLa cells, they were used in all subsequent experiments with the proof of concept constructs. Between the positive and negative FRET constructs, expression of mCerulean in cells transfected with FAP-TM-mCer was typically less bright and there were more aggregates than in cells expressing the FAP-mCer-TM construct. Average photon counts are 75 in cells expressing the positive FRET construct compared to 30 in the negative construct (Figure 3.1 B).
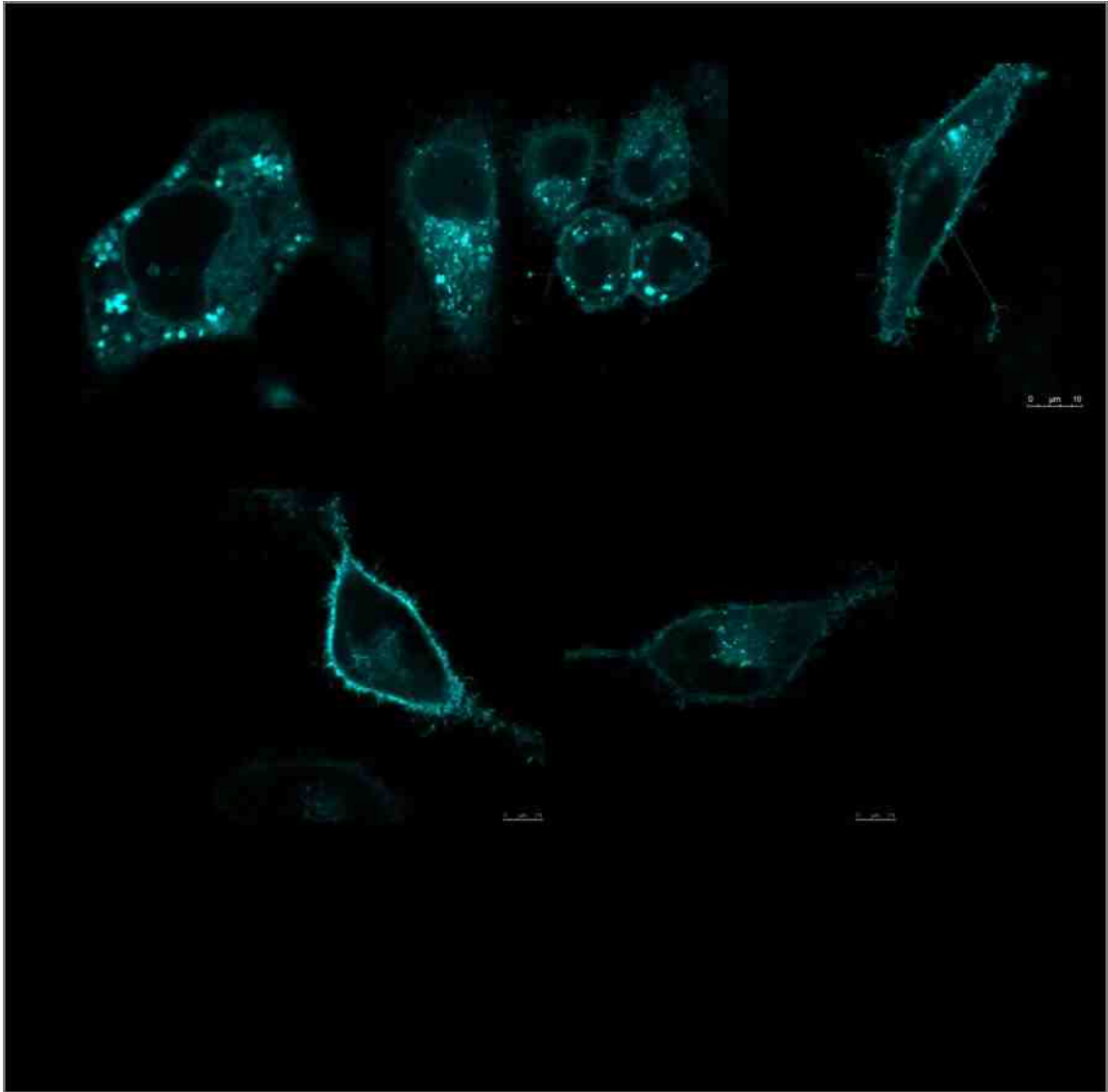
It was also confirmed that the membrane permeable and impermeable fluorogens bind

to both constructs as expected (Figure 3.2). MG binds to extracellular FAP within

seconds, as seen by the immediate appearance of fluorescence under the microscope.

The membrane permeant fluorogen, MG-nBu, shows intracellular binding to FAP several

minutes after addition with maximum binding around 15 min. The membrane

impermeable fluorogen, MG-βTau, binds to FAP expressed on the membrane but does

not cross the plasma membrane even after long periods of time, well past the 15 min

seen with MG-nBu. Neither fluorogen binds non-specifically to untransfected cells,

indicating that any detected signal is specific binding to FAPs.
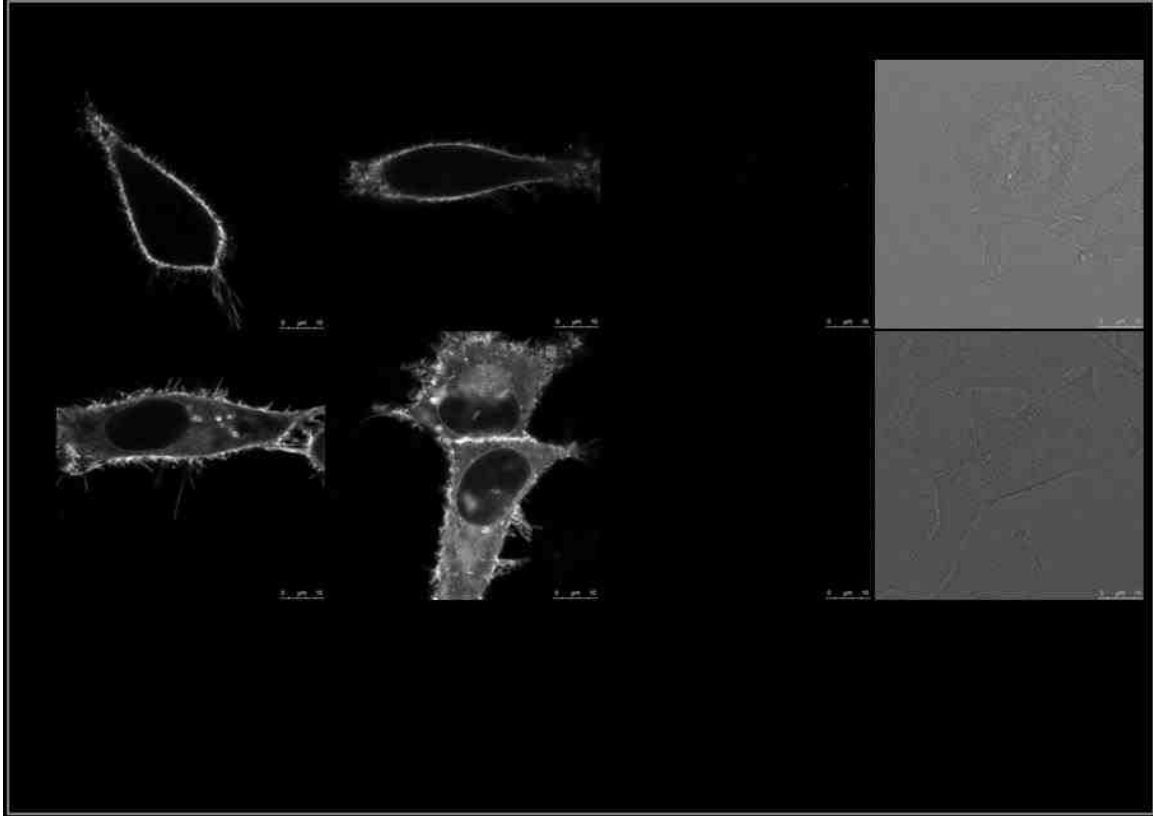
3.2 FRET can be visualized through sensitized emission and spectral imaging

Sensitized emission is a common method to measure FRET and as the large Stokes shift

of MG allows for mCerulean to participate as a FRET donor without contaminating the

FRET signal, this technique was used to evaluate the FRET with the proof of concept

constructs. A 405 nm laser was used to excited mCerulean and the sensitized emission

signal was collected in the far red, 640 nm to 740 nm (Figure 3.3). The simplicity of this

procedure should not be taken for granted; this is not possible when using traditional

FRET pairs, such as CFP and YFP. The bleed-through of CFP into the FRET channel makes

visualizing FRET impossible. Using a standard YFP emission filter, such as 550/50, 21% of

emission from CFP will be collected, masking the FRET signal, as shown in Figure 1.12 A.

This makes measuring sensitized emission difficult, especially considering that FRET

signals are typically low, requiring the many controls and corrections discussed in the

introduction.
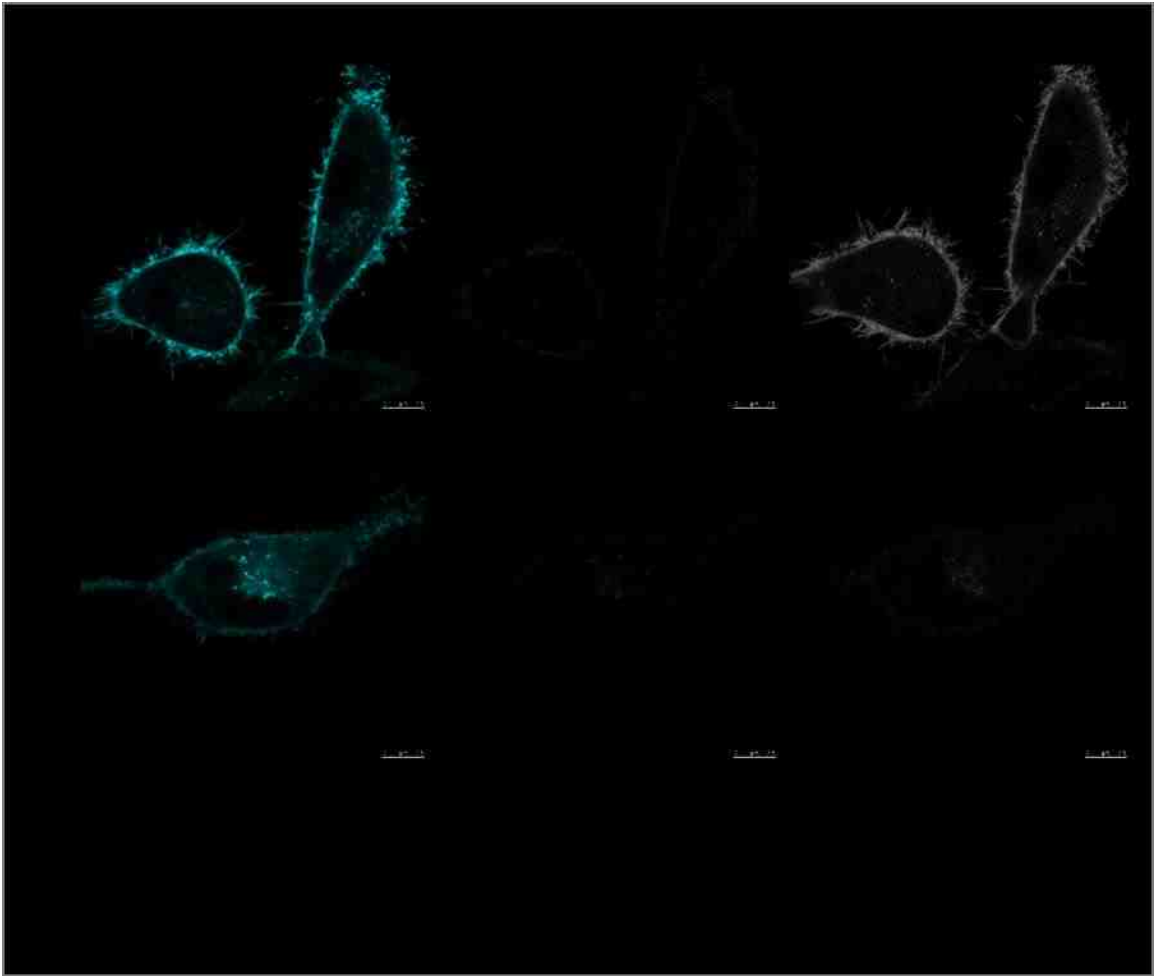
A HyD detector was used to collect the FRET signal, a photon counting detector capable

of acquiring raw photon counts where gain is not applied to the image, allowing for

intensity to be quantified. Unfortunately, raw FRET signals are typically low and images

from the FRET channel can be dim when using this detector. Displaying the images as a

ratio of the FRET channel over the donor channel enhances the visualization of the FRET

signal (Figure 3.4).
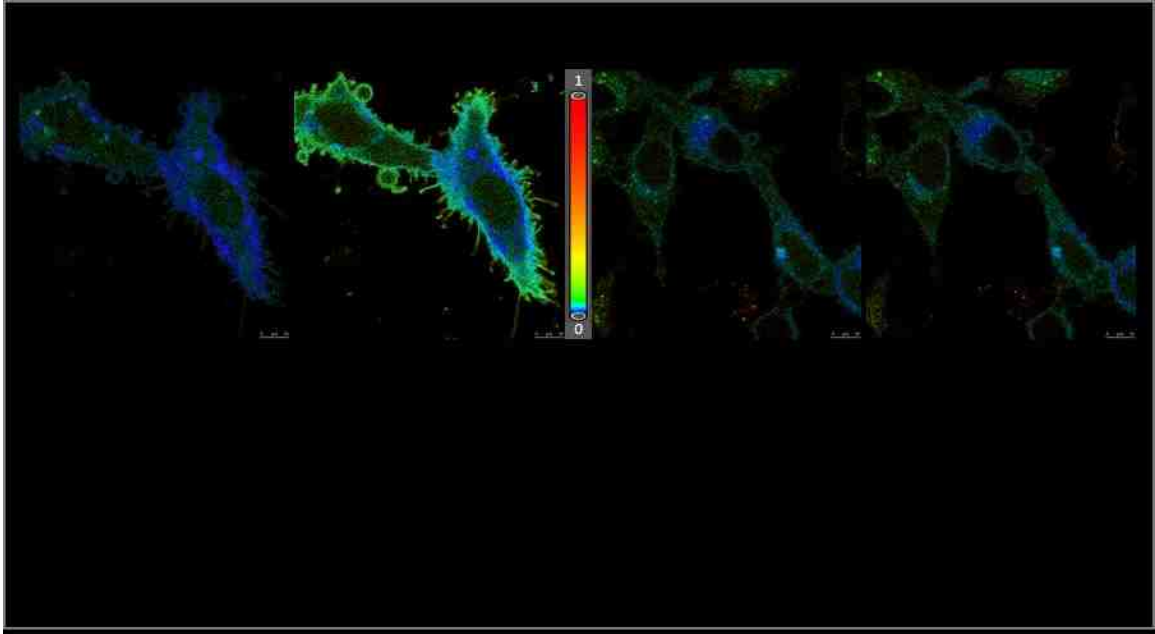
In addition to sensitized emission, FRET can be visualized with spectral imaging and was

used here to compare the positive and negative constructs to further evaluate the

mCerulean/MG FRET pair (Figure 3.5). With 405 nm excitation, images are acquired

across most of the visible spectrum, from 450 nm to 730 nm. The primary peak is

mCerulean emission but in cells expressing the positive FRET construct, FAP-mCer-TM,

the FRET signal is clearly visible as a small bump around 650 nm. This bump is greatly

reduced in cells expressing the negative construct, FAP-TM-mCer. The peak is 15% of

max in the FAP-mCer-TM image compared to 3% in the FAP-TM-mCer image.

Spectral Plot of FRET in cells expressing FAP-Cer-TM

Spectral Plot of FRET in cells expressing FAP-TM-Cer
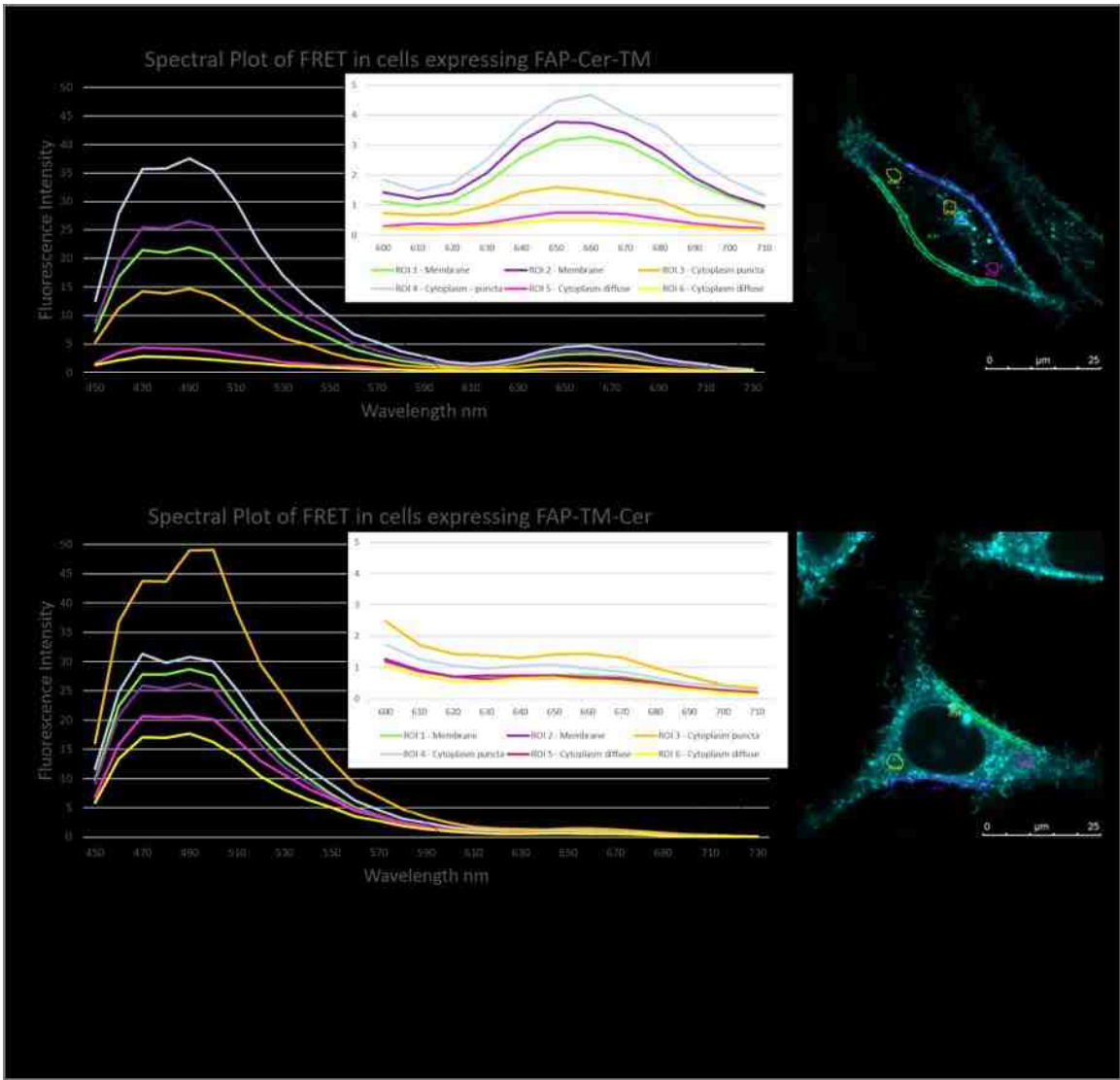
3.3 R_0 value supports mCerulean-MG as a suitable FRET pair

The Förster radius, R_0, is a useful calculation to determine the distance at which FRET is likely to occur for a given FRET pair based on the properties of the fluorophores. The larger the R_0 value, the greater the distance can be between fluorophores with energy transfer remaining possible. The R_0 value for mCerulean and MG was calculated using the following formula: $R_0 = (JK^2Q_0n^{-4})^{\frac{1}{6}} \times 8.8 \times 10^3 \text{Å}$, as described in the introduction, and automated with the Matlab script described in the Methods section. R_0 was found

50

to be 6.09 nm for mCerulean and MG (Figure 3.6 A), a value similar to R_0 calculated for

other commonly used FRET pairs, such as ECFP/EYFP (R_0 = 4.9 nm), mCerulean3/mVenus

(R_0 = 5.7 nm), and EGFP/mRFP1 (R_0 = 4.7 nm) (Müller et al., 2013). The spectral overlap

between mCerulean emission and MG absorption used in the calculation of J_{DA} is shown

in Figure 3.6 B. FRET efficiency versus distance was plotted to determine the range at

which detecting FRET is possible, with 5% FRET efficiency around 10 nm, indicating a

reasonable distance for measuring protein-protein interactions with this FRET pair

(Figure 3.6 C).

Q_D	K^2	n	J_{DA}	ε_A (M^{-1} cm^{-1})	R_0 (nm)
0.87	2/3	1.347	3.2980×10^{-13}	91,700	6.09

$$E = \frac{1}{1 + \left(r/R_0\right)^6}$$
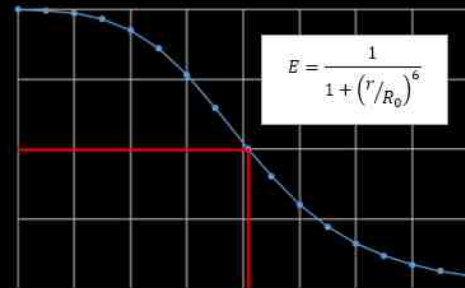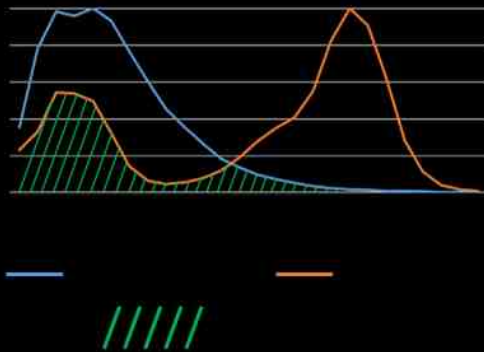
Aim 2: Quantify FRET efficiency of mCerulean-FAP FRET pair

3.4 FRET efficiency is significantly different between FAP-mCer-TM and FAP-TM-mCer

After demonstrating that mCerulean and MG should make a good FRET pair, the FRET efficiency of both constructs was quantified to support the hypothesis. Confocal images of the donor, mCerulean, were acquired to quantify FRET efficiency. The ability to add the acceptor MG at any time allows for 'donor only' and 'donor with acceptor' images to be acquired for the same cell (Figure 3.7 A). The decrease in intensity seen in the 'donor

with acceptor' image is not due to photobleaching, this is FRET. The Matlab script

described in the Methods section was used to determine the average intensity value

from the cell membrane of donor images acquired before and after adding the

fluorogen (Figure 2.2). The average intensity from the masked regions were applied to

the following FRET efficiency equation: $E = 1 - \frac{I_{D_A}}{I_D}$, where I_{D_A} is the intensity from the

'donor with acceptor' image, after the addition of MG, and I_D is the intensity from the

"donor only' image, before MG is added (Figure 3.7 B).
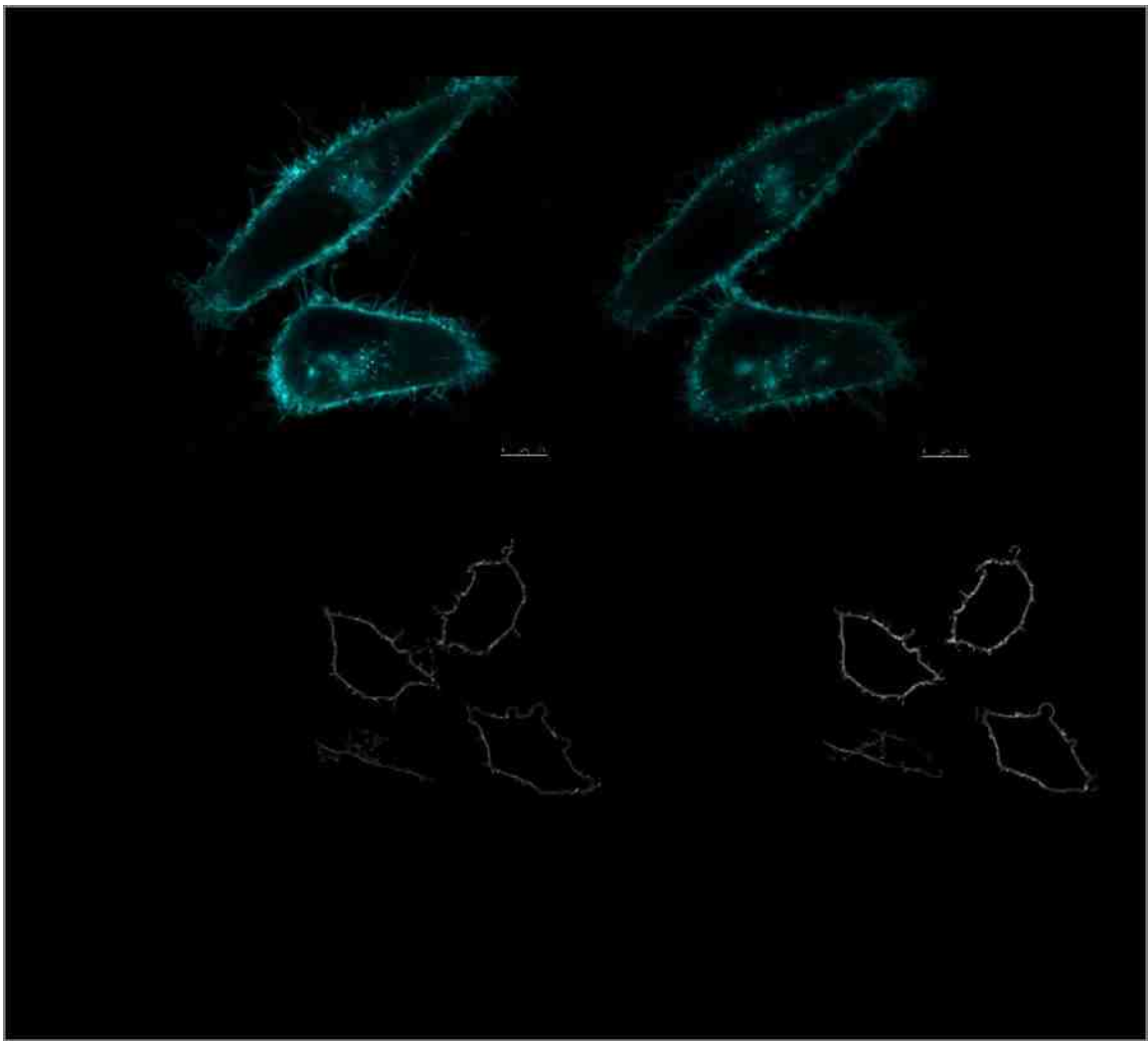
Cells expressing the positive FRET construct, FAP-mCer-TM, had FRET efficiencies of 29%

and 34% with MG-βTau and MG-nBu, respectively, whereas cells expressing the

negative FRET construct had FRET efficiencies of 3.7% and 5.8% using the same

fluorogens (Figure 3.8). A student's t-test showed a significant difference between FRET

efficiency values for the positive and negative FRET constructs with both fluorogens.
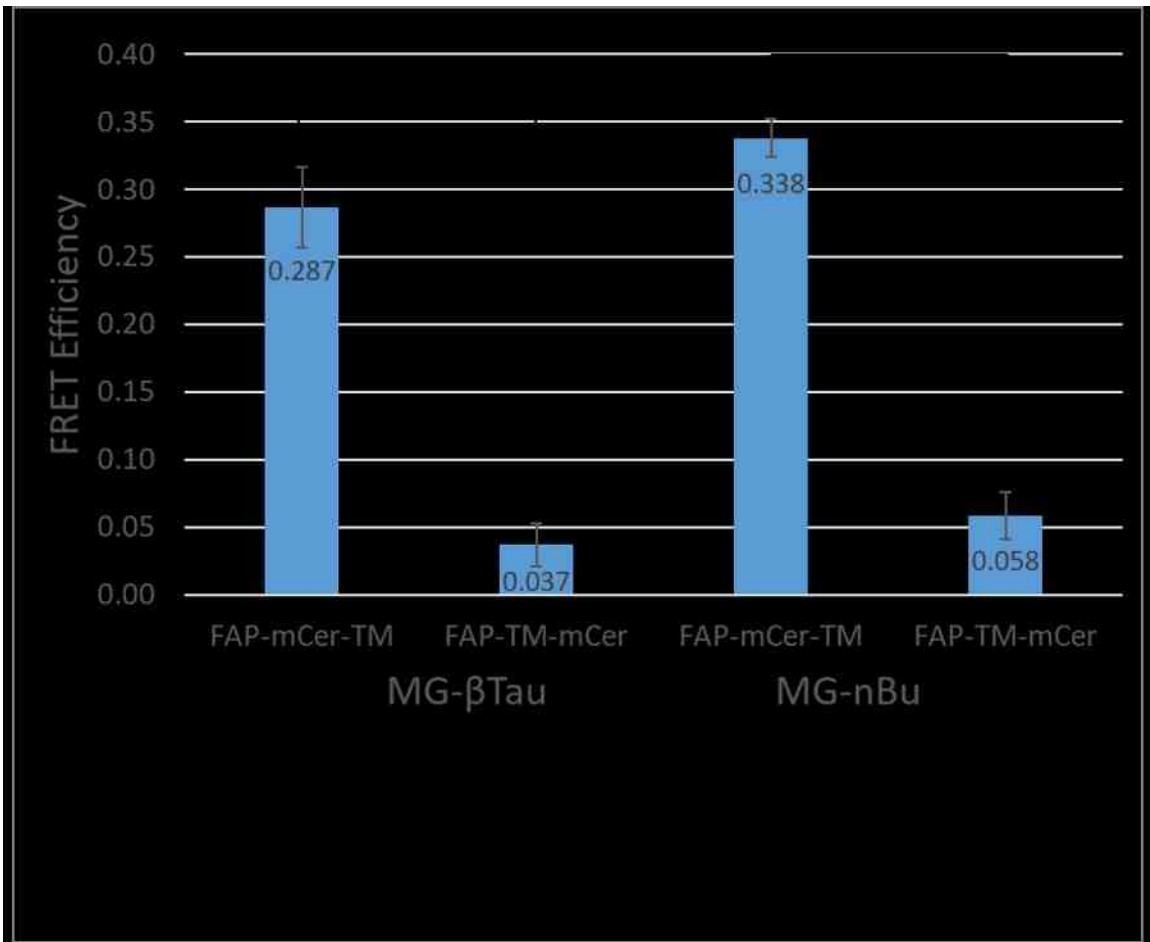
Preliminary intensity based FRET efficiency data was collected using the additional dyes

that were synthesized in the Bruchez lab and listed in Table 2.1. These data were

analyzed using an older version of the Matlab code that didn't mask the cell membrane

as accurately as the code used to analyze the MG-nBu and MG-βTau data. This data

must be re-analyzed using the newest code for accurate comparison. All MG dyes from the additional list will have the same R_0 value as MG-nBu and MG-βTau.

Aim 3: Determine if YFP-FAP make a good FRET pair using FLIM

3.5 R_0 value for YFP-MG indicate they are a good FRET pair and show proper expression

After determining that mCerulean can be a FRET donor for MG, we were interested in determining if any other fluorescent proteins could act as a donor. We chose to evaluate YFP as an option because it is a common fluorophore used for FRET and we can excite YFP with the white light laser on the Leica confocal microscope, allowing for FLIM-FRET measurements. The Bruchez lab made proof of concept constructs identical to the FAP-mCer-TM and FAP-TM-mCer constructs where mCerulean is replaced with SuperYFP2: FAP-YFP-TM and FAP-TM-YFP, as described in the Methods (Figure 2.1). Although it doesn't seem intuitive that FRET should occur between YFP and MG based on their spectra (Figure 3.9 B), the Bruchez lab at CMU measured FRET between YFP and MG using purified protein and sent us the new constructs to use for FLIM-FRET. The R_0 value was calculated for this YFP and MG using the Matlab script described in the Methods and was determined to be 5.58 nm, suggesting they will make a good FRET pair (Figure 3.9 A). Plotting FRET efficiency vs distance shows that 5% FRET efficiency can be detected when the fluorophores are approximately 9 nm apart, allowing for sufficient distance to measure protein-protein interactions (Figure 3.9 C).

Q_D	K^2	n	J_{DA}	ε_A (M^{-1} cm^{-1})	R_0 (nm)
0.68	2/3	1.347	2.4867 x 10^{-13}	91,700	5.58

$$E = \frac{1}{1 + \left(r/R_0\right)^6}$$
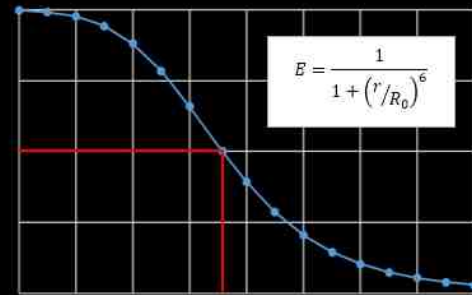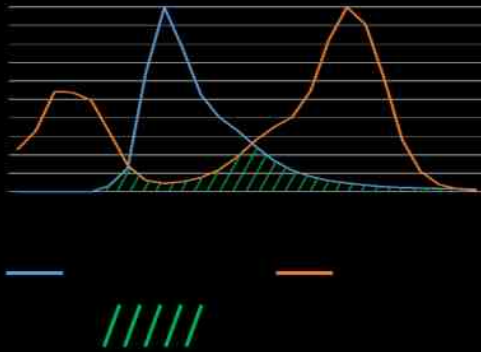
HeLa cells expressing the new constructs were imaged on the Leica confocal microscope

to evaluate protein expression and fluorogen binding. Images show that both YFP

constructs do express well, with proper membrane localization, few intracellular

aggregates, and sufficient fluorogen binding (Figure 3.10). Interestingly, the negative

FRET construct, FAP-TM-YFP, appeared brighter and contained fewer intracellular

aggregates than the mCerulean version.
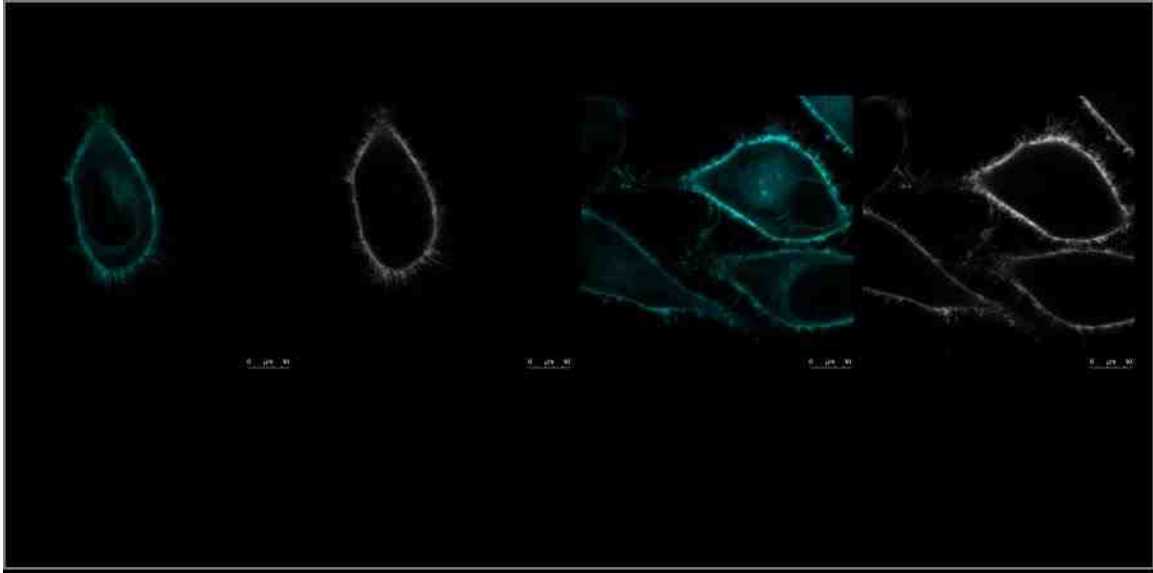
To evaluate YFP as a donor for FRET with MG, the lifetime of YFP was measured before

and after adding the acceptor, MG, for both proof of concept constructs, as the lifetime

of a fluorophore will decrease with FRET. YFP was excited with the 514 nm line from the

white light laser and donor lifetime values were recorded from 520-575 nm. Lifetime

images were acquired before and after adding the membrane impermeable dye, MG-

βTau. As lifetime values are measured for each pixel, localized changes in lifetime are

visible. In cells expressing FAP-YFP-TM, the lifetime clearly changes at the membrane

after adding MG-βTau, but not in cells expressing FAP-TM-YFP (Figure 3.11 A). ROIs of

the cell membrane were used for FLIM analysis to determine the average lifetime at the

membrane in each condition. As YFP has two lifetime components, a two component fit

was applied. The average lifetime of YFP decreased in the presence of the acceptor in

cells expressing the positive FRET construct, FAP-YFP-TM, from 2.4 ns to 1.7 ns,

indicating FRET with MG. There was no change in lifetime from cell expressing the FAP-

TM-YFP when the acceptor was added (Figure 3.11 B).
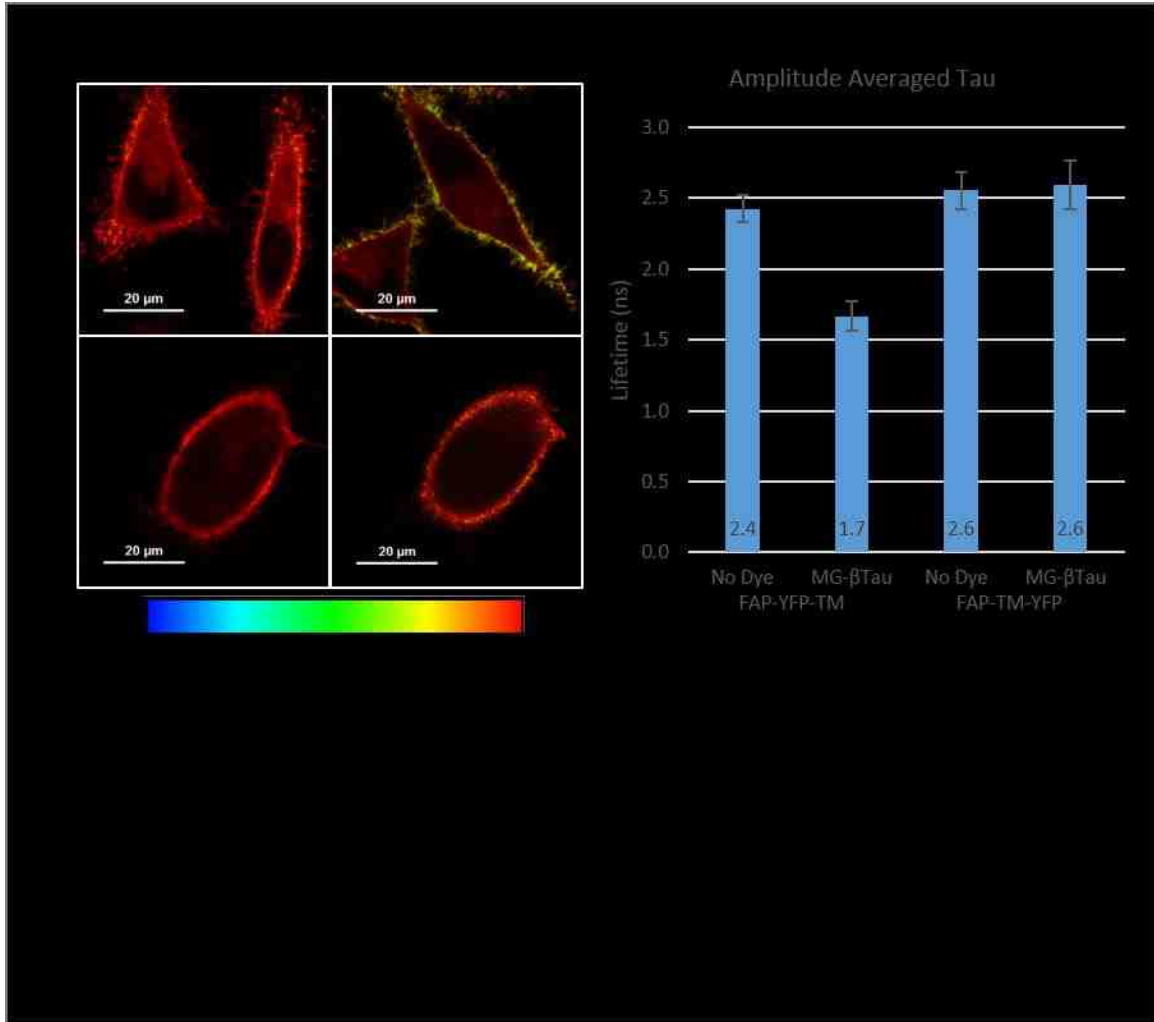
3.7 FRET efficiency is significantly different between constructs with MG-βTau

For further evaluation of YFP as a FRET donor to MG, FRET efficiency can be calculated

from lifetime values using the equation $E = 1 - \frac{\tau_{DA}}{\tau_D}$, where τ_{DA} is the lifetime of donor

in the presence of the acceptor (after dye) and τ_D is the lifetime of donor alone (before

dye). As we fit for two components, we use amplitude averaged tau (τ_Av_Amp) in the

FRET efficiency calculation to account for both lifetime components. The τ_Av_Amp

values from each image are averaged within each condition for use in the FRET

efficiency calculation. Cells expressing the positive FRET construct were calculated to

have a FRET efficiency of 29%, consistent with intensity-based calculations, whereas

cells expressing the negative construct showed a FRET efficiency of 0% (Figure 3.12).

Chapter 4

Discussion

4.1 Introduction

In this work we have generated and tested two proof of concept fluorescent constructs that demonstrate the utility of the FAP as a FRET acceptor, and have detailed the improvements to FRET detection made possible by the FAP system. Two membrane spanning constructs were generated by our collaborators at Carnegie Mellon University; a positive FRET construct in which the donor and acceptor fluorophores are expressed in tandem within the same sequence, and a negative FRET construct in which the donor and acceptor fluorophores are expressed on opposite sides of a biological membrane, and at a distance predicted to be too far for efficient energy transfer. These constructs were expressed in HeLa cells and it was demonstrated that the MG fluorogen, when bound to the FAP, can be a FRET acceptor for both mCerulean and YFP.

4.2 FRET efficiency

FRET efficiency was calculated to be approximately 30% in cells expressing the positive FRET construct when analyzed using both intensity-based and lifetime measurements. Different donor fluorophores were used for each technique, mCerulean for intensity-based measurements and YFP for lifetime. Additionally, two fluorogens were tested as FRET acceptors, MG-βTau and MG-nBu. These results match previous experiments carried out by the Bruchez lab at CMU, in which a FRET efficiency of ~30% was found using purified donor/acceptor proteins at high concentrations in solution (personal

60

communication). The consistency across techniques and constructs is impressive and strengthens the validity of the data.

There is an incredibly wide range of published FRET efficiencies, with reports higher than 90% (Ding, Cargill, Das, Medintz, & Claussen, 2015), depending on the size and optical property of the probe as well as the specific substrate being measured. Calculating 30% FRET efficiency for the positive proof of concept construct may be reasonable considering that with mCerulean as a donor, the spectral overlap with the secondary absorption peak of MG is only 50% of the primary peak, reducing the fluorescence emission from MG by 50%. Interestingly, using red-shifted YFP as a donor there is little spectral overlap with the secondary absorption peak of MG yet the FRET efficiency was also calculated to be approximately 30%, likely from sufficient overlap with the primary absorption peak. The R_0 values calculated for both donors were similar, 6.09 nm for mCerulean-MG and 5.58 nm for YFP-MG, supporting the similarity in FRET efficiency. Additionally, the barrel surrounding the fluorophore of mCerulean and YFP is not insignificant in size, approximately 2 nm x 4 nm, and will always limit the FRET efficiency when using fluorescent proteins.

Sensitized emission is a common technique to measure FRET, which was used here to evaluate the FP-FAP system for FRET. It was important to use a traditional method as a comparison to previously published FRET data to validate the results as well as demonstrate the simplicity of the FP-FAP FRET system. With a large Stokes shift between a blue-shifted donor and the far red emitting acceptor, MG, sensitized emission can be measured directly with FP-FAP FRET. This eliminates the need for

multiple transfections that are typically required for imaging controls, such as CFP alone and YFP alone, and the many corrections required to correct for cross-talk and variability in protein expression. Unlike FRET studies with two fluorescent proteins, using the FAP-MG as the acceptor, the donor image can be acquired with and without the acceptor for the same cell, simply by acquiring an image of the donor before and after adding the acceptor fluorogen. Therefore, calculating FRET efficiency is significantly simplified and data can be measured for individual cells and regions within cells.

The FP-FAP system greatly simplifies measuring sensitized emission and calculating FRET efficiency but precise pixel masking is necessary for accurate FRET data. Although FRET efficiency was calculated to be approximately 30% and standard error of the mean was reported, the standard deviation is large, approximately 0.133 and 0.077 for FAP-mCer-TM with MG-βTau and MG-nBu, respectively, for corresponding FRET efficiency values of 28.7% and 33.8%. The standard deviations were 0.07 for FAP-TM-mCer with MG-βTau and 0.095 with MG-nBu, for corresponding FRET efficiencies of 3.7% and 5.8%, nearly twice the values. This is likely due to poor membrane masking from the current Matlab script used for analysis. Once the proof of concept construct is expressed, the fluorescent protein is excitable regardless of the location in the cell, but the membrane impermeable fluorogens only have access to bind FAPs that have localized to the membrane with the proper extracellular orientation. Although membrane permeable fluorogens can bind intracellular FAPs, sufficient binding can take up to 15 min as the fluorogen diffuses across the membrane. Additionally, if the FP-FAP is within

intracellular vesicles in transport to the membrane, the fluorogen will be required to pass the vesicle membrane as well to bind vesicular FAPs. Depending when the donor with fluorogen image is acquire will affect the level of fluorogen binding to FAPs and therefore the amount of FP that cannot FRET. As the FP intensity before and after adding fluorogen are used to calculate FRET efficiency, masking FP pixels that are inaccessible to fluorogen will blunt FRET efficiency values. Variability in the morphology of the cell can also cause FRET positive regions of the plasma membrane be excluded from the mask, also reducing FRET efficiency. Inaccurate masking creates variability when calculating FRET efficiency and improvements to the masking code should continue. Dr. Bernd Rieger, at Delft University of Technology in The Netherlands, is an expert in image analysis and has agreed to help improve the script. A student, Wessel Hoff, applied a "snaking" technique to create a more accurate membrane mask.

4.3 Spectral imaging

Spectral images were also used to evaluate FRET within the proof of concept constructs. The FRET signal in the far-red is clearly visible in cells expressing the positive FRET construct, FAP-mCer-TM and is correlated with mCerulean intensity. While the signal is nearly negligible in cells expressing the negative FRET construct, FAP-TM-mCer, a small bump can be detected when the intensity of mCerulean is high. This could be from direct excitation of MG in regions of high protein expression or low levels of FRET across the plasma membrane. Two controls could be tested to determine the origin of the bump. Far red signal from 405 nm excitation of cells expressing a FAP only construct with MG would indicate direct excitation of the fluorogen and not FRET. Additionally, a

spectral image of cells expressing the proof of concept constructs acquired before the addition of MG would generate the pure mCerulean spectra, while a spectral image of untransfected cells would show any contribution of autofluorescence. Regardless of the source, the increase in FRET signal is clear in cells expressing the positive FRET construct, FAP-mCer-TM.

4.4 FLIM

Although FLIM-FRET is more sensitive than intensity-based techniques, it used less often because of the specific hardware required to acquire the data. Fortunately, the Leica SP8 has the ability to measure lifetime, allowing for evaluation of the constructs using FLIM. The lifetime of a fluorophore is not affected by typical parameters that affect intensity based measurements but is very sensitive to changes in environment, such as pH or the availability of an acceptor for FRET, as noted by the decrease in lifetime of a fluorophore with FRET and described in the introduction. The preliminary data of lifetime measurements of our two constructs suggest that FRET is occurring at the membrane in cells expressing the positive FRET construct, with a reduction in lifetime by about 30% when the acceptor MG-βTau is present. Cells expressing the negative FRET construct show no change in lifetime when MG-βTau is added, indicating the change in lifetime in cells expressing FAP-YFP-MG is due to FRET and not simply the presence of the fluorogen.

The sensitivity of FLIM-FRET maybe required when using the FP-FAP system in biological applications where FRET efficiency is potentially less than what was found with the

64

proof of concept constructs. Using the E vs r plot and an R_0 value of 6.09 nm for MG and mCerulean, the fluorophores of the FRET pair must be approximately 7 nm apart in the positive construct with a FRET efficiency of 30%. Considering that the size of the mCerulean barrel and the FAP are not insignificant, it is likely that the two proteins are less than 5 nm apart (Figure 4.1). When using the FP-FAP system in a biological application, the FRET signal is likely to be low as the proteins of interest must be quite close to detect FRET, and a technique as sensitive as FLIM may be advantageous.
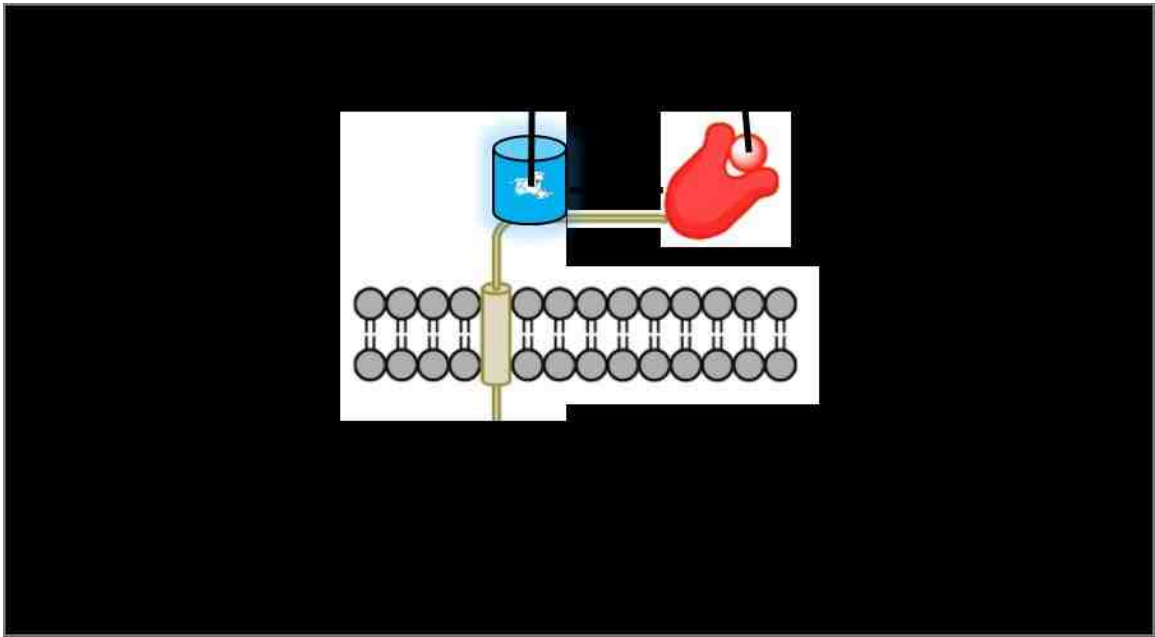
4.5 Additional dyes

The fluorogens that have been developed by the Bruchez lab at CMU have a wide range of FRET efficiencies, likely due to differences in quantum yields. Of the MG dyes tested, the MG-nBu and MG-βTau had the highest FRET efficiency with mCerulean but other variants could be useful in other applications, such as the need for reduced binding affinity. In addition to the MG variants, there are two versions of another fluorophore,

MHN. Both MHN fluorogens have a single excitation peak around 480 nm, but one has

an emission peak around 533 nm, similar to GFP, while the other is red-shifted with a

maximum peak around 588 nm. Although not tested here, the red-shifted version of

MHN could be used as a FRET acceptor with a blue-shifted fluorescent protein, such as

mCerulean, with similar advantages of mCerulean-MG-FAP FRET. The benefit of using

MHN over MG would be significantly higher spectral overlap between mCerulean

emission and MHN absorption, but the cross-talk of mCerulean into the FRET channel

would be higher than when using MG as the acceptor.

4.6 Conclusion

Through the use of proof of concept constructs, this work has shown that FAP-MG is a

viable FRET acceptor with two different fluorescent proteins as donors, mCerulean and

YFP, with several advantages over traditional FRET pairs. The large Stokes shift between

the emission of the donor and MG allows for direct detection of sensitized emission,

eliminating the need for the many imaging controls and correction factors typically

required to measure sensitized emission. Additionally, without the cross-talk from

typical pairs, such as CFP and YFP, FRET efficiency can be calculated with the simple

equation: $E = 1 - \frac{I_{DA}}{I_D}$. Another advantage of FP-FAP FRET is the ability to add the

acceptor at any time, allowing for 'donor only' and 'donor with acceptor' images to be

acquired for the same cell, inherently controlling for variability of protein expression

and allowing for FRET efficiency to be determined within regions of cells. When

comparing the R_0 value of FP-MG to standard FRET pairs, the Förster radius is congruent

with other pairs. The R_0 value of ECFP and EYFP is 4.9 nm (Hochreiter et al., 2015), which

is smaller than the R_0 value for mCerulean3 and MG (6.09 nm) as well as SuperYFP2 and

MG (5.58 nm), meaning that FP-MG allows for a wider range of distance at which FRET is

detectable compared to ECFP and EYFP. Finally, the FP-FAP system can be applied to the

same range of biological applications as the expression of fluorescent proteins, while

the FAP and fluorogen variants increase the versatility of this tool. Taken together, the

benefits offered by the FP-FAP FRET system are clear and can expand the use of FRET

beyond the traditional capacity.

Chapter 5

Future directions

5.1 Introduction to IgE, FcɛR1, and signaling proteins

Thorough characterization of the proof-of-concept constructs, provides confidence that the FP-FAP system can be applied to investigate biological interactions to simplify calculating FRET between proteins of interest. The Lidke lab studies signaling of the high affinity IgE receptor, FcɛRI, and while the signaling players have been identified the kinetics of these interactions remain unknown. The ability to measure transient interactions that occur between proteins in living cells is incredibly challenging and requires techniques such as FRET to confirm specific interactions. The FP-FAP FRET system simplifies acquisition and calculation of FRET data compared to traditional FRET methods, and can be applied to study signaling proteins associated with FcɛRI.

The FcɛRI is a multi-chain immune recognition receptor, a family of membrane spanning receptors that contain an extracellular ligand binding region and an intracellular signaling motif, the immunoreceptor tyrosine-based activation motif (ITAM) (Figure 5.1 A). ITAMs are sites of tyrosine phosphorylation commonly found on immune cells, including B cells and T cells, and are essential for appropriate reactions to the environment and communication between cells. For example, antigen binding to IgE on the FcɛRI results in several kinases binding to and phosphorylating the ITAM, initiating a signaling cascade that concludes with degranulation.
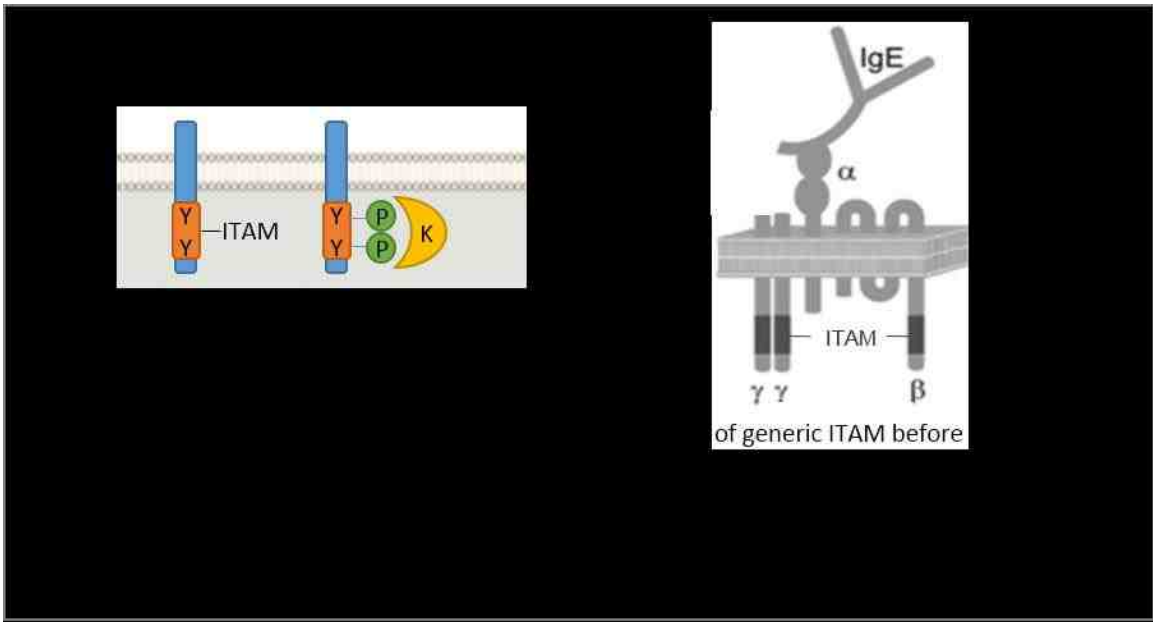
FcεRI is found on the surface of mast cells and basophils, which are white blood cells involved during an immune reaction through the release of granules containing cytokines and mediators of an allergic response. The receptor is a tetramer, composed of an α-chain, β-chain, and two γ-chains (Figure 5.1 B). The α-chain has a long extracellular portion that binds the Fc region of IgE with high affinity. The β and γ subunits each contain an ITAM for signaling upon receptor activation, leading to degranulation (Kraft & Kinet, 2007).

Two kinases involved in the initial signaling events of the IgE receptor are Lyn and Syk. Lyn is a Src family kinase approximately 55 kDa with an SH4 domain that results in association with the beta subunit of the IgE receptor in resting mast cells, and an SH2 domain that can phosphorylate tyrosine residues within ITAMs of β and γ subunits of cross-linked IgE receptors (Ortega et al., 1999; Vonakis et al., 2005). Additionally, Lyn can be found in membrane domains due to myristoylation of the protein (Wilson,

Pfeiffer, & Oliver, 2000). Syk is another kinase within the Src family that is approximately 72 kDa and contains two SH2 domains that can bind to the ITAM residues phosphorylated by Lyn. Binding of Syk to the IgE receptor tail leads to activation of the enzyme and downstream signaling. It is an essential signaling protein that when active, eventually results in cellular degranulation (Siraganian, Zhang, Suzuki, & Sada, 2001). We can express the FP-FAP components on these two proteins to measure their activity when the IgE receptor is activated.

The Bruchez lab has developed a number of constructs to study IgE receptor signaling (Table 5.1). Will Kanagy, a graduate student the Lidke lab, has transfected most of these constructs in RBL cells and evaluated them for proper expression. All have shown proper localization and response to receptor activation except Lyn-FAP, FcεR1-γ-FAP, and FAP-LAT, which still need to be optimized and are indicated with an asterisk in Table 5.1, while plasmids that have not been tested are indicated with two asterisks.

Plasmid Name	Plasmid Detail
FAP-GPI	(pcDNA-kappa-myc-dL5-2XG4S-GPI)
FAP-GPI **	(pBABE-kappa-myc-dL5-2XG4S-TM)
mCer-GPI	(pcDNA-kappa-myc-mCer3-2XG4S-GPI)
YFP-GPI	(pcDNA-kappa-myc-SYFP2-2XG4S-GPI)
FAP-FcεRI-γ	(pcDNA-kappa-HA-dL5-HA-FcERI-γ)
FcεRI-γ-dKFAP**	(pcDNA-KozATG-rFcεRIγ SP-rFcεRIγ-2XG4S-dKFAP)
FcεRI-γ-FAP*	(pcDNA-KozATG-rFcεRI-γ SP-rFcεRI-γ-2XG4S-dL5)
FcεRI-γ-mCer	(pcDNA-KozATG-rFcεRI-γ SP-rFcεRI-γ-2XG4S-mCer3)
Syk-FAP	(pcDNA-KozATG-myc-WTSyk-2XG4S-dL5)
Syk-dKFAP**	(pcDNA-KozATG-myc-WTSyk-2XG4S-dKFAP)
Syk-mCer	(pcDNA-KozATG-WTSyk-2XG4S-mCer)
Y130ESyk-mCer**	(pcDNA-KozATG-Y130ESyk-2XG4S-mCer)
Lyn-FAP*	(pcDNA-KozATG-Lyn-2XG4S-dL5)
Lyn-dKFAP**	(pcDNA-KozATG-Lyn-2XG4S-dKFAP)
FAP-LAT*	(pcDNA-kappa-myc-dL5-2XG4S-mmLAT)

5.2 Examining the association of Lyn with FcεRI

There are several questions surrounding the interactions of Lyn and the IgE receptor

that can be addressed using FAP-FP FRET, including confirming association of the two in

resting cells, determining if there is an increase in Lyn recruitment upon stimulation,

and understanding whether Lyn remains associated with the receptor or becomes

excluded after receptor aggregation. Wilson et al. has shown that Lyn is associated with

the beta subunit of the IgE receptor under resting conditions (Wilson et al., 2000). To

71

investigate this first question, we will transfect the Lyn-FAP construct and the FcεR1-γ-mCerulean3 into RBL cells. Using a Leica SP8 confocal microscope for intensity based FRET measurements in photon counting mode, we will take advantage of the ability to withhold the acceptor and acquire donor only images to get a baseline level of no FRET. We can then add the acceptor and acquire images to measure the FRET efficiency of mCerulean with MG in resting cells (Figure 5.2 A). As the association of Lyn with FcεRI-γ occurs at the membrane, these images can be analyzed using the membrane masking code as well as looking directly at changes in intensity in the FRET channel.
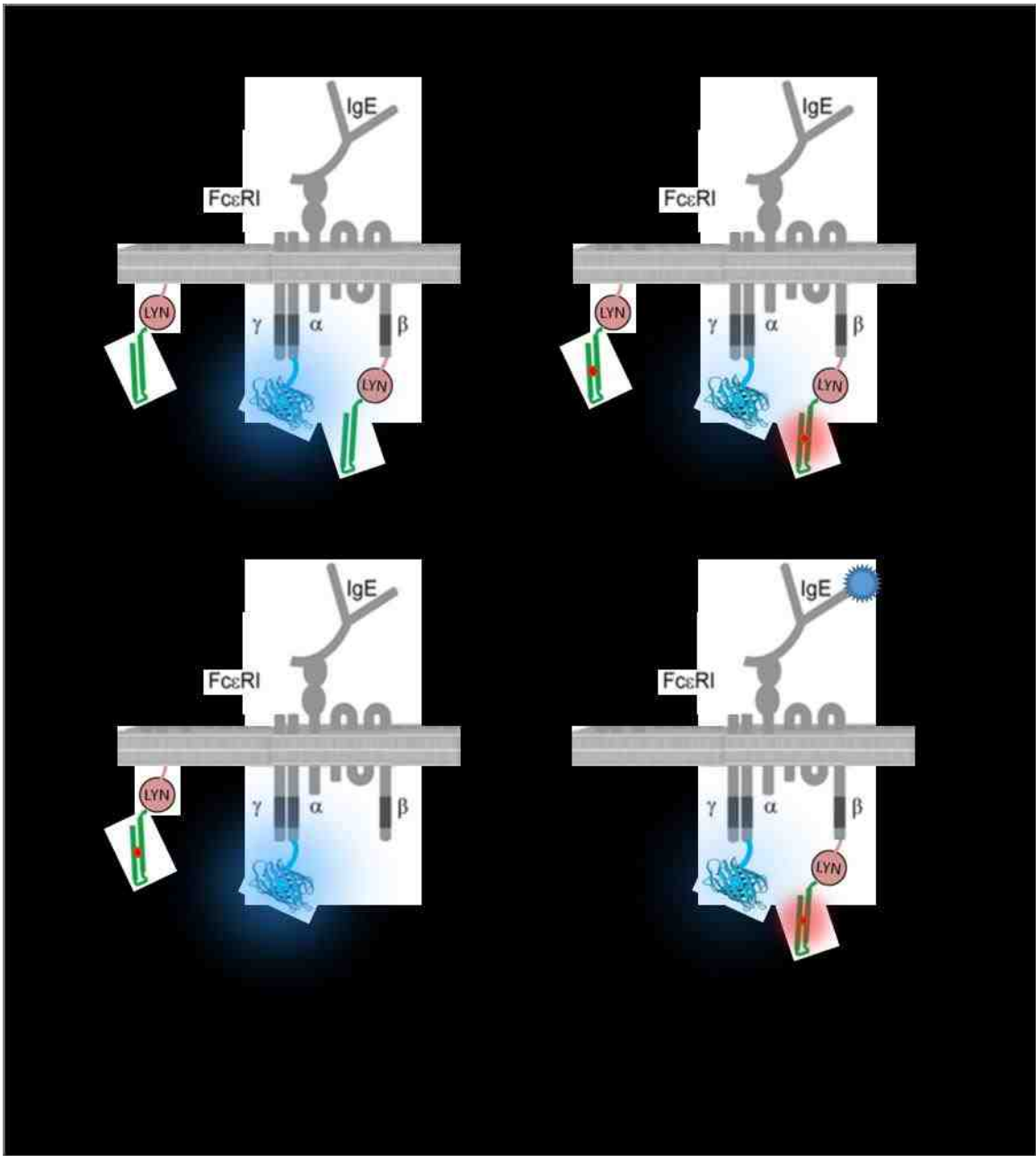
To investigate additional recruitment of Lyn after receptor activation, it is essential to measure changes in FRET between Lyn and the IgE receptor in live cells, acquiring images continuously over time. Generating intensity based FRET data to monitor recruitment is preferred as acquisition of FLIM and spectral images would take longer and could potentially miss the graduated increase in FRET signal. We will use RBL cells

and the same Lyn-FAP/ FcεRI-γ-mCerulean3 constructs from the first experiment to monitor changes in FRET after receptor crosslinking. We can acquire a donor only image at the beginning of the time series but it is necessary to add the acceptor before adding the crosslinker to measure the baseline FRET signal before activation. Additionally, the FAP is intracellular and therefore we will need to use the membrane permeable dye and wait 15 min to acquire the first donor with acceptor baseline image. This also means that the donor only image used to calculate FRET efficiency would not be available throughout the time series and it will be important to take advantage of the large Stokes shift between the donor and acceptor to directly monitor an increase of sensitized emission of MG over time (Figure 5.2 B). Any background or cross-talk is determined from images acquired before adding dye, which can be subtracted and average intensity from the FRET channel can be plotted over time.

It will be interesting to determine if FRET between Lyn and FcεRI-γ increases overtime and then reaches either a plateau or a peak followed by a decrease in FRET signal, indicating possible dissociation of Lyn from the receptor tail. Ortega et al. has shown evidence for this to occur (Ortega et al., 1999). Additionally, does the plateau or peak FRET signal coincide with the rate and size of receptor clustering? Receptor clustering can be measured using intensity and spatial data from the FcεRI-γ-mCerulean3 channel and compared to the FRET channel across time. Once the kinetics have been elucidated, additional FRET methods can be implored to investigate the level of Lyn dissociation from the receptor. Using the same cells and constructs as in the previous experiments and with a better understanding of the kinetics, cells can be fixed at critical time points

to allow for donor only (no fluorogen) and donor with acceptor (fluorogen added) to calculate FRET efficiency over time. If Lyn does disassociate from the receptor at some point after activation, we should see a decrease in FRET efficiency when Lyn is no longer associated. These experiments would strengthen the results from the live cell time series FRET data and confirm that a decrease in signal was not due to photobleaching over time.

5.3 Determining resting interactions of Syk with FcεRI and kinetics during activation

Investigating the specific interactions of Syk with FcεRI-γ is also of interest. If Lyn does FRET with the receptor tail in resting cells, this could indicate there are phosphorylated sites for Syk to bind in resting cells, and as Syk is critical for signal propagation, this is an important question to address. Live cell FRET imaging could capture these transient interactions in resting cells. As the association of Syk with the IgE receptor tail in unstimulated cells is thought to be infrequent and transient, it may be easiest to begin by measuring this potential interaction in fixed cells to get an estimate of the percentage of receptors associating with Syk at any given time. As FLIM is a relatively simple method to provide localized FRET measurements, this would be the preferred technique for these initial experiments, and as the cells are fixed, there is no concern about acquisition time. The Bruchez lab is currently developing an FcεRI-γ-YFP construct that could be used with Syk-FAP to measure FLIM FRET in fixed and unstimulated RBL cells.

We are also interested in the kinetics of Syk binding after activation and want to compare the accumulation of Syk at the receptor tail over time with the FRET data from Lyn. Using the FcεR1-γ-mCerulean and Syk-FAP constructs and following the same protocol for intensity based live cell FRET as used to acquire the kinetic data for Lyn would allow for this comparison. It will be interesting to see if Lyn and Syk are recruited to the receptor tail on the same time and at similar levels, or will it be possible to see that Lyn binds at earlier time points compared to Syk and potentially with differences in sensitize emission (Figure 5.3). FLIM-FRET could be used to determine if differences in the FRET signal were due to distance or protein concentration, as lifetime is insensitive to concentration.
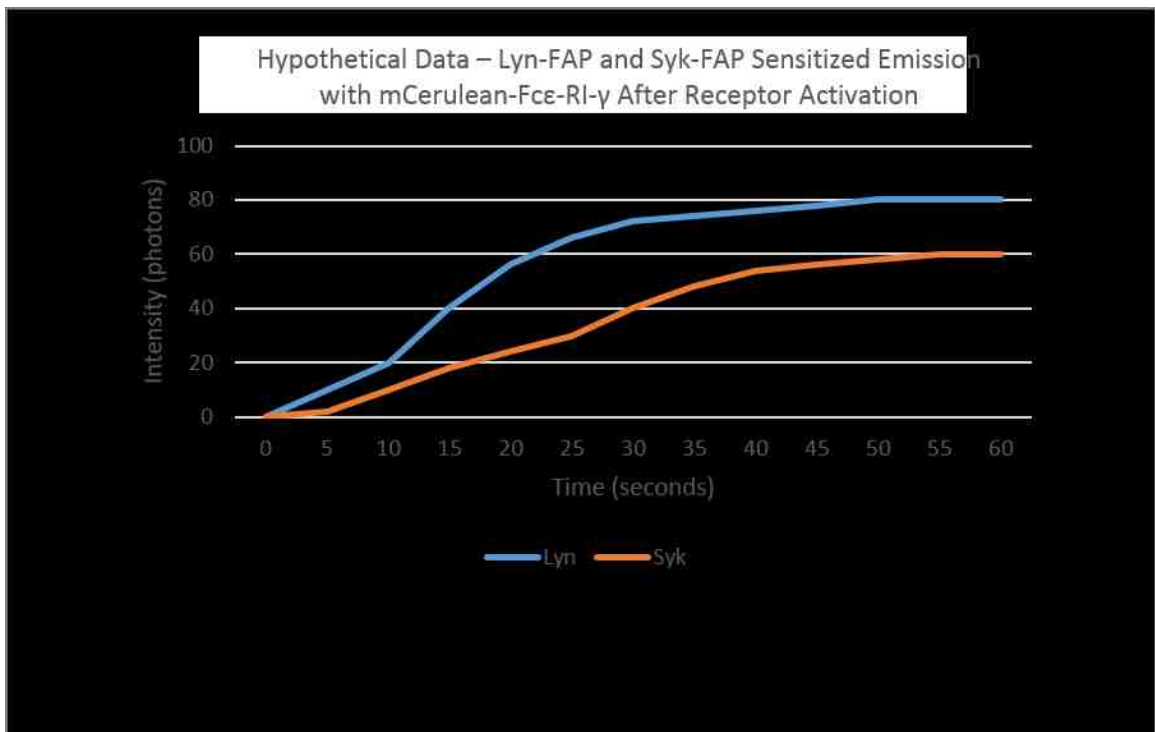
5.4 Using FAP-FP FRET to investigate the relationship between cluster size and signaling

The details of receptor clustering after activation is not well understood. It is known that cluster size increases with dose whereas degranulation occurs once antigen reaches a threshold (Andrews et al., 2009). We would like to use FAP-FP FRET to investigate recruitment of Lyn and Syk to the IgE receptor as a function of antigen dose and valency to better understand the signaling response to cluster size. Does recruitment of these kinase increase with cluster size, follow a similar pattern as degranulation, or something unique?

To answer this question, we will use live cells to measure the accumulation of FRET signal between FcεR1-γ-FP and either Lyn-FAP or Syk-FAP after activation, using a range of antigen doses (0, 0.001, 0.01, 0.1, 1, 3, and 10 µg/ml DNP-BSA) as well as antigens of low, medium, and high valency, such as DNP_4-BSA, DNP_{12}-BSA, DNP_{25}-BSA, respectively. As we will be investigating FRET signal at receptor clusters, it will be advantages to use FLIM to acquire localized FRET data, and as clusters form on a relatively long time scale, approximately 2 min, FLIM will be fast enough to capture these events. Another advantage of using FLIM is the lifetime of the donor is not expected to change under the various conditions so donor alone data is not necessary to acquire throughout the time series. We can acquire control FLIM time series data without the acceptor at several doses and with different antigens to confirm this, and then simply monitor the change in lifetime when FRET is occurring. It will be interesting to see if the change in donor lifetime, mCerulean3 on the receptor tail, is different for the different acceptor kinases,

either Lyn or Syk, and to characterize the recruitment pattern of each under the different antigen conditions.

If we find evidence of FRET between Syk and the IgE receptor tail in resting cells, it will be important to determine the length of these interactions, requiring live cell single molecule FRET measurements. FcεRI and the signaling molecules that interact with the receptor are all events that occur at the cell membrane, therefore TIRF can be used to image protein-protein interactions through FRET in live cells at the single molecule level. It will be important to image continuously over time to possibly capture these interactions. Using the FcεR1-γ-mCerulean and Syk-FAP constructs in live unstimulated RBL cells, we can acquire an image of donor alone, add the membrane permeable acceptor, wait 15 min, and then acquire images continuously until reaching the limit of photobleaching. Similar to the Lyn live cell FRET images, the FRET channel would be directly analyzed to identify any interactions and determine their length of time. Overall, there are many applications of the FP-FAP FRET system including the experiments described here to study the kinetics of FcεRI signaling molecules.

Chapter 6

Setting up TIRF for single molecule FRET

6.1 Using TIRF for single-molecule FRET

As described in the introduction, TIRF allows for imaging of fluorescence at the
coverslip-cell membrane interface by adjusting the angle of the laser through the
objective such that only molecules within approximately 200 nm of the coverslip are
excited. This optical section is much thinner than what can be achieved using a confocal
microscope and is the preferred imaging technique to examine events occurring at the
basal membrane. We can use TIRF to observe single molecule FRET and measure the
kinetics of signaling proteins with the FcεR1-gamma subunit. An EM-CCD camera is used
to collect fluorescence and can detect very low signal, a significant advantage when
measuring FRET at the single molecule level with even fewer photons than ensemble
FRET. Single molecule FRET can provide detail about the length of time that Syk or Lyn
associates with the IgE receptor tail. TIRF allows for proper tracking of single molecules
by restricting illumination to a thin optical section and eliminating background that
would obstruct protein localization.

6.2 Redesigning the optics on the Olympus IX-71

The Olympus IX-71 in the Cancer Center Microscopy Facility has been set up for TIRF but
needed to be updated. The two original lasers had been used in Keith Lidke's lab and
donated to the facility but were not performing optimally. The 472 nm laser was very
unstable and continuously fluctuated power while the 635 nm laser power output was

too low; both lasers needed to be replaced. It was also necessary to add lasers with

different wavelengths to the optical table for excitation of mCerulean and YFP to use the

TIRF microscope for FP-FAP FRET. The addition of two lasers required a number of other

components be added to the optical path, including a new optical fiber, an aspheric lens

for three of the lasers, and several mirrors and filters. The previous optical path and new

design are shown in Figure 6.1 and the new components are underlined in Figure 6.1 B.
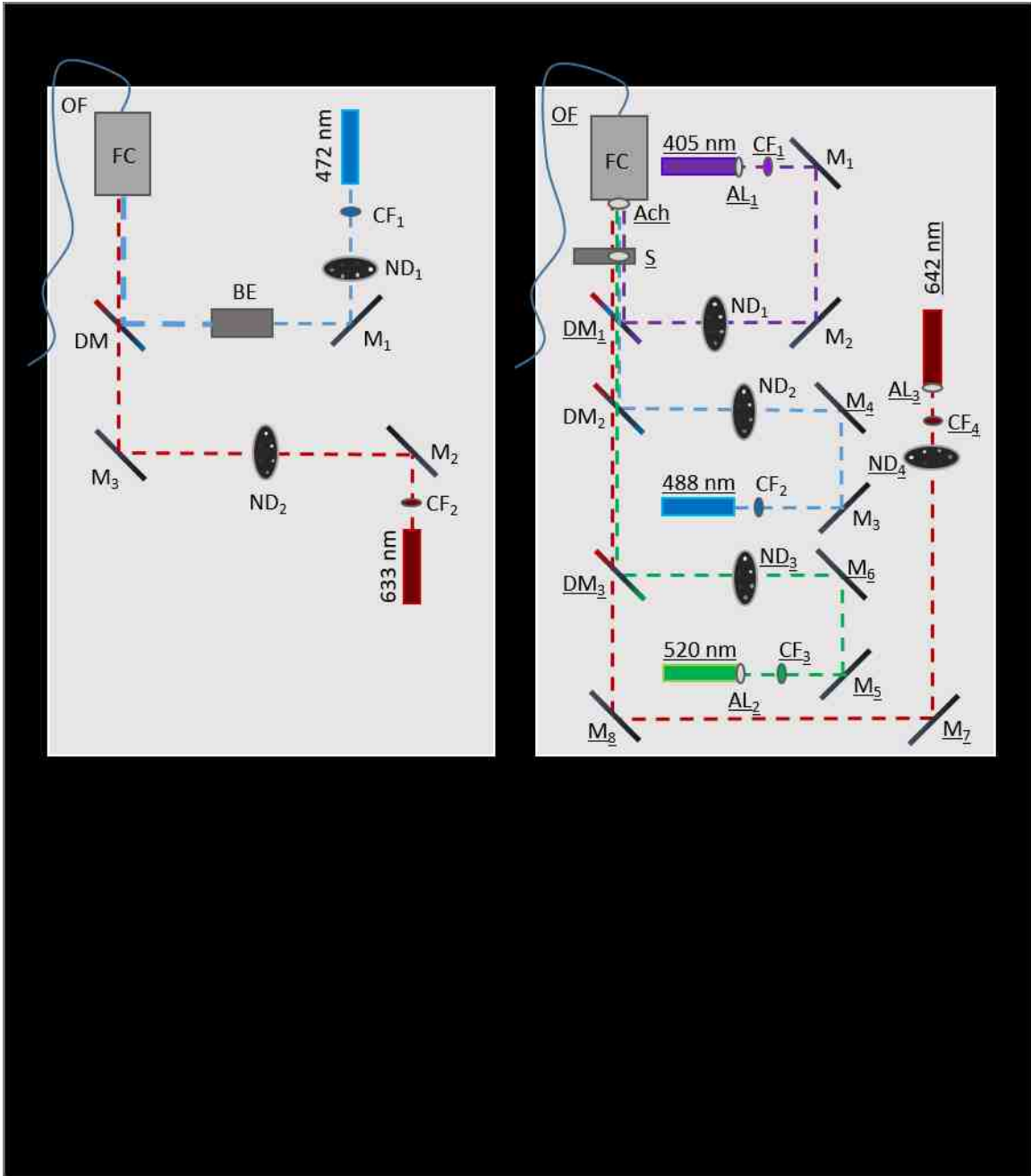
Two diode lasers, a 40 mW 405 nm and a 50 mW 520 nm, were purchased to excite

mCerulean and YFP, as well as a 150 mW 488 nm diode laser to replace the unstable 472

nm laser, and an 80 mW 642 nm diode laser to replace the 633. An electronic shutter

was purchased to quickly shutter the light during live cell experiments and can be

controlled through the imaging software. Aspheric lenses are required to collimate the

light for the 405 nm, 520 nm, and 642 nm lasers diodes. The 488 nm laser is collimated so an aspheric lens is not necessary. Calculations for the lens were based on a desired beam diameter of 1 mm. The achromatic lens corrects for the four different wavelengths coupling into the optical fiber. See supplement for lens calculations and a list of purchased parts. (S6.1 and S6.2)

To date, most of the optics have been assembled on the optical table, except the 488 nm laser, which has not yet arrived. Once the 488 nm laser has been added to the table, the lasers can be aligned to the fiber couple. The lasers can be used for excitation in either wide field or TIRF and can be broadly applied to microscopy experiments beyond single molecule FP-FAP FRET.

Supplement

S2.1 Detail of confocal imaging parameters

Confocal images were acquired with three imaging parameters at multiple positions before and after adding the fluorogen. 405 nm laser = 1%, 633 nm = 0% parameters:

Dimensions

Dimension	Logical Size	Physical Length	Start Position	End Position	Pixel Size / Voxel Size
X	1024	61.51 µm	0 µm	61.51 µm	0.06 µm
Y	1024	61.51 µm	0 µm	61.51 µm	0.06 µm
Z	1	0 µm	3.99 µm	-3.99 µm	0 µm

Channels

LUT		Resolution	Min	Max	STED: DetectorMode / Huygens saturation factor / Wavelength
Cyan		12	0	4095	--- / --- / ---
Gray		12	0	4095	--- / --- / ---

Confocal Settings

Name	Value
Rotator Angle	0 °
Scan Mode	xyz
Scan Direction X	Bidirectional
Scan Speed	400 Hz
Version Number	10
StagePosX	63367.57 µm
StagePosY	39476.63 µm
ZPosition	-3.99 µm
IsSuperZ	0
Magnification	63
ObjectiveName	HC PL APO CS2 63x/1.20 WATER
Immersion	WATER
NumericalAperture	1.2
RefractionIndex	1.33
Zoom	3
Pinhole	111.3 µm
PinholeAiry	999.01 mAU
EmissionWavelength for PinholeAiry Calculation	580 nm
FrameAverage	1
LineAverage	1
FrameAccumulation	3
Line_Accumulation	1
IsUserSettingNameSet	0
IsRoiScanEnable	0

Filter Wheels / Other Motorized Devices

Device Name	Filter Name/Position
Galvo Slider	Galvo X Normal
Notch FW 2	Empty
Polarization FW	Empty
Galvo Resonant Pan	Galvo X Pan Center
Simple Beam Expander	No FRAP Booster
Target Slider	Target Park
X2 Lens Changer	CS2 UV Optics 1

Lasers

LaserName	OutputPower
405 Diode	On
WLL	On, 70.0000 %
Argon	Off

Laser Lines

Laser Line	Intensity
UV (405 nm)	Shutter: on, Intensity: 1.0005%
Supercontinuum Visible (633 nm)	Shutter: on, Intensity: 0.0000%
Supercontinuum Visible (552 nm)	Shutter: on, Intensity: 0.0000%
Supercontinuum Visible (631 nm)	Shutter: on, Intensity: 0.0000%
Supercontinuum Visible (473 nm)	Shutter: on, Intensity: 0.0000%
Supercontinuum Visible (667 nm)	Shutter: on, Intensity: 0.0000%
Supercontinuum Visible (668 nm)	Shutter: on, Intensity: 0.0000%
Supercontinuum Visible (669 nm)	Shutter: on, Intensity: 0.0000%
Supercontinuum Visible (670 nm)	Shutter: on, Intensity: 0.0000%
Visible (458 nm)	Shutter: off, Intensity: 0.0000%
Visible (476 nm)	Shutter: off, Intensity: 0.0000%
Visible (488 nm)	Shutter: off, Intensity: 0.0000%
Visible (496 nm)	Shutter: off, Intensity: 0.0000%
Visible (514 nm)	Shutter: off, Intensity: 0.0000%

Detectors

Name	Channel	Type	Location	Active	Gain	Offset	Gate Start	Gate End	Gate Ref. Wavelength
HyD 1	Channel 1	HyD (450nm - 550nm) Counting mode	Internal	Active	10	-0.01	-- Time Gating not activated --		
HyD SMD 2	Channel 2	HyD (568nm - 574nm) Standard mode	Internal	Inactive	100	-0.01	0.6 ns	11.9 ns	633 nm
PMT 3	Channel 3	PMT (574nm - 579nm)	Internal	Inactive	0	0	-- Time Gating not supported --		
HyD SMD 4	Channel 4	HyD (579nm - 585nm) Standard mode	Internal	Inactive	100	-0.01	-- Time Gating not activated --		
HyD 5	Channel 5	HyD (640nm - 740nm) Counting mode	Internal	Active	10	-0.01	0.6 ns	11.9 ns	633 nm
PMT Trans	Transmission Channel	PMT	TLD	Inactive	296.8	0	-- Time Gating not supported --		

84

405 nm laser = 0%, 633 nm = 5% parameters:

Dimensions

Dimension	Logical Size	Physical Length	Start Position	End Position	Pixel Size / Voxel Size
X	1024	61.51 µm	0 µm	61.51 µm	0.06 µm
Y	1024	61.51 µm	0 µm	61.51 µm	0.06 µm
Z	1	0 µm	3.99 µm	-3.99 µm	0 µm

Channels

LUT		Resolution	Min	Max	STED: DetectorMode / Huygens saturation factor / Wavelength
Cyan		12	0	4095	--- / --- / ---
Gray		12	0	4095	--- / --- / ---

Confocal Settings

Name	Value
Rotator Angle	0 °
Scan Mode	xyz
Scan Direction X	Bidirectional
Scan Speed	400 Hz
Version Number	10
StagePosX	63367.57 µm
StagePosY	39476.63 µm
ZPosition	-3.99 µm
IsSuperZ	0
Magnification	63
ObjectiveName	HC PL APO CS2 63x/1.20 WATER
Immersion	WATER
NumericalAperture	1.2
RefractionIndex	1.33
Zoom	3
Pinhole	111.3 µm
PinholeAiry	999.01 mAU
EmissionWavelength for PinholeAiry Calculation	580 nm
FrameAverage	1
LineAverage	1
FrameAccumulation	3
Line_Accumulation	1
IsUserSettingNameSet	0
IsRoiScanEnable	0

Filter Wheels / Other Motorized Devices

Device Name	Filter Name/Position
Galvo Slider	Galvo X Normal
Notch FW 2	Empty
Polarization FW	NF 488/561/633
Galvo Resonant Pan	Galvo X Pan Center
Simple Beam Expander	No FRAP Booster
Target Slider	Target Park
X2 Lens Changer	CS2 UV Optics 1

Lasers

LaserName	OutputPower
405 Diode	On
WLL	On, 70.0000 %
Argon	Off

Laser Lines

Laser Line	Intensity
UV (405 nm)	Shutter: on, Intensity: 0.0000%
Supercontinuum Visible (633 nm)	Shutter: on, Intensity: 4.9998%
Supercontinuum Visible (552 nm)	Shutter: on, Intensity: 0.0000%
Supercontinuum Visible (631 nm)	Shutter: on, Intensity: 0.0000%
Supercontinuum Visible (473 nm)	Shutter: on, Intensity: 0.0000%
Supercontinuum Visible (667 nm)	Shutter: on, Intensity: 0.0000%
Supercontinuum Visible (668 nm)	Shutter: on, Intensity: 0.0000%
Supercontinuum Visible (669 nm)	Shutter: on, Intensity: 0.0000%
Supercontinuum Visible (670 nm)	Shutter: on, Intensity: 0.0000%
Visible (458 nm)	Shutter: off, Intensity: 0.0000%
Visible (476 nm)	Shutter: off, Intensity: 0.0000%
Visible (488 nm)	Shutter: off, Intensity: 0.0000%
Visible (496 nm)	Shutter: off, Intensity: 0.0000%
Visible (514 nm)	Shutter: off, Intensity: 0.0000%

Detectors

Name	Channel	Type	Location	Active	Gain	Offset	Gate Start	Gate End	Gate Ref. Wavelength
HyD 1	Channel 1	HyD (450nm - 550nm) Counting mode	Internal	Active	10	-0.01	-- Time Gating not activated --		
HyD SMD 2	Channel 2	HyD (568nm - 574nm) Standard mode	Internal	Inactive	100	-0.01	0.6 ns	11.9 ns	633 nm
PMT 3	Channel 3	PMT (574nm - 579nm)	Internal	Inactive	0	0	-- Time Gating not supported --		
HyD SMD 4	Channel 4	HyD (579nm - 585nm) Standard mode	Internal	Inactive	100	-0.01	-- Time Gating not activated --		
HyD 5	Channel 5	HyD (640nm - 740nm) Counting mode	Internal	Active	10	-0.01	0.6 ns	11.9 ns	633 nm
PMT Trans	Transmission Channel	PMT	TLD	Inactive	296.8	0	-- Time Gating not supported --		

405 nm laser = 1%, 633 nm = 5% parameters:

Dimensions

Dimension	Logical Size	Physical Length	Start Position	End Position	Pixel Size / Voxel Size
X	1024	61.51 µm	0 µm	61.51 µm	0.06 µm
Y	1024	61.51 µm	0 µm	61.51 µm	0.06 µm
Z	1	0 µm	5.2 µm	-5.2 µm	0 µm

Channels

LUT		Resolution	Min	Max	STED: DetectorMode / Huygens saturation factor / Wavelength
Cyan		12	0	4095	--- / --- / ---
Gray		12	0	4095	--- / --- / ---

Confocal Settings

Name	Value
Rotator Angle	0 °
Scan Mode	xyz
Scan Direction X	Bidirectional
Scan Speed	400 Hz
Version Number	10
StagePosX	63371.26 µm
StagePosY	39499.24 µm
ZPosition	-5.2 µm
IsSuperZ	0
Magnification	63
ObjectiveName	HC PL APO CS2 63x/1.20 WATER
Immersion	WATER
NumericalAperture	1.2
RefractionIndex	1.33
Zoom	3
Pinhole	111.3 µm
PinholeAiry	999.01 mAU
EmissionWavelength for PinholeAiry Calculation	580 nm
FrameAverage	1
LineAverage	1
FrameAccumulation	3
Line_Accumulation	1
IsUserSettingNameSet	0
IsRoiScanEnable	0

Filter Wheels / Other Motorized Devices

Device Name	Filter Name/Position
Galvo Slider	Galvo X Normal
Notch FW 2	Empty
Polarization FW	NF 488/561/633
Galvo Resonant Pan	Galvo X Pan Center
Simple Beam Expander	No FRAP Booster
Target Slider	Target Park
X2 Lens Changer	CS2 UV Optics 1

Lasers

LaserName	OutputPower
405 Diode	On
WLL	On, 70.0000 %
Argon	Off

Laser Lines

Laser Line	Intensity
UV (405 nm)	Shutter: on, Intensity: 1.0005%
Supercontinuum Visible (633 nm)	Shutter: on, Intensity: 4.9998%
Supercontinuum Visible (552 nm)	Shutter: on, Intensity: 0.0000%
Supercontinuum Visible (631 nm)	Shutter: on, Intensity: 0.0000%
Supercontinuum Visible (473 nm)	Shutter: on, Intensity: 0.0000%
Supercontinuum Visible (667 nm)	Shutter: on, Intensity: 0.0000%
Supercontinuum Visible (668 nm)	Shutter: on, Intensity: 0.0000%
Supercontinuum Visible (669 nm)	Shutter: on, Intensity: 0.0000%
Supercontinuum Visible (670 nm)	Shutter: on, Intensity: 0.0000%
Visible (458 nm)	Shutter: off, Intensity: 0.0000%
Visible (476 nm)	Shutter: off, Intensity: 0.0000%
Visible (488 nm)	Shutter: off, Intensity: 0.0000%
Visible (496 nm)	Shutter: off, Intensity: 0.0000%
Visible (514 nm)	Shutter: off, Intensity: 0.0000%

Detectors

Name	Channel	Type	Location	Active	Gain	Offset	Gate Start	Gate End	Gate Ref. Wavelength
HyD 1	Channel 1	HyD (450nm - 550nm) Counting mode	Internal	Active	10	-0.01	-- Time Gating not activated --		
HyD SMD 2	Channel 2	HyD (568nm - 574nm) Standard mode	Internal	Inactive	100	-0.01	0.6 ns	11.9 ns	633 nm
PMT 3	Channel 3	PMT (574nm - 579nm)	Internal	Inactive	0	0	-- Time Gating not supported --		
HyD SMD 4	Channel 4	HyD (579nm - 585nm) Standard mode	Internal	Inactive	100	-0.01	-- Time Gating not activated --		
HyD 5	Channel 5	HyD (640nm - 740nm) Counting mode	Internal	Active	10	-0.01	0.6 ns	11.9 ns	633 nm
PMT Trans	Transmission Channel	PMT	TLD	Inactive	296.8	0	-- Time Gating not supported --		

These parameters were repeated over the same positions after adding dye, which was additionally repeated for cells expressing FAP-TM-mCer and FAP-mCer-TM.

S2.2 Matlab script

Script to extract original Leica images (.lif) and run the "createMembraneMask" script:

```matlab
1    % input params
2    % script for extracting and matching masks for 'multi-position' data on
3    % Leica. Creates appropriate file name and calls the createMembraneMask
4    % function on those images.
5
6    datadir = 'G:\Leica data\8-9-16';% location of .lif files
7    lif_filename = '8-11-16 HeLa MG-bTau_405-1_633-off ONLY.lif';% .lif file
8    %names -can make cell array of names or use uigetfiles to select
9    savedir = 'G:\Leica data\8-9-16\MC code analysis\8-11-16';
10   savestr = '160811'; % any addition info to be included in the savestr
11   coverslip_name = {'HeLa_SamI_','HeLa_SamII_'};
12   dye_types = {'MG-bTau','MG-bTau'};
13
14   membranethickness = {50,25,15};
15
16   assert(numel(coverslip_name)==numel(dye_types));
17   lifObj = lif(datadir,lif_filename);
18   % first we want to find the before and after dye files to match up for the
19   % particular coverslip
20   for cc = 1: numel(coverslip_name) %--- for loop over each coverslip name---
21   % extrac only those files from this coverslip
22   covsl_idx = cellfun(@(x) strfind(x,coverslip_name{cc}),lifObj.SeriesName,
23   'UniformOutput',false);
24   covsl_id = find(cell2mat(cellfun(@(x) ~isempty(x),covsl_idx,
25   'UniformOutput',false)));
26   for ii = covsl_id(1:numel(covsl_id)/2)' % loop of each position, make both
27       %files masks and save
28       pos = lifObj.SeriesName{ii}(strfind(lifObj.SeriesName{ii},'Position')
29       :end);
30       svnm = [coverslip_name{cc} dye_types{cc} savestr pos];
31       % pre file is lifObj series(covsl_id)
32       lif_im_predye = lifObj.loadSeries(ii); %lif_im_predye(:,:,1) is mCer
33       %channel
34       lif_im_postdye = lifObj.loadSeries(ii+numel(covsl_id)/2); % post file
35       %is id of pre file plus half the number of total series
36       for mm = 1:numel(membranethickness)
37       savename1 = fullfile([svnm 'MemThick=' num2str(membranethickness{mm})
38           '_predye']);
39       createMembraneMask(lif_im_predye(:,:,1),savename1,savedir,
40       membranethickness{mm})
41       savename2 = fullfile([svnm 'MemThick=' num2str(membranethickness{mm})
42           '_postdye']);
43       createMembraneMask(lif_im_postdye(:,:,1),savename2,savedir,
44       membranethickness{mm})
45       end
46
47   end
48   end
```

"createMembraneMask" script:

```
1   function createMembraneMask(im,filename,savedir,membranethickness)
2   % This function takes in an image im and generates a series of masks
3   % for isolating the membrane - later used for calculating FRET
4   % im: 2D grey image to threshold
5   % membranethickness: input for masking
6   % filename: filename to save the resulting masks
7   % savedir: directory where filename should be saved
8   % file will have following variables:
9       % im: 2D double grey valued image
10      % ThickMembraneMask: 2D binary mask of thick crude membrane mask
11      % CytoMask: 2D binary mask of the cytosol'
12      % MaskFullCell: 2D binary mask of thresholde of full cell
13      % MembraneMask: resulting membranemask
14      % params: structure with all parameters used to calculate masks
15  if nargin<4
16      membranethickness = 20;
17  end
18  %-- input params
19  params.erosionPar1 = 40;
20  params.erosionPar2 = 40;
21  params.MinPix = 1000;
22  params.thresholdParameter = Inf;
23  params.fillholes = 2;
24  params.membranethickness = membranethickness;
25
26  %--- find crude mask
27  [out,~] = threshold(im,'isodata',params.thresholdParameter);
28  out2=berosion(bdilation(out,params.erosionPar1),params.erosionPar2);
29  CM=fillholes(out2,params.fillholes);
30  %get rid of small objects
31  LI=label(CM);
32  for ii=1:max(LI)
33      if sum(LI==ii)<params.MinPix
34          LI(LI==ii)=0;
35      end
36  end
37  Mask=LI>0;
38  DTim=dt(Mask);
39  %now do distance transform
40  ThickMembraneMask = (DTim<params.membranethickness)&(DTim>0);
41
42  %--- get cytosolic mask
43  FullCellMask = threshold(im,'isodata',params.thresholdParameter);
44  CytoMask = FullCellMask - ThickMembraneMask;
```

```
45
46     %--- make membrane mask
47 -   MembraneMask = FullCellMask - CytoMask;
48 -   FinalMembrane = im.*MembraneMask;
49
50     %--- save results
51     save(fullfile(savedir,filename),'im','FinalMembrane','MembraneMask',
52     'CytoMask','FullCellMask','ThickMembraneMask','params');
53     % png files:
54     % --original image
55 -   dip_image(im)
56 -   saveas(gcf,fullfile(savedir,[filename '_image']),'png');
57 -   close(gcf);
58     % --membrane mask over original image
59 -   overlay(im,MembraneMask)
60 -   saveas(gcf,fullfile(savedir,[filename '_overlay']),'png');
61 -   close(gcf);
62     % -- final membrane
63 -   FinalMembrane
64 -   saveas(gcf,fullfile(savedir,[filename '_FinalMembrane']),'png');
65 -   close(gcf);
66     % --FullCellMask
67 -   FullCellMask
68 -   saveas(gcf,fullfile(savedir,[filename '_FullCellMask']),'png');
69 -   close(gcf);
70     % --Membrane Mask
71 -   MembraneMask
72 -   saveas(gcf,fullfile(savedir,[filename '_MembraneMask']),'png');
73 -   close(gcf);
74     % --Cyto Mask
75 -   CytoMask
76 -   saveas(gcf,fullfile(savedir,[filename '_CytoMask']),'png');
77 -   close(gcf);
78     % --ThickMembrane Mask
79 -   ThickMembraneMask
80 -   saveas(gcf,fullfile(savedir,[filename '_ThickMembrane']),'png');
81 -   close(gcf);
82 -   end
```

S2.3 Detail of spectral imaging parameters

Spectral confocal images were acquired with two imaging parameters before and after

adding the fluorogen. 405 nm laser = 1%, emission 450 nm – 750 nm:

Dimensions

Dimension	Logical Size	Physical Length	Start Position	End Position	Pixel Size / Voxel Size
X	1024	92.26 µm	0 µm	92.26 µm	0.09 µm
Y	1024	92.26 µm	0 µm	92.26 µm	0.09 µm
Lambda	29	0.28 µm	0.45 µm	0.73 µm	µm

Channels

LUT		Resolution	Min	Max	STED: DetectorMode / Huygens saturation factor / Wavelength
Cyan		12	0	4095	--- / --- / ---

Confocal Settings

Name	Value
Rotator Angle	0 °
Scan Mode	xyλ
Scan Direction X	Bidirectional
Scan Speed	400 Hz
Version Number	10
StagePosX	78966.88 µm
StagePosY	40315.51 µm
ZPosition	-8.36 µm
IsSuperZ	0
Magnification	63
ObjectiveName	HC PL APO CS2 63x/1.20 WATER
Immersion	WATER
NumericalAperture	1.2
RefractionIndex	1.33
Zoom	2
Pinhole	111.3 µm
PinholeAiry	999.01 mAU
EmissionWavelength for PinholeAiry Calculation	580 nm
FrameAverage	1
LineAverage	1
FrameAccumulation	3
Line_Accumulation	1
IsUserSettingNameSet	0
IsRoiScanEnable	0

Filter Wheels / Other Motorized Devices

Device Name	Filter Name/Position
Galvo Slider	Galvo X Normal
Notch FW 2	Empty
Polarization FW	Empty
Galvo Resonant Pan	Galvo X Pan Center
Simple Beam Expander	No FRAP Booster
Target Slider	Target Park
X2 Lens Changer	CS2 UV Optics 1

Lasers

LaserName	OutputPower
405 Diode	On
WLL	On, 70.0000 %
Argon	Off

Laser Lines

Laser Line	Intensity
UV (405 nm)	Shutter: on, Intensity: 1.0005%
Supercontinuum Visible (633 nm)	Shutter: on, Intensity: 0.0000%
Supercontinuum Visible (552 nm)	Shutter: on, Intensity: 0.0000%
Supercontinuum Visible (631 nm)	Shutter: on, Intensity: 0.0000%
Supercontinuum Visible (473 nm)	Shutter: on, Intensity: 0.0000%
Supercontinuum Visible (667 nm)	Shutter: on, Intensity: 0.0000%
Supercontinuum Visible (668 nm)	Shutter: on, Intensity: 0.0000%
Supercontinuum Visible (669 nm)	Shutter: on, Intensity: 0.0000%
Supercontinuum Visible (670 nm)	Shutter: on, Intensity: 0.0000%
Visible (458 nm)	Shutter: off, Intensity: 0.0000%
Visible (476 nm)	Shutter: off, Intensity: 0.0000%
Visible (488 nm)	Shutter: off, Intensity: 0.0000%
Visible (496 nm)	Shutter: off, Intensity: 0.0000%
Visible (514 nm)	Shutter: off, Intensity: 0.0000%

Detectors

Name	Channel	Type	Location	Active	Gain	Offset	Gate Start	Gate End	Gate Ref. Wavelength
HyD 1	Channel 1	HyD (640nm - 660nm) Counting mode	Internal	Active	10	-0.01	-- Time Gating not activated --		
HyD SMD 2	Channel 2	HyD (780nm - 785nm) Standard mode	Internal	Inactive	100	-0.01	0.6 ns	11.9 ns	633 nm
PMT 3	Channel 3	PMT (785nm - 790nm)	Internal	Inactive	0	0	-- Time Gating not supported --		
HyD SMD 4	Channel 4	HyD (790nm - 795nm) Standard mode	Internal	Inactive	100	-0.01	-- Time Gating not activated --		
HyD 5	Channel 5	HyD (795nm - 800nm) Counting mode	Internal	Inactive	10	-0.01	0.6 ns	11.9 ns	633 nm
PMT Trans	Transmission Channel	PMT	TLD	Inactive	296.8	0	-- Time Gating not supported --		

93

633 nm laser = 5%, emission 640 nm – 750 nm:

Dimensions

Dimension	Logical Size	Physical Length	Start Position	End Position	Pixel Size / Voxel Size
X	1024	92.26 µm	0 µm	92.26 µm	0.09 µm
Y	1024	92.26 µm	0 µm	92.26 µm	0.09 µm
Lambda	10	0.09 µm	0.64 µm	0.73 µm	µm

Channels

LUT		Resolution	Min	Max	STED: DetectorMode / Huygens saturation factor / Wavelength
Cyan		12	0	4095	--- / --- / ---

Confocal Settings

Name	Value
Rotator Angle	0 °
Scan Mode	xyλ
Scan Direction X	Bidirectional
Scan Speed	400 Hz
Version Number	10
StagePosX	78966.88 µm
StagePosY	40315.51 µm
ZPosition	-8.36 µm
IsSuperZ	0
Magnification	63
ObjectiveName	HC PL APO CS2 63x/1.20 WATER
Immersion	WATER
NumericalAperture	1.2
RefractionIndex	1.33
Zoom	2
Pinhole	111.3 µm
PinholeAiry	999.01 mAU
EmissionWavelength for PinholeAiry Calculation	580 nm
FrameAverage	1
LineAverage	1
FrameAccumulation	3
Line_Accumulation	1
IsUserSettingNameSet	0
IsRoiScanEnable	0

Filter Wheels / Other Motorized Devices

Device Name	Filter Name/Position
Galvo Slider	Galvo X Normal
Notch FW 2	Empty
Polarization FW	NF 488/561/633
Galvo Resonant Pan	Galvo X Pan Center
Simple Beam Expander	No FRAP Booster
Target Slider	Target Park
X2 Lens Changer	CS2 UV Optics 1

Lasers

LaserName	OutputPower
405 Diode	**On**
WLL	**On, 70.0000 %**
Argon	**Off**

Laser Lines

Laser Line	Intensity
UV (405 nm)	Shutter: on, Intensity: 0.0000%
Supercontinuum Visible (633 nm)	Shutter: on, Intensity: 4.9998%
Supercontinuum Visible (552 nm)	Shutter: on, Intensity: 0.0000%
Supercontinuum Visible (631 nm)	Shutter: on, Intensity: 0.0000%
Supercontinuum Visible (473 nm)	Shutter: on, Intensity: 0.0000%
Supercontinuum Visible (667 nm)	Shutter: on, Intensity: 0.0000%
Supercontinuum Visible (668 nm)	Shutter: on, Intensity: 0.0000%
Supercontinuum Visible (669 nm)	Shutter: on, Intensity: 0.0000%
Supercontinuum Visible (670 nm)	Shutter: on, Intensity: 0.0000%
Visible (458 nm)	Shutter: off, Intensity: 0.0000%
Visible (476 nm)	Shutter: off, Intensity: 0.0000%
Visible (488 nm)	Shutter: off, Intensity: 0.0000%
Visible (496 nm)	Shutter: off, Intensity: 0.0000%
Visible (514 nm)	Shutter: off, Intensity: 0.0000%

Detectors

Name	Channel	Type	Location	Active	Gain	Offset	Gate Start	Gate End	Gate Ref. Wavelength
HyD 1	Channel 1	HyD (730nm - 750nm) Counting mode	Internal	Active	10	-0.01	-- Time Gating not activated --		
HyD SMD 2	Channel 2	HyD (780nm - 785nm) Standard mode	Internal	Inactive	100	-0.01	0.6 ns	11.9 ns	633 nm
PMT 3	Channel 3	PMT (785nm - 790nm)	Internal	Inactive	0	0	-- Time Gating not supported --		
HyD SMD 4	Channel 4	HyD (790nm - 795nm) Standard mode	Internal	Inactive	100	-0.01	-- Time Gating not activated --		
HyD 5	Channel 5	HyD (795nm - 800nm) Counting mode	Internal	Inactive	10	-0.01	0.6 ns	11.9 ns	633 nm
PMT Trans	Transmission Channel	PMT	TLD	Inactive	296.8	0	-- Time Gating not supported --		

S2.4 Detail of FLIM imaging parameters

FLIM images were acquired with the following imaging parameters before and after

adding the fluorogen:

Dimensions

Dimension	Logical Size	Physical Length	Start Position	End Position	Pixel Size / Voxel Size
X	256	61.51 µm	0 µm	61.51 µm	0.241 µm
Y	256	61.51 µm	0 µm	61.51 µm	0.241 µm
Z	1	0 µm	4.73 µm	-4.73 µm	0 µm

Channels

LUT		Resolution	Min	Max	STED: DetectorMode / Huygens saturation factor / Wavelength
Green		8	0	255	--- / --- / ---

Confocal Settings

Name	Value
Rotator Angle	0 °
Scan Mode	xyz
Scan Direction X	Unidirectional
Scan Speed	200 Hz
Version Number	10
ZPosition	-4.73 µm
IsSuperZ	0
Magnification	63
ObjectiveName	HC PL APO CS2 63x/1.20 WATER
Immersion	WATER
NumericalAperture	1.2
RefractionIndex	1.33
Zoom	3
Pinhole	111.4 µm
PinholeAiry	1 AU
EmissionWavelength for PinholeAiry Calculation	580 nm
FrameAverage	16383
LineAverage	1
FrameAccumulation	1
Line_Accumulation	1
IsUserSettingNameSet	0
IsRoiScanEnable	0

Filter Wheels / Other Motorized Devices

Device Name	Filter Name/Position
Galvo Slider	Galvo X Normal
Notch FW 2	Empty
Polarization FW	NF 514
Galvo Resonant Pan	Galvo X Pan Center
Simple Beam Expander	No FRAP Booster
Target Slider	Target Park
X2 Lens Changer	CS2 UV Optics 1

Lasers

LaserName	OutputPower
405 Diode	Off
WLL	On, 70.0000 %
Argon	Off

Laser Lines

Laser Line	Intensity
UV (405 nm)	Shutter: off, Intensity: 0.0000%
Supercontinuum Visible (514 nm)	Shutter: on, Intensity: 3.5007%
Supercontinuum Visible (471 nm)	Shutter: on, Intensity: 0.0000%
Supercontinuum Visible (472 nm)	Shutter: on, Intensity: 0.0000%
Supercontinuum Visible (473 nm)	Shutter: on, Intensity: 0.0000%
Supercontinuum Visible (667 nm)	Shutter: on, Intensity: 0.0000%
Supercontinuum Visible (668 nm)	Shutter: on, Intensity: 0.0000%
Supercontinuum Visible (669 nm)	Shutter: on, Intensity: 0.0000%
Supercontinuum Visible (670 nm)	Shutter: on, Intensity: 0.0000%
Visible (458 nm)	Shutter: off, Intensity: 0.0000%
Visible (476 nm)	Shutter: off, Intensity: 0.0000%
Visible (488 nm)	Shutter: off, Intensity: 0.0000%
Visible (496 nm)	Shutter: off, Intensity: 0.0000%
Visible (514 nm)	Shutter: off, Intensity: 0.0000%

Detectors

Name	Channel	Type	Location	Active	Gain	Offset	Gate Start	Gate End	Gate Ref. Wavelength
HyD 1	Channel 1	HyD (401nm - 443nm) Standard mode	Internal	Inactive	100	-0.01			-- Time Gating not activated --
HyD SMD 2	Channel 2	HyD (520nm - 575nm) Standard mode	Internal	Active	10	-0.01			-- Time Gating not activated --
PMT 3	Channel 3	PMT (649nm - 654nm)	Internal	Inactive	0	0			-- Time Gating not supported --
HyD SMD 4	Channel 4	HyD (654nm - 696nm) Standard mode	Internal	Inactive	10	-0.01			-- Time Gating not activated --
HyD 5	Channel 5	HyD (737nm - 779nm) Standard mode	Internal	Inactive	100	-0.01			-- Time Gating not activated --
PMT Trans	Transmission Channel	PMT	TLD	Inactive	0	0			-- Time Gating not supported --

S6.1 Lens calculations for TIRF
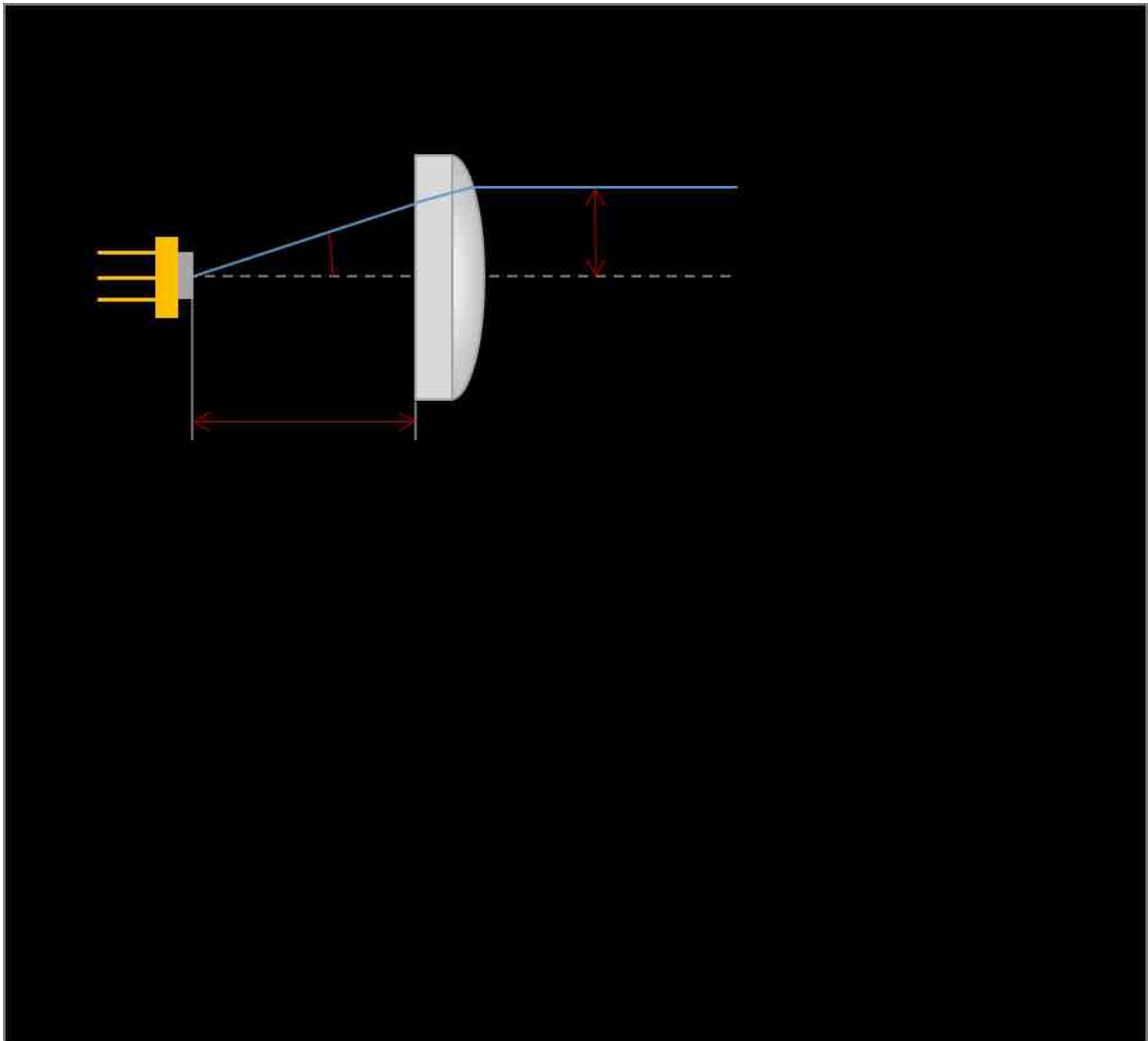
S6.2 Purchased components for TIRF

Part Description	Quantity	Company	Part Number	Price/unit	Total
achromatic lens	1	Edmund	49-270	$ 95.00	$ 95.00
aspheric lens for 405	1	Thorlabs	C110TMD-A	$ 83.30	$ 83.30
aspheric lens for 642	1	Thorlabs	C110TMD-A	$ 83.30	$ 83.30
aspheric lens for 520	1	Thorlabs	C110TMD-A	$ 83.30	$ 83.30
aspheric lens adapter	3	Thorlabs	E09RMS	$ 32.00	$ 96.00
assembly rods 4", 4 pack	1	Thorlabs	ER4-P4	$ 26.37	$ 26.37
cage plate					
clamping fork, short, 5 pack	3	Thorlabs	CF125-P5	$ 41.50	$ 124.50
clean up filter for 405	1	Thorlabs	FB405-10	$ 98.00	$ 98.00
clean up filter for 642	1	Thorlabs	FB640-10	$ 84.67	$ 84.67
clean up filter for 520	1	Thorlabs	FB520-10	$ 84.67	$ 84.67
clean up filter for 488	1	Thorlabs	FL05488-10	$ 46.20	$ 46.20
Dichromatic mirror for 405	1	Thorlabs	DMLP425	$ 165.00	$ 165.00
Dichromatic mirror for 520	1	Thorlabs	DMLP550	$ 165.00	$ 165.00
filter wheel with 6 positions, with mount and 5 filters	1	Thorlabs	FW1AND	$ 294.00	$ 294.00
filter wheel mount	1	Newport	FWM	$ 123.00	$ 123.00
laser diode, 520 nm	1	Thorlabs	L520P50	$ 120.00	$ 120.00
laser diode controller	1	Thorlabs	TLD001	$ 773.00	$ 773.00
Power supply for diode	1	Thorlabs	TSP002	$ 105.00	$ 105.00
laser diode mount	1	Thorlabs	LDM9T/M	$ 702.00	$ 702.00
lens mount for clean up filters	3	Thorlabs	LMR1S	$ 26.25	$ 78.75
mirror mount translational, empty	1	Thorlabs	KM100	$ 38.70	$ 38.70
mirror mount translational, with mirror	5	Thorlabs	KM100-E02	$ 103.50	$ 517.50
ND filters OD 1.5	1	Newport	FSR-OD150	$ 38.00	$ 38.00
ND filters OD 1.0	1	Newport	FSR-OD100	$ 38.00	$ 38.00
ND filters OD 0.7	1	Newport	FSR-OD70	$ 38.00	$ 38.00
ND filters OD 0.3	1	Newport	FSR-OD30	$ 38.00	$ 38.00
optical fiber for 405	1	Thorlabs	P1-405BPM-FC-2	$ 234.00	$ 234.00
optical post, 1.5", 5 pack	1	Thorlabs	TR1.5-P5	$ 22.37	$ 22.37
post holder	6	Thorlabs	PH2E	$ 23.50	$ 141.00
x-y translator cage	3	Thorlabs	CXY1	$ 169.05	$ 507.15
TOTAL					$ 5,043.78

References

Aitken, C. E., Marshall, R. A., & Puglisi, J. D. (2008). An oxygen scavenging system for

improvement of dye stability in single-molecule fluorescence experiments.

Biophysical Journal, 94(5), 1826-1835. http://doi.org/10.1529/biophysj.107.117689

Andrews, N. L., Pfeiffer, J. R., Martinez, A. M., Haaland, D. M., Davis, R. W., Kawakami,

T., … Lidke, D. S. (2009). Small, Mobile FcεRI Receptor Aggregates Are Signaling

Competent. *Immunity*, *31*(3), 469–479.

http://doi.org/10.1016/j.immuni.2009.06.026

Bajar, B., Wang, E., Zhang, S., Lin, M., & Chu, J. (2016). A Guide to Fluorescent Protein

FRET Pairs. *Sensors*, *16*(9), 1488-1512. http://doi.org/10.3390/s16091488

Berezin, M. Y., & Achilefu, S. (2010). Fluorescence lifetime measurements and biological

imaging. *Chemical Reviews*, *110*(5), 2641–2684. http://doi.org/10.1021/cr900343z

Campbell, R. E., Campbell, R. E., Tour, O., Tour, O., Palmer, A. E., Palmer, A. E., … Tsien,

R. Y. (2002). A monomeric red fluorescent protein. *Proceedings of the National

Academy of Sciences of the United States of America*, *99*(12), 7877–7882.

http://doi.org/10.1073/pnas.082243699

Coons, A. H. (1961). The beginnings of immunofluorescence. *Journal of Immunology*, *87*,

499–503.

Ding, S., Cargill, A. A., Das, S. R., Medintz, I. L., & Claussen, J. C. (2015). Biosensing with

förster resonance energy transfer coupling between fluorophores and nanocarbon

allotropes. *Sensors*, *15*(6), 14766–14787. http://doi.org/10.3390/s150614766

Fernández-Suárez, M., & Ting, a. (2008). Fluorescent probes for super-resolution imaging in living cells. *Nature Reviews Molecular Cell Biology*, *9*(12), 929–943. http://doi.org/10.1038/nrm2531

Fitzpatrick, J. A. J., Yan, Q., Sieber, J. J., Dyba, M., Schwarz, U., Szent-Gyorgyi, C., … Bruchez, M. P. (2009). STED nanoscopy in living cells using fluorogen activating proteins. *Bioconjugate Chemistry*, *20*(10), 1843–1847. http://doi.org/10.1021/bc900249e

Goedhart, J., von Stetten, D., Noirclerc-Savoye, M., Lelimousin, M., Joosen, L., Hink, M. A., … Royant, A. (2012). Structure-guided evolution of cyan fluorescent proteins towards a quantum yield of 93%. *Nature Communications*, *3*, 751-760. http://doi.org/10.1038/ncomms1738

Hell, S. W., Dyba, M., & Jakobs, S. (2004). Concepts for nanoscale resolution in fluorescence microscopy. *Current Opinion in Neurobiology*, *14*(5), 599–609. http://doi.org/10.1016/j.conb.2004.08.015

Hochreiter, B., Garcia, A. P., & Schmid, J. A. (2015). Fluorescent proteins as genetically encoded FRET biosensors in life sciences. *Sensors*, *15*(10), 26281–26314. http://doi.org/10.3390/s151026281

Kenworthy, A. K. (2001). Imaging protein-protein interactions using fluorescence resonance energy transfer microscopy. *Methods*, *24*(3), 289–296.

http://doi.org/10.1006/meth.2001.1189

Khrenova, M., Topol, I., Collins, J., & Nemukhin, A. (2015). Estimating orientation factors

in the FRET theory of fluorescent proteins: The TagRFP-KFP pair and beyond.

Biophysical Journal, *108*(1), 126–132. http://doi.org/10.1016/j.bpj.2014.11.1859

Kraft, S., & Kinet, J. P. (2007). New developments in FcepsilonRI regulation, function and

inhibition. *Nature Reviews Immunology*, *7*(5), 365–378.

http://doi.org/10.1038/nri2072

Kremers, G. J., Goedhart, J., Van Munster, E. B., & Gadella, T. W. J. (2006). Cyan and

yellow super fluorescent proteins with improved brightness, protein folding, and

FRET Förster radius. *Biochemistry*, *45*(21), 6570–6580.

http://doi.org/10.1021/bi0516273

Lavis, L. D., & Raines, R. T. (2007). Bright Ideas for Chemical Biology. *ACS Chemical

Biology*, *3*(3), 142-155. http://doi.org/10.1021/cb700248m

Li, I. T., Pham, E., & Truong, K. (2006). Protein biosensors based on the principle of

fluorescence resonance energy transfer for monitoring cellular dynamics.

Biotechnology Letters, *28*(24), 1971–1982. http://doi.org/10.1007/s10529-006-

9193-5

Liu, H., Zhang, H., & Jin, B. (2013). Fluorescence of tryptophan in aqueous solution.

Spectrochimica Acta - Part A: Molecular and Biomolecular Spectroscopy, *106*, 54–

59. http://doi.org/10.1016/j.saa.2012.12.065

Mäntele, W., & Deniz, E. (2017). UV–VIS absorption spectroscopy: Lambert-Beer reloaded. *Spectrochimica Acta Part A: Molecular and Biomolecular Spectroscopy, 173*, 965-968. http://doi.org/10.1016/j.saa.2016.09.037

Matz, M. V, Fradkov, A. F., Labas, Y. a, Savitsky, A. P., Zaraisky, A. G., Markelov, M. L., & Lukyanov, S. a. (1999). Fluorescent proteins from nonbioluminescent Anthozoa species. *Nature Biotechnology*, *17*(10), 969–973. http://doi.org/10.1038/13657

Mellors, R. C. (1968). The Application of Labeled Antibody Technics in Studying Cell Antigens. *Cancer Research*, *28*(7), 1372–1381.

Mérola, F., Fredj, A., Betolngar, D. B., Ziegler, C., Erard, M., & Pasquier, H. (2014). Newly engineered cyan fluorescent proteins with enhanced performances for live cell FRET imaging. *Biotechnology Journal*, *9*(2), 180–191. http://doi.org/10.1002/biot.201300198

Müller, S., Galliardt, H., Schneider, J., Barisas, B., & Seidel, T. (2013). Quantification of Förster resonance energy transfer by monitoring sensitized emission in living plant cells. *Frontiers in Plant Science*, *4*, 413-433. http://doi.org/10.3389/fpls.2013.00413

Ortega, E., Lara, M., Lee, I., Santana, C., Martinez, A. M., Pfeiffer, J. R., … Oliver, J. M. (1999). Lyn dissociation from phosphorylated Fc epsilon RI subunits: a new regulatory step in the Fc epsilon RI signaling cascade revealed by studies of Fc epsilon RI dimer signaling activity. *Journal of Immunology*, *162*(1), 176–185.

Pratt, C. P., He, J., Wang, Y., Barth, A. L., & Bruchez, M. P. (2015). Fluorogenic green-

inside red-outside (GIRO) labeling approach reveals adenylyl cyclase-dependent control of BKα surface expression. *Bioconjugate Chemistry*, *26*(9), 1963–1971. http://doi.org/10.1021/acs.bioconjchem.5b00409

Qian, J., Yao, B., Wu, C., & Wu, C. (2014). Fluorescence resonance energy transfer detection methods: Sensitized emission and acceptor bleaching. *Experimental and Therapeutic Medicine*, *8*(5), 1375–1380. http://doi.org/10.3892/etm.2014.1928

Sanders, J. K. M., & Jackson, S. E. (2009). The discovery and development of the green fluorescent protein, GFP. *Chemical Society Reviews*, *38*(10), 2821–2822. http://doi.org/10.1039/b917331p

Saunders, M. J., Liu, W., Szent-Gyorgyi, C., Wen, Y., Drennen, Z., Waggoner, A. S., & Meng, W. S. (2013). Engineering fluorogen activating proteins into self-assembling materials. *Bioconjugate Chemistry*, *24*(5), 803–810. http://doi.org/10.1021/bc300613h

Schermelleh, L., Heintzmann, R., & Leonhardt, H. (2010). A guide to super-resolution fluorescence microscopy. *Journal of Cell Biology*, *190*(2), 165–175. http://doi.org/10.1083/jcb.201002018

Schwartz, S. L., Yan, Q., Telmer, C. A., Lidke, K. A., Bruchez, M. P., & Lidke, D. S. (2015). Fluorogen-activating proteins provide tunable labeling densities for tracking FcRI independent of IgE. *ACS Chemical Biology*, *10*(2), 539–546. http://doi.org/10.1021/cb5005146

Seong, J., Ouyang, M., Kim, T., Sun, J., Wen, P. C., Lu, S., … Wang, Y. (2011). Detection of focal adhesion kinase activation at membrane microdomains by fluorescence resonance energy transfer. *Nature Communications*, *2*, 406-414. http://doi.org/10.1038/ncomms1414

Siraganian, R. P., Zhang, J., Suzuki, K., & Sada, K. (2001). Protein tyrosine kinase Syk in mast cell signaling. *Molecular Immunology*, *38*(2001), 1229–1233.

Stryer, L. (1978). Fluorescence energy transfer as a spectroscopic ruler. *Annual Review of Biochemisiry*, *47*(5), 819-846.

Szent-Gyorgyi, C., Schmidt, B. A. F., Schmidt, B. A. F., Creeger, Y., Fisher, G. W., Zakel, K. L., … Waggoner, A. (2008). Fluorogen-activating single-chain antibodies for imaging cell surface proteins. *Nature Biotechnology*, *26*(2), 235–240. http://doi.org/10.1038/nbt1368

Szent-Gyorgyi, C., Stanfield, R. L., Andreko, S., Dempsey, A., Ahmed, M., Capek, S., … Bruchez, M. P. (2013). Malachite green mediates homodimerization of antibody VL domains to form a fluorescent ternary complex with singular symmetric interfaces. *Journal of Molecular Biology*, *425*(22), 4595–4613. http://doi.org/10.1016/j.jmb.2013.08.014

Teale, F. W., & Weber, G. (1957). Ultraviolet fluorescence of the aromatic amino acids. *The Biochemical Journal*, *65*(3), 476–482.

Vogelsang, J., Kasper, R., Steinhauer, C., Person, B., Heilemann, M., Sauer, M., &

Tinnefeld, P. (2008). A reducing and oxidizing system minimizes photobleaching and blinking of fluorescent dyes. *Angewandte Chemie - International Edition*, *47*(29), 5465–5469. http://doi.org/10.1002/anie.200801518

Voicescu, M., Ionescu, S., & Gatea, F. (2014). Effect of pH on the fluorescence characteristics of some flavones probes. *Spectrochimica Acta - Part A: Molecular and Biomolecular Spectroscopy, 123*, 303-308. http://doi.org/10.1016/j.saa.2013.12.040

Vonakis, B. M., Gibbons, S. P., Rotté, M. J., Brothers, E. a, Kim, S. C., Chichester, K., & MacDonald, S. M. (2005). Regulation of rat basophilic leukemia-2H3 mast cell secretion by a constitutive Lyn kinase interaction with the high affinity IgE receptor (Fc epsilon RI). *Journal of Immunology*, *175*(7), 4543–4554. http://doi.org/10.4049/jimmunol.175.7.4543

Walker, C. L., Lukyanov, K. A., Yampolsky, I. V., Mishin, A. S., Bommarius, A. S., Duraj-Thatte, A. M., … Solntsev, K. M. (2015). Fluorescence imaging using synthetic GFP chromophores. *Current Opinion in Chemical Biology*, *27*(June), 64–74. http://doi.org/10.1016/j.cbpa.2015.06.002

Wegner, K. D., & Hildebrandt, N. (2015). Quantum dots: bright and versatile in vitro and in vivo fluorescence imaging biosensors. *Chemical Society Reviews*, *44*(14), 4792–4834. http://doi.org/10.1039/c4cs00532e

Wilson, B. S., Pfeiffer, J. R., & Oliver, J. M. (2000). Observing Fc epsilon RI signaling from the inside of the mast cell membrane. *Journal of Cell Biology*, *149*(5), 1131–1142.

http://doi.org/10.1083/jcb.149.5.1131

Yan, Q., Schmidt, B. F., Perkins, L. A., Naganbabu, M., Saurabh, S., Andreko, S. K., & Bruchez, M. P. (2015). Near-instant surface-selective fluorogenic protein quantification using sulfonated triarylmethane dyes and fluorogen activating proteins. *Organic & Biomolecular Chemistry*, *13*(7), 2078–2086. http://doi.org/10.1039/C4OB02309A

Yan, Q., Schwartz, S. L., Maji, S., Huang, F., Szent-Gyorgyi, C., Lidke, D. S., … Bruchez, M. P. (2014). Localization microscopy using noncovalent fluorogen activation by genetically encoded fluorogen-activating proteins. *Chemphyschem : A European Journal of Chemical Physics and Physical Chemistry*, *15*(4), 687–695. http://doi.org/10.1002/cphc.201300757

Yang, F., Moss, L. G., Phillips, G. N., Phillips Jr., G. N., & Phillips, G. N. (1996). The molecular structure of green fluorescent protein. *Nature Biotechnology*, *14*(10), 1246–1251. http://doi.org/10.1038/nbt1096-1246

Zacharias, D. A., Violin, J. D., Newton, A. C., & Tsien, R. Y. (2002). Partitioning of lipid-modified monomeric GFPs into membrane microdomains of live cells. *Science*, *296*(5569), 913–916. http://doi.org/10.1126/science.1068539

Zgierski, M. Z., Fujiwara, T., & Lim, E. C. (2010). Role of the pisigma* state in molecular photophysics. *Accounts of Chemical Research*, *43*(4), 506–517. http://doi.org/10.1021/ar9002043

Zimmer, M. (2009). GFP: from jellyfish to the Nobel prize and beyond. *Chemical Society Reviews*, *38*(10), 2823–2832. http://doi.org/10.1039/B904023D